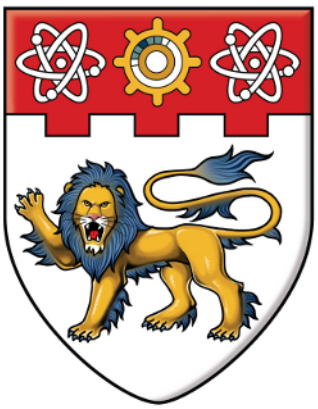

NANYANG TECHNOLOGICAL UNIVERSITY

IMPROVING SELECTIVITY OF GOLD NANOPARTICLES FOR GLYCEROL ELECTRO-OXIDATION VIA INTERACTION WITH NON-NOBLE METALS

THIA YI PING LARISSA

Interdisciplinary Graduate School

NEWRI-Residues & Resource Reclamation Centre

2016

IMPROVING SELECTIVITY OF GOLD NANOPARTICLES FOR GLYCEROL ELECTRO-OXIDATION VIA INTERACTION WITH NON-NOBLE METALS

THIA YI PING LARISSA

Interdisciplinary Graduate School
NEWRI- Residues & Resource Reclamation Centre

A thesis submitted to the Nanyang Technological University in partial fulfilment of the requirement for the degree of
Doctor of Philosophy

2016

To my parents, with gratitude.

Acknowledgements

First and foremost, I would like to thank my supervisor, Prof Wang Xin, for giving me the opportunity to join his research group and work on this project. Your patience and support over the course of my PhD studies has been instrumental in helping me persist despite my numerous failures. I have also benefited greatly from the academic advice you have given me.

To my lab mates, both past and present, including: Zhou Huiming, Yan Ya, Xiao Peng, Xia Baoyu, Peng Yuecheng and Nsanzimana Jean Marie Vianney thanks for the help and support. Special thanks goes out to: Li Nan, for your encouragement when I needed it the most. Also for help with the XPS tests. Xie Mingshi, for helping me in countless large and small ways (certainly too many to be listed). Wang Jiong and Lu Yizhong for the insightful discussions that I have had with you guys over the past 8 months. Also for help with ICP and TEM. Finally, to Wang Haibo, thanks for pulling me through the past year (and all the times in between) as I worked towards completing my thesis and publications. I couldn't have done it without you.

To the friends that I have made during my PhD studies: Yan Yibo, Chen Xiaoping, Zhao Jun and Huang Lin, thanks for all the laughter, friendship and generosity. To Jaslyn, thanks for being such a pal. Glad to have made it through this PhD journey with you. I would also like to thank my other friends, especially Bri and Angie, for their unwavering support and encouragement. Thanks for always being available.

Lastly, my gratitude goes out to my parents for the immense sacrifices they have made for me over the years. Thanks for giving me the best in life and for always believing in me despite all the odds. This thesis is dedicated to the both of you.

Abstract

This thesis begins by examining the current state of the art for glycerol electro-oxidation. Extensive research has been carried out to determine the effect of size, morphology, shape, support, experimental conditions and catalyst preparation methods on the catalytic performance of both Au and Pt based catalysts. While the effect of non-noble metal promoters has been relatively well studied for Pt group catalysts, the same cannot be said for Au based catalysts. Thus, the research work presented in this thesis aims to demonstrate how the selectivity of carbon supported Au nanoparticles for glycerol electro-oxidation can be improved via interaction of Au/C with non-noble metals.

Enhanced selectivity towards C3 products, glycerate and tartronate, was achieved by simple electro-deposition of Cu onto Au nanoparticles. Initial studies showed that the most selective catalysts were obtained when Cu electro-deposition occurred at -0.1 V and +0.015 V for 30 min. Enhancement in C3 selectivity was attributed to the presence of an Au^{+} species that was generated via electron transfer between Au and electro-deposited Cu_2O. C3 selectivity was maximized at double that of pure carbon supported Au nanoparticles when Cu electro-deposition took place at +0.015 V for 90 min. This result is attributed to the doubling of Au^{+} content that takes place at this experimental condition.

Electro-deposition of Ni onto Au nanoparticles also gave rise to enhanced C3 selectivity. The most selective catalysts were obtained when Ni electro-deposition occurred at -0.3 V for 40 min. Au^{+} species was similarly identified post Ni electro-deposition and it was generated due to electron transfer between Au and NiOOH species. When Ni electro-deposition occurred at more negative potentials, the resultant thick Ni surface layer partially shielded Au from the reaction medium thus reduced access of glycerol molecules to the Au active sites. As such, C3 selectivity of the Ni-Au/CB catalysts prepared under these conditions were relatively similar

to that of pure Au/CB. Any possible synergistic effect between Au and Ni was thus nullified by the thick Ni surface coverage.

Lastly, residual Ag containing porous Au structures were prepared and tested for glycerol electro-oxidation. These catalysts were highly active and selective towards C-C bond breaking products, glycolate and formate. Porous Au catalysts were obtained by etching alloyed AuAg sheets in concentrated nitric acid. However, etching does not completely remove all traces of Ag, hence small amounts are still present. Additionally, low temperature annealing enhanced selectivity and product conversion due to the increase in mixed Au-Ag sites after annealing.

Keywords: glycerol electro-oxidation, Cu electro-deposition, Ni electro-deposition, porous Au, Au nanoparticles

Table of Contents

List of figures

List of tables

List of publications

1) L,Thia.; M, Xie.; Z, Liu.; X, Ge.; Y, Lu.; E, Fong.; X, Wang. *Chemcatchem*, 2016, 8, 3272-3278.

2) L.Thia.; M, Xie, D, Kim, X, Wang.; *Catal. Sci. Technol.*, 2017, **7**, 874-881.
(This article was selected as part of the themed collection: 2017 Catalysis, Science and Technology Hot Articles)

3) Wang, H.; Thia, L.; Li, N.; Ge, X.; Liu, Z.; Wang. X. *Applied Catalysis. B*, 2015, 166-167, 25-31.

4) Wang, H.; Thia, L.; Li, N.; Ge, X.; Liu, Z.; Wang. X. *ACS Catalysis*, 2015, 5, 3174-3180.

5) H. Wang.; M. Xie.; L. Thia.; A. Fisher.; and X. Wang. *The Journal of Physical Chemistry Letters*, 2014, **5**, 119-125.

Chapter 1

Introduction and Scope of Thesis

1.1. Introduction

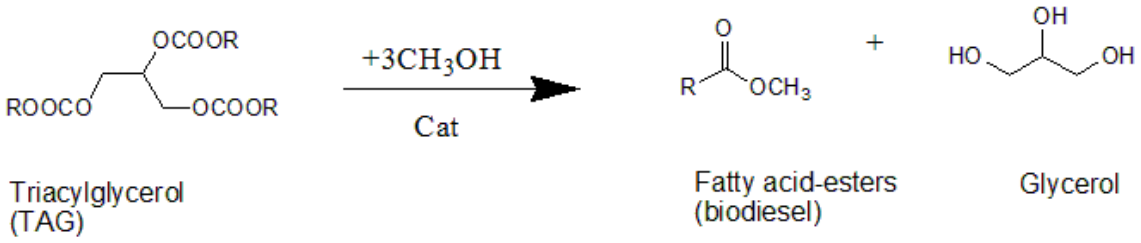

Scheme 1. Transesterification of vegetable oils and fats yielding biodiesel, and glycerol as a by-product. Reprinted with permission from ref 1. Copyright Royal Society of Chemistry.

The progressively rapid depletion of fossil fuels has driven the search for alternative energy sources that are based on renewable raw materials. In line with this, the Directive on the Promotion of the use of biofuels and other renewable fuels for transport (2003/30/EC) was enforced within the European Union (EU) in 2003 to promote the use of biofuels for transport and reduce dependency on petroleum. Biodiesel is conventionally produced via the transesterification of vegetable oils or animal or waste fats. The homogeneous process is catalysed by a strong base which simultaneously cleaves fatty acids from the glycerol backbone and transforms them into methyl esters, leaving glycerol behind as a by-product (Scheme 1).[1] Consequently, global production of glycerol from biodiesel has increased sharply in the past decade. Between 2003 and 2012, global glycerol production was ramped up by more than ten times from 200,000 tonnes in 2003 to more than 2 million tonnes in 2012.[2]

1.2. Rationale: the need to valorise glycerol via electro-oxidation

Although glycerol is widely employed in a variety of industries, the current biodiesel production boom has flooded the market with a large excess of glycerol which classical industries have struggled to absorb. As such, new strategies to valorise glycerol are necessary to absorb this surplus.

The highly functionalized glycerol molecule can be used as a platform chemical to produce new polymers, fine chemicals and pharmaceuticals. Amongst the available methods, electrochemical oxidation of glycerol in direct alcohol fuel cells (DAFCs) is extremely attractive, owing to its ability to co-generate electricity and valuable chemicals. As a fuel, glycerol is a viable alternative to methanol and ethanol, which are the two classical fuels for liquid fuel cells. Energy density for glycerol is 5.0 kWh kg^{-1}, which is comparable to that of methanol and ethanol at 6.1 and 8.0 kWh kg^{-1} respectively.[3] Glycerol also has a lower fuel cross-over and is less toxic and volatile. More importantly, converting surplus glycerol to high value added chemicals helps offset the cost of biodiesel production and enables the process to be more economical.

Glycerol oxidation occurs either by the primary or secondary oxidation pathway. The primary oxidation pathway produces glyceric acid (GLYA), tartronic acid (TA) and mesoxalic acid (MA) as the principle C3 oxidation products while the secondary oxidation pathway generates dihydroxacetone (DHA) and hydropyruvic acid (HYPA) as the main products. While GLYA is the dominant product generated under most experimental conditions tested, it has yet to find any practical applications. Nevertheless, it is a crucial intermediate to produce TA and MA. TA is a very expensive reagent (1564 US$/g). Owing to its high costs, TA is primarily utilized in the treatment of osteoporosis and obesity.[4] TA also has potential as an anti-corrosive protective agent that can be employed for high temperature applications.[5] Similarly, MA, the direct oxidation product of TA, is also an expensive fine chemical (156 USD$/g). It has potential applications as a complexing agent and is a precursor in the synthesis of 4-chlorophenylhydrazoned mesoxalic acid, which is a demonstrated anti-HIV agent.[6] The calcium or potassium salt of MA can also be used in the treatment of diabetes.[7] On the other hand, DHA (150 USD$/kg), the secondary oxidation product, is the active ingredient in sunless tanning agents. Currently, DHA is commercially produced via fermentation, which is

necessitated given the strict quality requirements for cosmetic grade DHA. However, the conventional fermentation process is not very efficient owing to the low concentration of starting material used.

Despite their potential to be utilized for a wide variety of applications, C3 products derived from partial oxidation of glycerol are currently limited to high value applications such as for medicine due to their high cost. Yet, the significantly higher commercial value of these oxidation products compared to crude and purified glycerol (less than 0.3 US$/kg and about 0.6 US$/kg respectively), provides motivation to optimize the glycerol oxidation process such that these chemicals can be selectivity produced in high concentrations. However, the glycerol oxidation pathway is highly complex and the ability to tune the oxidation pathway to produce specific products selectively remains challenging. In addition to the above mentioned C3 products, a variety of C2 and C1 products such as oxalic acid, glycolic acid, formic acid and CO_2 are typically generated during the reaction. These C1 and C2 products also lend themselves to many industrial applications. For example, glycolic acid is also widely used in textile dyeing, leather tanning and personal care products while major applications of formic acid include silage and animal feed preservation.

1.3. Scope of thesis

1.3.1 Objectives

The goal of this study is to develop a general strategy to tune the selectivity of carbon supported Au nanoparticles (Au/C) towards specific products during glycerol electro-oxidation. Specifically, this work aims to investigate the ability of non-noble metals to influence the selectivity of Au/C. To date, a general strategy to tune the selectivity of Au/C towards specific products in the glycerol electro-oxidation pathway has yet to be proposed.

1.3.2. Hypothesis

Presence of electro-deposited transition metals may influence the catalytic performance of the Au/C through the following ways (i) synergistic interaction between the two metals (ii) electronic modification of Au/C via electron transfer (iii) ability of the electro-deposited species to alter the glycerol oxidation pathway on Au/C. A thicker catalyst layer will result post electro-deposition and this will likely be favourable for the formation of deeper oxidation products. Hence, this thesis aims to determine if the electro-deposition of transition metals will influence the selectivity of Au/C for glycerol electro-oxidation and the underlying factors which drive these changes.

The detailed scope of this thesis is as follows:

Chapter 1: gives a short introduction on why there is a surplus of glycerol in the market and rationalizes the need to valorise surplus glycerol via electro-oxidation. The objectives and hypothesis of our research work as well as the scope of this thesis is also outlined.

Chapter 2: provides a detailed literature review on the various catalytic systems which have been studied for both glycerol oxidation and electro-oxidation. Successful strategies that have been developed to improve the catalytic performance of metal catalysts are highlighted. The glycerol electro-oxidation mechanism over gold and platinum electrodes under different pH conditions is also discussed.

Chapter 3: evaluates the ability of electro-deposited Cu species to influence the selectivity of Au/C. C3 selectivity of the resulting catalysts were significantly enhanced due to synergistic interaction between Au and the electro-deposited Cu species. Furthermore, extent of improvement in C3 selectivity was dependent on deposition time and potential, with the highest improvement obtained after Cu electro-deposition occurred for 90 minutes at +0.015 V. Presence of electro-deposited Cu led to electronic modification of Au/C and the generation of an Au^{+} species in the catalyst. Au^{+} was generated via electron transfer between Au and electro-

deposited Cu_2O. Catalysts containing the Au^+ species observed increased selectivity to glycerate and tartronate while simultaneously suppressing C-C bond cleavage to glycolate and formate.

Chapter 4: evaluates the ability of electro-deposited Ni to influence the selectivity of Au/C. C3 selectivity of Au/C for glycerol electro-oxidation was enhanced after Ni electro-deposition. Au/C underwent electronic modification because of interaction with the electro-deposited Ni species. The most selective catalysts contained an Au^+ species which was generated via interaction between Au and NiOOH species.

Chapter 5: examines the ability of residual Ag containing porous Au structures to achieve high selectivity towards glycolate and formate. Porous Au structures were obtained by etching AuAg sheets in concentrated nitric acid. However, the etching process does not completely dealloy Ag and residual amounts remained embedded within the porous 3D framework. Residual Ag tuned the product distribution towards glycolate and formate when glycerol electro-oxidation occurred under alkaline conditions. Heat treatment of the catalysts after dealloying resulted in further improvements in selectivity as annealing caused residual Ag to diffuse and precipitate onto the surface of the porous framework. Presence of greater amounts of exposed Ag was the driving factor for improved selectivity to glycolate and formate.

Chapter 6: provides a summary of this thesis and gives recommendations for future work.

Chapter 2

Literature Review

2.1. Introduction

Heterogeneous catalytic oxidation of glycerol can be carried out using inexpensive oxidizing agents such as air and oxygen or via electrochemical methods. Glycerol oxidation is usually carried out in an autoclave or glass reactor under elevated temperature and pressure, using water as a solvent. Glycerol is also a potential fuel for direct alcohol fuel cells (DAFC). Utilization of glycerol as a fuel in DAFCs is advantageous as it enables the co-generation of electricity and valuable chemicals. Applied potential can also be used as means to further tune catalytic selectivity during the reaction.

Most studies investigating the catalytic (electro)-oxidation of glycerol have focused on using supported Pd, Pt, Au noble metal catalysts since non-noble metal catalysts tend to perform poorly. Hence, this chapter will provide an overview of the catalytic performance of Au, Pt and Pt based catalysts under both electro-catalytic and oxidative conditions. In particular, we will highlight the various strategies that have been undertaken in order to improve innate performance of these noble metal catalysts.

2.2. Glycerol Oxidation

2.2.1. Platinum group catalysts

Platinum group based catalysts (Pt and Pd) have been widely investigated as catalytic systems for glycerol (electro)-oxidation.[8-13] Supported Pt and Pd catalysts produce glycerate as the main product when the reaction occurs under base free and basic conditions.[14, 15] Employment of Pt catalysts is particularly attractive owing to their high activity under base free conditions. Consequently, oxidation products generated do not need to undergo additional neutralization and acidification steps to obtain the free acid.

In general, Pt nanoparticles smaller than 6 nm were more active for glycerol oxidation under base free conditions while particles larger than 6 nm, though less active, were more selective to glyceric acid.[9, 16-19] Particle and catalyst morphology also influenced catalytic activity.[20] Highly faceted Pt nanocrystals possessing a greater number of exposed facets observed greater activity due to the presence of a higher number of atomic and terrace steps. However, it is not conclusive whether an increase in the number of (111)[19] or (100)[21] facets drives higher activity for glycerol oxidation. Furthermore, type of exposed facet also affects selectivity. Computation and experimental studies showed that the Pt(111) electrode produced glyceraldehyde, glyceric acid, and dihydroxyacetone as products of glycerol electro-oxidation while only glyceraldehyde was detected on the Pt(100) electrode.[22]

2.2.1.2. Disadvantages

Catalyst deactivation due to Pt surface oxidation is the biggest obstacle in the large-scale application of Pt based catalysts for glycerol oxidation. High temperatures and a low partial pressure of oxygen are usually required in order to stabilize the catalytically active zero valent Pt species and prevent oxygen poisoning.[23, 24] Platinum group based catalysts are also highly susceptible to poisoning either by by-products or adventitious species.[23, 24] In addition, strongly coordinated products generated in-situ may lead to reversible metal dissolution–precipitation which in turn increases mobility of metal atoms at the catalyst surface.[23, 25] Increased mobility results in particle growth leading to a decrease in specific surface area and consequently turnover frequency (TOF). On the other hand, irreversible dissolution results in loss of catalyst as it is leached into solution.[26]

2.2.2 Gold based catalysts

2.2.2.1. Advantages

Au based catalysts are more stable and more resistant to oxidation[27] compared to Pt group catalysts. This is due to the high electrode potential (E^o = +1.69 V) of Au which is responsible

for its inert nature. Indeed, bulk Au displays little to no catalytic activity. However, supported Au in the nanoscale region (typically with diameters below 10 nm) is surprisingly active, especially at low temperatures.[28-31] Additionally, Au based catalysts tend to be more selective than Pt/Pd based catalysts as they are able to discriminate between different chemical groups and geometrical positions, leading to superior yields of desired products. For example, glycols are selectively oxidised to monocarboxylates[32] whilst unsaturated alcohols are fully converted to unsaturated aldehydes[33] when their respective reactions are catalysed by Au nanoparticles. Au nanoparticles, especially those prepared by sol-immobilization, are also relatively tolerant towards poisoning chemical groups such as aliphatic and aromatic amines.[34, 35] Au is also subject to poisoning from ternary ammoniums when used as a catalyst in direct glycerol alkaline membrane fuel cells.[36] Ternary ammoniums are possible degradation products of quaternary ammonium functional groups that are mainly contained in the anion exchange membranes. However, since the adsorption of these N-containing species was induced by the anodic nature of Au, the normal water washing off under no load condition should remove these species from the catalyst layer. Furthermore, the types of amine groups used in the anion exchange membranes can be optimized to reduce Au deactivation as methyl group substituted amines were found to be more suitable than larger substituted amines for the Au-based catalysts. Given the abovementioned disadvantages of Pt based catalysts and the relative merits of Au based catalysts, this thesis will focus on the catalytic performance of Au catalysts for glycerol (electro)-oxidation under alkaline conditions. The following section provides an in-depth discussion on the various factors which influence the catalytic performance of Au based catalysts for glycerol (electro)-oxidation.

2.2.2.2. Size Effect

Catalytic performance of Au based catalysts for glycerol oxidation is significantly influenced by the size of the Au nanoparticles.[32-37] In general, smaller Au nanoparticles (average diameter

< 20 nm) exhibited turnover frequencies (TOFs) that were about an order of magnitude higher than larger Au nanoparticles (average diameter ≥ 20 nm). However, the latter demonstrated higher selectivity for glyceric acid. On average, selectivity to glyceric acid was about 10% higher with larger Au nanoparticles. Extending Au particle size beyond 20 nm resulted in catalytic performance similar to that of bulk Au. Additionally, judicious selection of particle size in conjunction with careful tuning of reaction conditions led to even greater improvements in glyceric acid selectivity.[38] 100% glyceric acid selectivity was achieved when glycerol oxidation was carried out over 1% Au/charcoal or 1% Au/graphite catalysts, under mild conditions.

Ideal particle size to achieve optimal catalytic performance is also dependent on the type of support used.[39, 40] Au nanoparticles on carbon support display optimal activity when they possess an average diameter of 7-8 nm. Au nanoparticles smaller than 8 nm tend to lie deep in the carbon support and are less accessible to glycerol during the reaction. As such, catalytic activity declines when particle size decreases beyond 8 nm. In comparison, oxide supported Au nanoparticles perform better with smaller average diameters. Presumably, the shielding of smaller Au nanoparticles does not exist when they are deposited on oxide supports. Hence catalytic activity continued to increase with decreasing particle size.

2.2.2.3. Effect of Preparation methods

Preparation methods influence nanoparticle size and dispersion and this in turn affects their catalytic performance.[41-44] Supported Au nanoparticles are typically prepared via sol-immobilization or incipient-wetness methods. Sol-immobilization consists of reducing aqueous metal precursors in the presence of stabilizers followed by depositing the pre-formed sols onto a support. On the other hand, incipient-wetness method first involves impregnating the support with appropriate amounts of aqueous metal precursor. The catalyst is then dried and activated via calcination. Sol-immobilization is more effective for preparing catalysts that

possess the following characteristics: smaller nanoparticles, narrower size dispersion, good surface exposition and high dispersion. The classical incipient wetness method tends to result in larger particles (average particle diameter > 10 nm) which tend to aggregate. As such, activated carbon supported Au nanoparticles prepared by sol-immobilization are generally more active and consequently less selective for glyceric acid. In comparison, catalysts prepared by the incipient wetness method exhibited lower activity but higher selectivity to glyceric acid due to their larger sized nanoparticles.

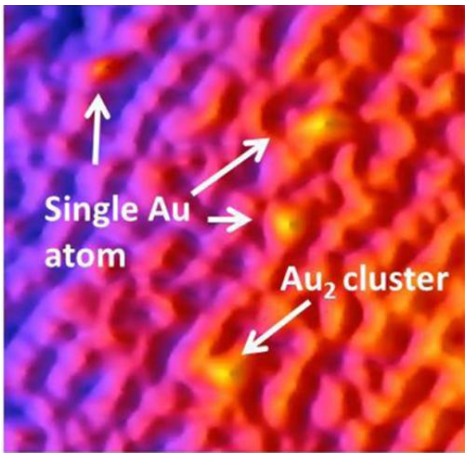

Fig. 2.1. High resolution HAADF STEM images of single Au atom and Au_2 cluster. Reprinted with permission from ref 33. Copyright ACS Publications.

Additionally, the solvent system (a mixture of water and ethanol) and reaction temperature used during sol-immobilization can be further tuned to produce Au catalysts with improved catalytic performances and durability.[45] Au/TiO_2 catalysts prepared in water (Au/TiO_2-water), at 1 ^oC, exhibited the highest activity for glycerol oxidation. Its TOF was about 10 times higher than that observed for a similarly sized catalyst, which was prepared with a 50/50 ethanol/water ratio at 0 ^oC. Superior activity of Au/TiO_2-water was associated with the presence of ultra-small Au clusters (1-5 atoms) (Fig. 2.1).

Interaction between PVA and solvent system also appeared to affect catalytic performance. This was observed from experiments showing that Au nanoparticles possessing the same average size but prepared with different solvent systems gave rise to varying catalytic

performances. Au/TiO_2-water was also highly durable and catalytic activity only decreased slightly after 10 successive recycling tests due to aggregation of the very small Au clusters.

2.2.2.4. Influence of protecting agent

Protecting agents like poly(vinyl)alcohol (PVA) and Poly(diallyldimethylammonium chloride) (PDDA) can affect catalytic performance by limiting access to active sites and influencing metal–support and reactant–metal interactions. Stearic stabilizers like PVA are more effective than electrostatic stabilizers like THPC for preparing small Au nanoparticles for glycerol (electro)-oxidation.[46] Similar observations were made when PVA and THPC were used to prepare AuPd alloys for glycerol oxidation.[46, 47] PVA protected Au seeds resulted in small, highly dispersed and homogeneously alloyed AuPd nanoparticles. In comparison, THPC protected Au seeds resulted in agglomerated AuPd alloys which were not homogenously alloyed. These structural differences led to differences in catalytic activities. PVA protected alloys were most active while THPC protected alloys were less active compared to its monometallic counterparts.

PVA to Au wt/wt ratio affects Au particle size and distribution.[48, 49] However, this is also dependent on Au concentration used. With low Au concentrations, higher PVA to Au wt/wt ratio gave rise to smaller particle sizes and narrower size distributions. When high Au concentrations are used, particle size is relatively independent of PVA to Au wt/wt ratio. Additionally, regardless of Au concentration, nanoparticle size increases in the presence of excess PVA. Excess PVA causes difficultly in immobilizing Au nanoparticles onto the support, thus resulting in partial aggregation and coalescence of Au.

When PVA was completely removed from the Au nanoparticle surface, TOF decreases drastically.[50] Furthermore, this decrease is not commensurate with the corresponding increase in particle size. As such, PVA not only functions as a stabilizing agent but may also be actively involved in the reaction. PVA appeared to mediate selectivity as well since C3 selectivity

increased with increasing amounts of PVA. That is, C3 selectivity increased with decreasing particle size. Improvement in C3 selectivity was attributed to the ability of PVA to direct the adsorption mode of glycerol. PVA arrangement on Au nanoparticles surface created a sort of porous structure that directed the adsorption of glycerol to the Au active sites by interacting with their OH groups (Fig. 2.2).

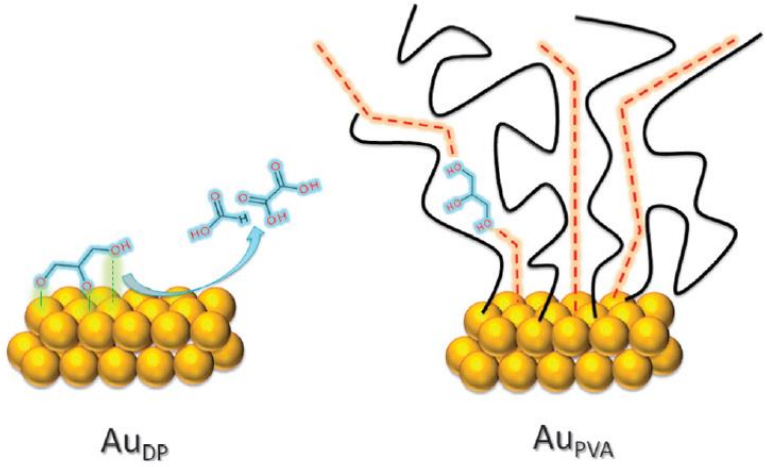

Fig. 2.2. Mode of glycerol adsorption on Au nanoparticles (a) in the presence of PVA, (b) on its free surface. Reprinted with permission from ref 34. Copyright Royal Society of Chemistry.

Prati and co-workers also observed that carbon supports can function as stabilizing agents in the absence of PVA.[51] This is particularly true for activated carbon (AC), which is a highly functionalized and defective support that possesses a great number of anchoring sites. Au supported on AC is protected against coarsening even when PVA is completely removed. In comparison, the number of functional groups on crystalline graphite and TiO_2 are too low to efficiently anchor the nanoparticles and aggregation was observed after complete PVA removal.

2.2.2.5. Influence of platinum group metals on catalytic performance of Au

AuPd and AuPt bimetallic catalysts have been widely investigated to determine how Pd and Pt influence catalytic performance of Au for glycerol oxidation.[52, 53] In general, bimetallic catalysts (typically alloys or core-shell structures) engenders significant improvements in catalytic performance compared to monometallic catalysts.[54, 55] Resistance to poisoning also improves with the addition of Au to Pd or Pt.[56]

Supported AuPd alloys have merited intensive investigation as its catalytic performance supersedes that of Au.[57-62] This is due to (i) synergistic effect between Au and Pd in the alloy (ii) Au and Pd being able to form a continuous solid solution over the whole range of gold/palladium compositions and (iii) Pd altering the electronic and geometrical properties of Au, which in turn positively affects its catalytic activity, stability and product distribution. [63, 84] For example, single phase activated carbon supported AuPd catalysts (AuPd/AC) was about 6-7 times more active for glycerol oxidation compared to Au and Pd/AC.[64]

Preparation method used to synthesize supported AuPd alloys is key to influencing its catalytic performance. Synergistic effects of Au and Pd alloying is only realized with uniformly alloyed, single-phase homogeneously dispersed bimetallic Au-Pd catalysts. Uniformly alloyed, AuPd catalysts can be synthesized via a 2 step procedure that makes use of Au as the nucleation centre for Pd.[64] Preformed Au sol was first immobilized on activated carbon (AC) using $NaBH_4$ as the reducing agent. Pd sol was then generated in the presence of Au/AC using H_2 as a second reducing agent as $NaBH_4$ easily results in Pd segregation. Slowing down the reduction rate of Pd salt is key to avoiding Pd segregation or homogenous nucleation that results in a mixture of monometallic phase.[56] Alternatively, AuPd/C was prepared by depositing Au onto the surface of commercially purchased Pd/C (3 nm), using H_2 as a reducing agent.[65] However, the resulting particles remained largely bimetallic (i.e. no bulk alloying) and no improvement in catalytic activity was observed. However, compared to AuPd/C prepared by sol-immobilization (AuPd-sol/C), AuPd/C managed to improve glyceric acid selectivity. This was attributed to surface Pd exposure which aided H_2O_2 decomposition on the Au surface. H_2O_2 is correlated with the formation of C–C cleavage products.

Sol-immobilization and wet impregnation methods were also investigated for the preparation of supported AuPd alloys for glycerol oxidation.[66] AuPd alloys prepared by sol-immobilization ($AuPd_{SI}$) were more active than those prepared by wet impregnation ($AuPd_{IW}$), even though

both methods produced alloys with similar size distributions. In general, sol-immobilization enhanced activity by a factor of ca. 2–3 for all catalysts tested. Selectivity to glycerate also improved. Enhanced catalytic performance of $AuPd_{SI}$ was attributed to formation of homogenous alloys with narrow particle size distributions. In comparison, $AuPd_{IW}$ were larger particles with enhanced levels of surface Pd and in addition displayed Pd^{2+} exclusively. As such, surface Au-Pd alloying is the key parameter in tuning catalytic activity.

Using the 2 step nucleation method, surface Au-Pd alloying can be further controlled by tuning Au : Pd ratio.[67-69] Catalytic activity improved with increasing Au/Pd molar ratio and the highest activity corresponded to a highly Au-rich Au system. When Au : Pd ratios were varied at 9 : 1, 8 : 2 and 6 : 4, single phased alloys with significantly improved catalytic activity for glycerol oxidation were achieved.[68] In this report, an Au : Pd ratio of 9 : 1 possessed optimum surface configuration for glycerol oxidation. However, another report suggests that an Au80–Pd20 ratio maximizes activity instead.[69] Improvement in activity was attributed to the presence of a considerable number of Pd monomer sites that are isolated by Au atoms. Dispersed Pd sites and the Pd monomers in contact with Au are the suggested active sites.[70-72] Surface Pd monomer sites can also help inhibit the formation undesirable by-products by breaking down H_2O_2. On the other hand, Au : Pd ratios of 2 : 8 and 9.5 : 0.5 showed inhomogeneous Pd distribution, with parts of the catalyst surface being Pd rich. Pd segregation weakened the synergistic effects of bimetallic catalysts and was detrimental to their catalytic performance.

Support identity also influenced catalytic performance of supported AuPd alloys.[66] However, its influence is dependent on preparation method employed. TiO_2 supported AuPd ($AuPd/TiO_2$) was more active than carbon supported AuPd (AuPd/C) when the alloys are prepared by impregnation. Lower activity of the carbon supported catalyst was due to a wider particle size distribution. In comparison, $AuPd/TiO_2$ and AuPd/C catalysts prepared by sol-immobilisation have very similar particle size distributions and display similarly high activity.

Effect of varying Pd surface with carbon supported AuPd bimetallic structures (Pd-on-Au/AC) was also studied.[73, 74] Higher activity of Pd-on-Au/AC compared to Au/AC was attributed to the former having lower activation energies for the β-C–H bond cleavage rate limiting step. Presence of Pd on Au lowered activation energy by about 5 kJ mol^{-1}. Furthermore, Pd-on-Au/AC catalysts weakened adsorption strength for the glycerolate intermediate and this contributed to its higher activity and enhanced selectivity to glyceric acid. Notably, catalytic activity exhibited a volcano dependence on Pd surface coverage. That is, catalytic activity increased with increasing Pd surface coverage, until maximum activity was reached at 80% Pd surface coverage. At Pd surface coverages greater than 80%, catalysts became more susceptible to deactivation either by CO poisoning or by adsorbate fouling. These catalysts were also more prone to undergoing oxidation and subsequent deactivation during the reaction.

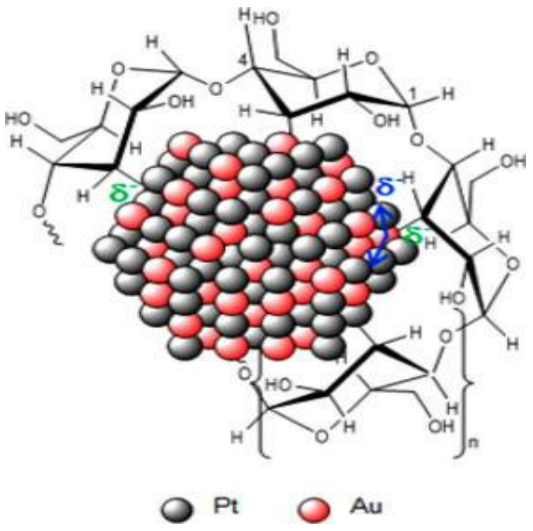

Fig. 2.3. Possible electron transfer from starch ligand to alloy PtAu−Starch NPs and from Au Atoms to adjacent Pt atoms. Reprinted with permission from ref 44. Copyright ACS Publications.

Supported AuPt catalysts have been less intensively investigated compared to supported AuPd catalysts. Catalytic performance of AuPt alloys is similarly dependent on the Pt : Au ratio. This was observed with hydrotalcite supported PtAu alloyed catalysts (PtAu-starch/HT) using starch as a stabilizing and reducing agent.[75] Activity increased with increasing Pt to Au ratio while conversely, glyceric acid selectivity decreased. Notably, alloying Pt with Au inhibited the over-

oxidation of glycerol oxidation intermediates to CO_2 and 100% mass balance could be attained. Enhanced catalytic performance of PtAu-starch/HT was also due to geometric and electronic changes brought about when starch was used as a protecting agent (Fig. 2.3). Both Pt and Au atoms gained negative charges from the starch ligand. Furthermore, excess electrons on the Au atoms were also transferred to the Pt atoms. The negatively charged Pt atoms likely enhanced oxygen absorption and generated anionic O_2 species such as superoxo or peroxo oxygen that initiated the polyol oxidation catalytic cycle. Replacement of active Pt atoms with inactive Au atoms also changed the geometry of the Pt surface and this could have contributed to the enhanced performance of AuPt-starch/HT.

Most importantly, supported AuPt catalysts have demonstrated enhanced ability to catalyse glycerol oxidation under base free conditions. Although H-mordenite supported Au and Pt catalysts can catalyse glycerol oxidation under base free conditions with high glyceric acid selectivity (70% and 79% selectivity respectively), the catalysts suffer from low conversion rates. Alloying Au with Pt in a 6 : 4 ratio led to enhanced conversion and high glyceric acid selectivity (81% at full conversion). Alloying also improved catalyst life and prevent metal leaching.[76] Herein, choice of support played in key role in ensuring high glyceric acid selectivity as the amount of H_2O_2 generated with H-mordenite as support was 30 times less than that with activated carbon. Monometallic catalysts supported on H-mordenite were also much less selective to C_1 products than those supported on neutral or basic supports such as TiO_2 and $MgAl_2O_4$. On the other hand, by fine tuning Au to Pt ratio, AuPt catalysts on basic MgO support (AuPt/MgO) could similarly achieve high activity for glycerol oxidation under base free conditions and ambient temperature.[77] Furthermore, AuPt/MgO was both more active (higher conversion rates) and selective to glyceric acid compared to AuPd/MgO under similar conditions.

Other types of bimetallic structures have also been investigated for glycerol oxidation. Notably, carbon supported Pd-Ag (Pd-Ag/C) catalysts exhibited exceptionally high selectivity (up to 85%) towards dihydroxyacetone (DHA).[78] Alloying Pd with Ag thus altered the inherent selectivity of Pd/C. Although, catalytic activity of the Pd-Ag/C catalysts was relatively low, it could be improved with pre-treatment. Alternatively, alloying Pt with Cu significantly improved stability of Pt, which is prone to deactivation.[18] PtCu/C catalysts maintained its catalytic performance during recycling and was more selective to glyceric acid compared to Pt/C catalysts having the same Pt loading. Thus, presence of Cu in Pt supressed C-C bond cleavage and decreased selectivity to C1 side products.

Contrary to expectations, TiO_2 supported Au-Pt-Pd trimetallic catalysts (Au-Pt-Pd/ TiO_2) were not more active for glycerol oxidation as compared to Au-Pd/TiO_2 and Pd-Pt/TiO_2 at longer reaction times of 4 h.[79] Furthermore, Au-Pt-Pd/ TiO_2 also performed poorly under base free conditions, even at high temperatures. In terms of selectivity, Au containing catalysts displayed higher C3 selectivity compared to Pd-Pt/TiO_2.

2.2.3. Effect of support

2.2.3.1 Carbon supports

Although unsupported Au nanoparticles may be able to achieve high catalytic activity for glycerol oxidation,[46, 80, 81] there are certain advantages to be realized when nanoparticles are immobilized onto a support. Supported nanoparticles have longer catalyst lives and can be recycled. Thus, they are more economical for industrial applications. They are also more stable compared to their respective sols and undergo a smaller degree of agglomeration during catalysis and storage. This is particularly important for structure sensitive reactions such as glycerol oxidation, as catalytically active species need to maintain their highly dispersed states to ensure that high catalytic activity is sustained throughout the reaction. Lastly, the properties of nanoparticles may be altered due to metal-support interactions. Tuning the metal-support

interaction may therefore be a way to mediate catalytic performance of supported nanoparticles.[82-85]

Support selection is based on a series of desirable characteristics: inertness, stability under reaction, regeneration conditions, adequate mechanical properties, appropriate physical form for the given reactor, high surface area, porosity and chemical nature.[86] For glycerol oxidation, carbon based supports have proven to be an enduring choice as they give rise to comparatively better catalytic activity than oxide supports.[32, 87-89] Nature of the carbon support affects activity of Au nanoparticles but has little influence on its selectivity.[89] Instead, selectivity is dependent on the size and nature of catalytic entities employed.[43] For instance, Au supported on activated carbon (Au/AC) achieved an estimated 6 times increase in TOF compared to Au supported on titanium dioxide (Au/TiO_2). However, no significant improvements in selectivity was observed. Additionally, fraction of micropores present in the carbon support and their structure could exert some influence over the resulting catalytic activity.[88] Activated carbon supports possessing a lower fraction of micropores exhibited higher activity for glycerol oxidation. This may be due to the shielding effect experienced by smaller nanoparticles as a result of being embedded within the micropores.

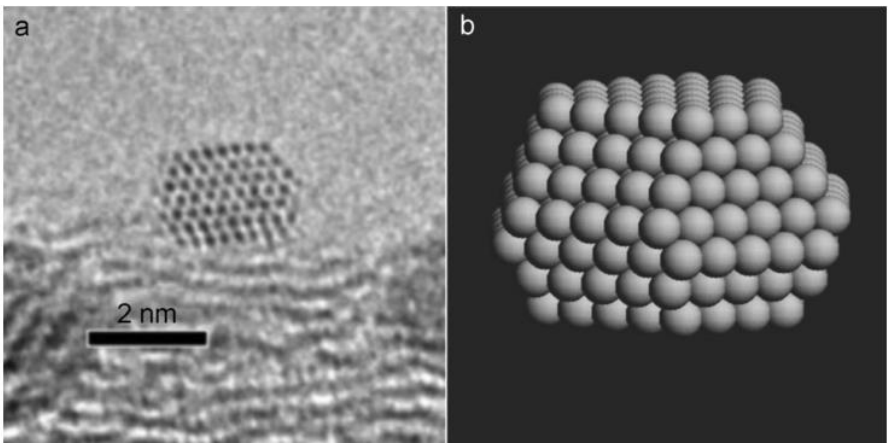

Fig. 2.4. Aberration-corrected HRTEM images of Au particles supported on highly graphitized CNF support. a) A representative 2–4 nm particle with (111) surface epitaxially parallel to the graphitic layer of CNF. b) Structure model derived from the image in part a. Reprinted with permission from ref 56. Copyright John Wiley and Sons.

Degree of graphitization[90] and crystallinity[91] are other key considerations that should be taken into account when selecting a carbon support. A high degree of graphitization provides many anchor sites for the formation of small, highly dispersed Au nanoparticles while high crystallinity ensures that a large fraction of these graphitic edges are exposed in an orderly manner. For example, Au supported on highly crystalline supports such as graphite (Au/G) demonstrated higher glycerol oxidation activity than when supported on poorly crystalline carbon supports like activated carbon (Au/AC) and carbon nanofibers (Au/CNFS). Significant nanoparticle agglomeration was also observed with Au/CNFS. On the other hand, Au/G was more selective towards C3 oxidation products (glyceric acid and hydroxypyruvic acid) while Au/CNFs and Au/AC exhibited high selectivity towards glycolic acid.[92] Surprisingly, while carbon nanospheres (CNS) possessed even poorer crystallinity compared to CNF, Au/CNS exhibited comparable performance with Au/G. CNS consists of graphene sheets in the form of waving flakes that follow the curvature of the sphere. These graphitic flakes in turn provide reactive "dangling bonds" which have been proposed to enhance surface reactions.[93]

Crystallinity of CNFS may determine the orientation in which Au nanoparticles are immobilized onto the support and this in turn impacts its catalytic performance.[94] Highly ordered graphitic layers on the CNF surface (Au/CNFs-LHT) led to preferential immobilization of Au on its (111) plane, exhibiting more facet area (Fig. 2.4). In comparison, disordered CNF surfaces (Au/CNFs-PS) led to random orientation of supported nanoparticles. Au/CNFs-LHT and Au/CNFs-PS possess similar particle sizes and thus exhibit similar TOF values. However, Au/CNFs-LHT was 34% less selective to glyceric acid and 20% more selective to formic acidcompared to Au/CNFs-PS and Au/C, both of which shared similar product distributions. Poor glyceric acid selectivity of Au/CNFs-LHT suggests that exposure of low index Au surfaces in Au/CNFs-LHT likely promoted C-C bond cleavage.

2.2.3.2. Oxide Supports

2.2.3.2.1. Influence of basic/acidic nature of oxide supports

Oxide supported nanoparticles tend to exhibit poorer catalytic activity for glycerol oxidation compared to carbon supported nanoparticles. However, the use of oxide supports has engendered significant improvements in C3 selectivity even under base free conditions and ambient temperature.[77]

Product distribution and/or C3 selectivity of oxide supported nanoparticles can be tuned by modifying the acidic/basic nature of the oxide supports.[95] Basic supports tend to result in higher catalytic activity compared to acidic supports under base free conditions.[96] Glycerol oxidation proceeds via oxidative dehydrogenation and basic supports enhance β-hydride abstraction, which is the rate limiting step.[97] In terms of product distribution, acidic supports favour high selectivity towards glyceraldehyde whilst basic supports promote its sequential oxidation to glyceric acid, tartronic acid and other C2 and C1 side products. Basic sites also bind strongly to the glycerol oxidation products and prevented their desorption until complete conversion to CO_2.[98] As such, basic supports also observed lower mass balance. Sequential oxidation of glyceric acid to over oxidation products can also be inhibited by doping the strongly basic sites with a weak base.[98]

In particular, acidic nature and strength of different oxide supports (SiO_2, MCM-41, H-mordenite, sulfated ZrO_2 (S-ZrO_2) was found to influence catalytic performance of supported AuPt nanoparticles for glycerol oxidation under base free conditions.[99] Total acid strength was the most significant factor in governing catalytic activity. More acidic supports resulted in lower catalytic activity. However, only Bronsted acid sites contributed to total acid strength while Lewis acid sites did not. On the other hand, selectivity to glyceraldehyde was enhanced with weakly acidic supports. Successive transformation of glyceraldehyde to glyceric acid proceeds via an acid catalyzed germinal diol formation and its dehydrogenation to a carboxylic

acid. Weaker acids only enable this process to a limited extent and thus favour the formation of glyceraldehyde.

Basic hydrotalcite (HT) was investigated as a support for glycerol oxidation.[75, 100] Catalytic performance of Pt/HT was linked to the degree of basicity of HT which influenced Pt nanoparticle size and thus, its final oxidation state. Basic strength of HT was tuned by varying its Mg/Al ratio.[101-105] Higher Mg/Al ratios led to more basic supports and larger Pt^0 nanoparticles.[104] Larger Pt^0 nanoparticles are less susceptible to oxidation when exposed to air and are better able to maintain their zero valent state. Since effective glycerol oxidation required more than 35% of the nanoparticles to exist as Pt^0, HT supports with higher basicity promoted enhanced catalytic activity. On another note, C3 selectivity of Au nanoparticles could be tuned by varying the Al/Mg ratios of crystalline $MgAl_2O_4$ spinel supports.[106] In general, $MgAl_2O_4$ supports possessing lower Al/Mg ratios were more selective to glyceric acid as the Al-rich surface promoted C – C bond cleavage. On the other hand, supports with similar Al/Mg ratios resulted in similar C3 selectivity, even if Au particle sizes differed.

2.2.3.2.2. Nickel oxide supports

While nickel based catalysts have been extensively investigated for glycerol steam reforming[107-111], their catalytic application towards glycerol oxidation is limited owing to poor catalytic performance[112]. However nickel oxide (NiO) based materials have shown some promise as supports for Au nanoparticles[113] during glycerol oxidation. In particular, Au nanoparticles supported on NiO nanoparticles (Au/nNiO) and NiO-TiO_2 mixed oxide supports (Au/NiO-TiO_2) demonstrated high catalytic performance for glycerol oxidation.[114] Amongst all the catalysts tested, Au/nNiO demonstrated the highest activity for glycerol oxidation under basic conditions. Although presence of TiO_2 in the support decreased activity by up to 3 times, there was a corresponding 20% improvement in selectivity to glyceric acid. Au was found to be preferentially deposited onto NiO in the NiO-TiO_2 supports. This indicated that the NiO

nano-crystalline thin sheets anchored and stabilized the Au nanoparticles. Improved glyceric acid selectivity presented by Au/NiO-TiO_2 was attributed to changes in its interaction with glycerol as opposed to changes in electronic structure of either oxide support or Au nanoparticles. Preferential confinement of Au on NiO likely introduced new interfaces in close proximity to the TiO_2. This in turn influenced diffusion and binding of reactants during the reaction.

2.2.3.2.3. Copper oxide supports

CuO supported Au nanoparticle (Au/CuO) catalyst are extremely selective for dihydroxyacetone under base free conditions.[115] 100% selectivity towards DHA could be obtained under the appropriate reaction conditions although glycerol conversion was only 1 %. However, reaction conditions could be further optimized to result in high DHA selectivity with high glycerol conversion. These results are significant as this is the first report identifying that supported Au catalysts can selectively oxidize the secondary alcohol group and the conditions under which they are able to do so. In contrast, when glycerol oxidation was carried out over Au/CuO in alkaline conditions, glyceric acid was once again the main oxidation product and dihydroxyacetone was not produced.

2.2.4. Influence of reactor design

Most of the experimental investigations discussed in this chapter were conducted in stainless steel autoclaves (semi-batch reactors)[116-118] or in glass reactors under optimized conditions. However, the results of these preliminary, small scale investigations might not translate well when the reaction is conducted under actual industrial conditions. In view of this, catalytic testing in alkaline membrane fuel cells and fixed bed reactors, enable a more realistic simulation of actual industrial conditions.[119]

Type of reactor employed influences both activity and selectivity. For example, supported PtBi catalysts in fixed bed reactors gave rise to higher glycerol conversion and DHA selectivity

when compared to semi-batch reactors.[120, 121] On the other hand, catalytic performance of Pt/C improved significantly when the reaction was carried out in a continuous flow electro-catalytic reactor instead of an electro-catalytic batch reactor.[122] Reactor design must also take into account reactor configuration which has a reported effect on product selectivity. For example, diacid (TA and/or OA) selectivity observed with Au/C is dependent on whether the reaction was carried out in a fixed bed or semi-batch reactor. [123, 124] TA selectivity was about 3 times higher when the reaction was carried out in a fixed bed reactor. Observed differences in selectivity were attributed to differences in flow rate and fluid volume. Additionally, Au on carbon coated monolith (Au/CM) was able to produce both dihydroxyacetone and glyceric acid when glycerol oxidation took place in a continuous flow structured reactor with mesoscale structured down flow slurry bubble column (SBCR) design.[125] However, only glyceric acid was observed when the reaction took place in a structured monolith reactor or autoclave. Production of dihydroxyacetone is attributed to higher oxygen availability in SBCR, which is in turn a result of enhanced interaction between bubbles and particles from meso-scale structuration.

2.2.5. Copper based catalysts

Catalytic performance of copper (Cu) based materials as catalysts or supports have been investigated for glycerol oxidation. Cu nanoparticles are attractive owing to their ability to catalyse glycerol oxidation under base free conditions. For example, 15-20 nm Cu(0) nanoparticles supported on ordered mesoporous cobalt monoxide (Cu/CoO) managed 86% glycerol conversion in the absence of base.[126] Cu/CoO favours the formation of C-C bond breaking products (glycolic acid, formic acid and CO_2) and these account for 75% - 95% of the total product distribution in all cases.

Cu has also been utilized as an additive to improve the catalytic performance of other materials for glycerol oxidation. For example, catalytic performance of MgAl layered double hydroxides

(LDH) improved after the addition of Cu.[127] Catalytic performance of CuMgAl was tuned by varying the amount of Cu. Increasing Cu content generally improved glycerol conversion and selectivity to glyceric acid until a maximum was reached. Calcination of CuMgAl was crucial to its high catalytic performance as different active species are present in the calcined and uncalcined samples. In the uncalcined sample, Cu existed as $Cu(OH)_2$. However, after calcination $Cu(OH)_2$ was oxidized to CuO. Since the calcined sample was more active than the uncalcined sample, it follows that Cu^{2+} existing in the form of $Cu(OH)_2$ was less active than Cu^{2+} present in the calcined mixed oxide sample.

CuNiAl hydrotalcites (HT) are moderately active and selective for glycerol oxidation under basic conditions although their catalytic performance does not exceed that of Au/C.[128] However, modifying CuNiAl HT with amino groups (CuNiAl-$C_5H_{10}N_2H_3$) resulted in improved glyceric acid selectivity and comparable glycerol conversion vis-à-vis Au/C. CuNiAl-$C_5H_{10}N_2H_3$ continued to be highly selective to glyceric acid even under base free conditions even though glycerol conversion decreased significantly. Synergistic effect of the Cu species, Lewis base sites and Bronsted base sites present on the hydrophobic surface of the CuNiAl-$C_5H_{10}N_2H_3$ catalysts contributed to its noteworthy catalytic performance.

AuCu alloys supported on niobium oxide (AuCu/Nb_2O_5) have also been investigated for glycerol oxidation.[129] Alloying Cu with Au resulted in elevated C-C bond breaking and glyceric acid selectivity exhibited by AuCu/Nb_2O_5 was between 20% - 30% lower than that of Au/Nb_2O_5. Additionally, there appeared to be very limited synergistic effect between Au and Cu when the alloy was supported on Nb_2O_5. Glycerol conversion attained by AuCu/Nb_2O_5 was only 11% higher than that of Au/Nb_2O_5 when the reaction was carried out at 60^{o}C while at 90^{o}C, both catalysts obtained comparable glycerol conversions.

2.3. Glycerol electro-oxidation

2.3.1. Mechanism

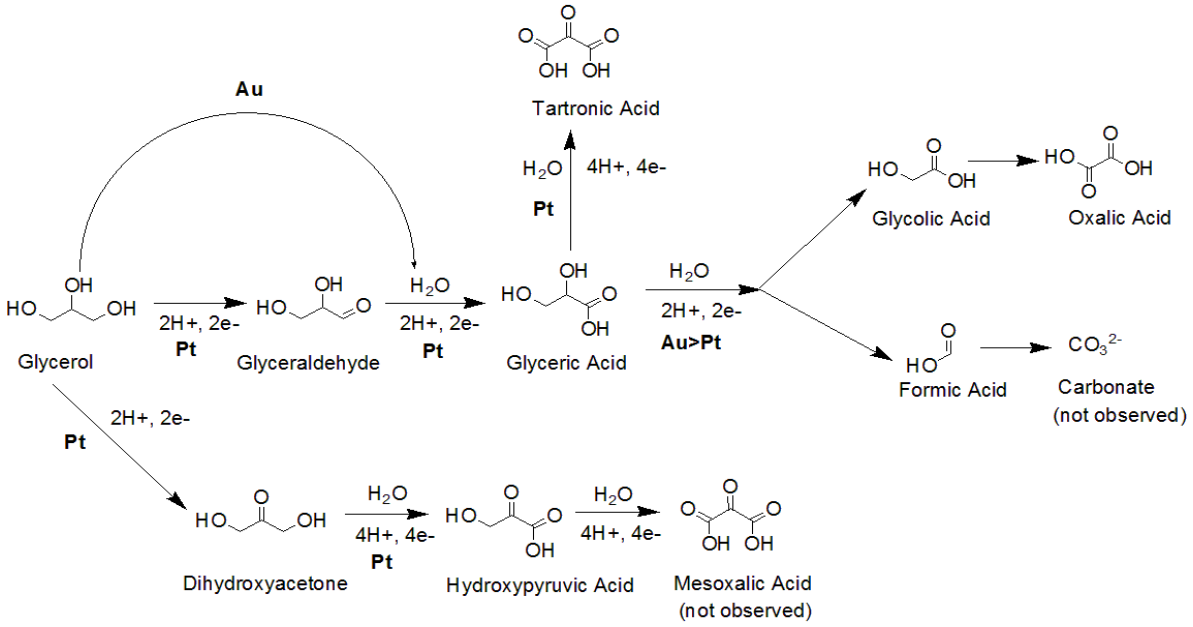

Scheme 2. The glycerol oxidation mechanism on Au and Pt electrodes in alkaline media under different pH conditions. Reprinted with permission from ref 84. Copyright John Wiley and Sons.

Koper and co-workers studied the mechanism of glycerol oxidation when the reaction was carried over Au and Pt electrodes under different pH conditions (Scheme 2).[130] Their studies were carried out by using a combination of cyclic voltammetry (CV) and high performance liquid chromatography (HPLC) that adopted a rapid online sample collection process with a modified micrometer-sized sample collecting tip.[131] All potentials reported for this work were measured with respect to the reversible hydrogen electrode (RHE).

The Pt electrode was active over the entire pH range. Furthermore, the glycerol oxidation pathway taken over the Pt electrode is essentially the same, regardless of pH. Pt electrode was most active under alkaline conditions and least active under acidic conditions. In terms of selectivity, glyceraldehyde was the dominant oxidation product generated over the Pt electrode. It was first obtained at low applied potentials and continued to be present throughout the entire potential range. Glyceraldehyde was subsequently converted to glyceric acid then glycolic acid,

formic acid and CO_2 as the applied potentials increased.[132] Interestingly, the PtO_x surface generated at high applied potentials appeared to be active for glycerol oxidation under neutral and acidic conditions but not in alkaline media. In neutral conditions, the PtO_x surface continued to generate glyceraldehyde even at higher applied potentials. However, the selectivity of PtO_x to glyceraldehyde was less than that of the clean Pt surface as glyceraldehyde was subsequently oxidized to glyceric acid and other side products. Under acidic conditions, the PtO_x surface facilitated high selectivity to formic acid and CO_2 at high applied potentials. Formic acid and CO_2 were generated via C-C bond breakage of glyceric acid and glycolic acid. To account for these observations, Koper and co-workers suggested that either the Pt surface at these high potentials was not fully oxidized to PtO_x in the presence of glycerol or that the high anodic potential makes PtO_x catalytically active. The secondary alcohol oxidation pathway was also observed at the Pt electrode over the entire pH range. Dihydroxyacetone and its corresponding oxidation product, hydroxypyruvic acid, were both detected in the reaction solutions. In addition, the acidic media was observed to be particularly favourable for secondary alcohol oxidation and under these conditions, the highest concentration of DHA was attained.

In contrast, the Au electrode was highly active for glycerol oxidation in alkaline media, especially at higher applied potentials, but inactive under acidic conditions. Under basic conditions, current density of the Au electrode at high applied potentials was nearly 10 times that of the Pt electrode. The higher activity of Au could be ascribed to its delayed surface oxidation compared to Pt; onset potential was 0.4 V and 0.8 V for Pt and Au respectively in alkaline media. Having said that, the Pt electrode was more active than the Au electrode in the potential region in which both electrodes were not covered by an oxide layer. Product distribution over the Au electrode was also significantly influenced by its onset potential. Glyceric acid instead of glyceraldehyde was detected as the main product. The acid

intermediate was then actively oxidized to glycolic acid and formic acid each with about 45% selectivity when applied potential was greater than 0.8 V. In contrast, only a small amount of glycolic acid and formic acid were observed over the Pt electrode in alkaline media; the main oxidation product derived from Pt was glyceric acid. These differences in product distribution and selectivity was ascribed to the wider potential range available for further oxidation over the Au electrode.

Pt was more active than Au for glycerol oxidation under neutral conditions and it exhibited a significantly higher current density. However, reaction kinetics for both electrodes are generally more sluggish under neutral conditions compared to alkaline conditions. The current density of glycerol oxidation on Pt and Au electrodes under neutral conditions was, respectively, 10 and 50 times lower than under alkaline conditions. These observations strongly suggest that OH^- promotes the glycerol oxidation and plays an important role of a proton acceptor or a reaction mediator, especially on an Au electrode.[133] Furthermore, glyceraldehyde was the only product observed over the Au electrode under neutral conditions. Small amounts of CO_2 were later detected by online electrochemical mass spectrometry. This indicated that some glycolic acid and formic acid were also produced but not detected. In line with these observations, Koper and co-workers subsequently showed that the presence of OH^- in solution accelerated C-C bond cleavage of glyceric acid to glycolic acid and formic acid, even in the absence of catalyst.[134] This stemmed from their observation that glyceraldehyde could independently convert to a range of products including glyceric acid, glycolic acid and formic acid, under alkaline conditions in the absence of Au (Fig. 2.5). The role that OH^- plays during the selective oxidation of alcohols in aqueous phase over supported metal catalysts was first investigated by Davis and co-workers (Fig. 2.6). Theoretical calculations revealed that the presence of surface bound hydroxide intermediates facilitated O-H bond activation of the alcohols via proton transfer in much the same way as it occurs in solution.

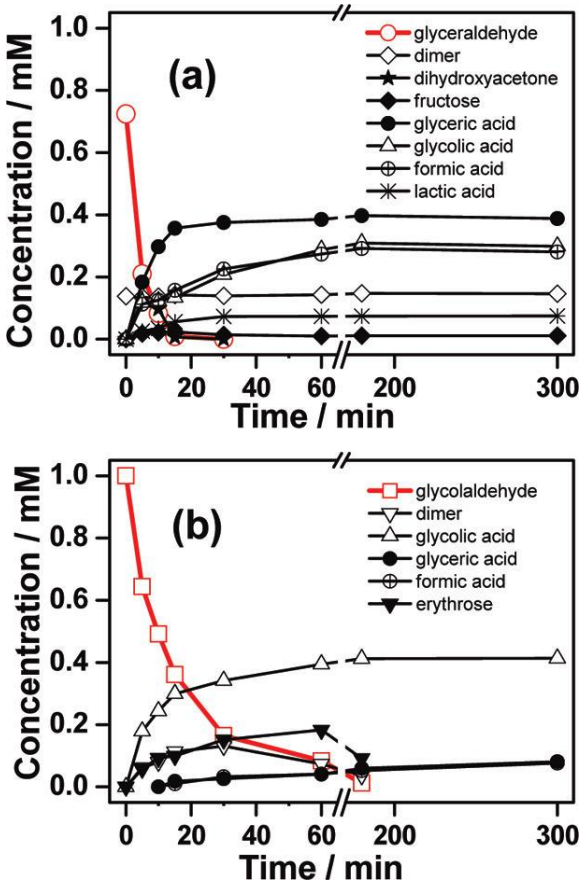

Fig. 2.5. Decomposition of (a) glyceraldehyde and (b) glycolaldehyde, the primary oxidation products of glycerol and ethylene glycol, respectively, in a nondeaerated O2-containing 0.1 M NaOH solution in the absence of gold, as determined by HPLC. Reprinted with permission from ref 88. Copyright ACS Publications.

Calculated activation barrier for the deprotonation process is very high and O-H bond activation by the metal alone is unlikely. However, the presence of adsorbed hydroxyl groups on the surface of Pt and Au significantly reduces the activation energy required for this rate limiting step. For instance, the calculated activation barriers for the dissociative adsorption of ethanol over the Au(111) and Pt(111) surfaces in water are 204 and 116 kJ mol^{-1} respectively. However, the presence of adsorbed hydroxyl intermediates was calculated to have lowered the activation barrier to 22 and 18 kJ mol^{-1} for Au(111) and Pt1(111) respectively. The resulting ethoxy anion species resulting from deprotonation is a highly reactive species and consequently forms the acetaldehyde product with ease.[135]

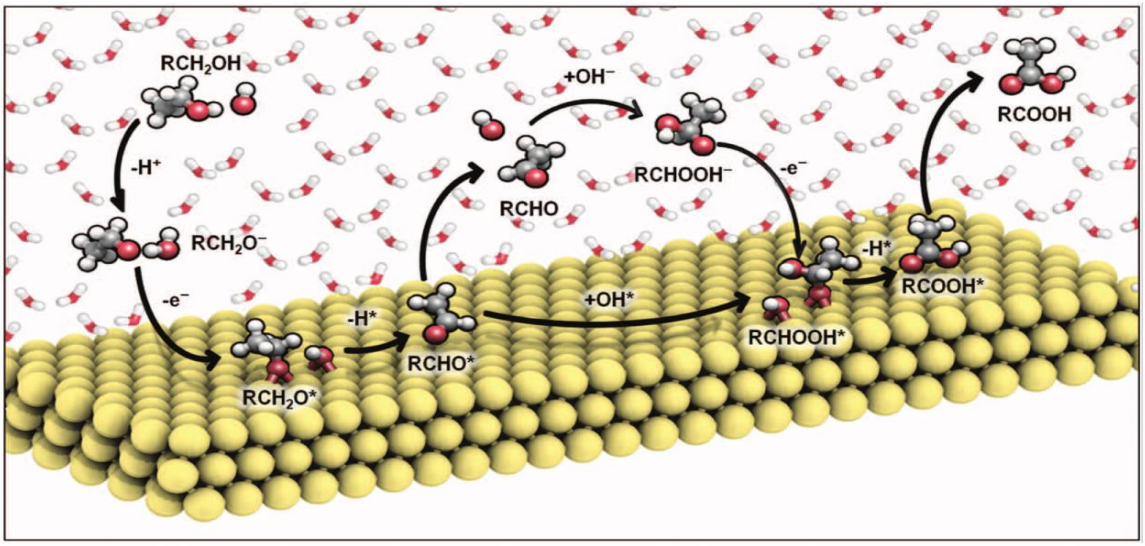

Fig. 2.6. Reaction scheme for the oxidation of alcohols to acids over Au surface in water at high pH. Reprinted with permission from ref 90. Copyright Nature Publishing Group.

Koper and co-workers later proved that the rate limiting deprotonation step is base catalysed and is facilitated solely by the added OH^- without the involvement of Au.[134] Moreover, the amount of base required to form the alkoxide intermediate is dependent on the pKa of the alcohol. Reactivity of the alcohol and its pKa share a Hamette type relationship such that alcohols with lower pKa values are more reactive. Glycerol and other sugar alcohols proved to have high oxidation activity at pH=11, corresponding to their low pKa values. In contrast, alcohols with a high pKa, such as isopropanol and isobutanol, were significantly less active. Both Koper and Davis's studies posited that the Pt and Au electrodes investigated only became involved during the β-hydride elimination step to form the aldehyde intermediate. The adsorbed hydroxide intermediates continued to lower the activation barrier for the subsequent activation of the C-H bond of the ensuing alkoxide intermediate to form the aldehyde over Au. However, for Pt, this step already has a very low barrier and it does not require further assistance from the adsorbed OH. Since OH^- in solution can independently facilitate further oxidation and C-C bond cleavage of glyceraldehyde to glyceric acid, glycolic acid and formic acid, it is possible to conclude that Au plays a limited role during the alcohol oxidation process. Having said that, importance of the interaction between Au and the adsorbed hydroxyl

intermediates during β-hydride elimination cannot be undermined. Some interaction of the alkoxide with the (hydroxylated) gold surface is still mandatory (Fig. 2.6).

2.3.2. Factors affecting catalytic performance

2.3.2.1. Effect of metal-support interactions

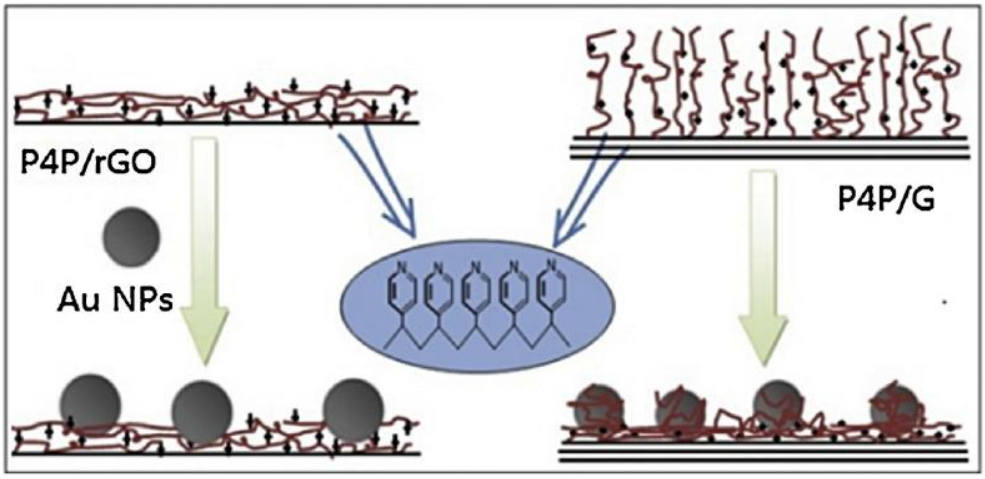

Fig. 2.7. The schematic drawing of the loading of Au NPs on P4P/rGO and P4P/G. Reprinted with permission from ref 91. Copyright Elsevier Publications.

Our group investigated the use of modified graphene supports to improve the catalytic performance of Au and Pd nanoparticles for glycerol electro-oxidation. In the first report, we prepared Au nanoparticles supported on poly(m-aminophenol) (Au-PmAP/G) and poly(4-vinylpyridine) (Au-P4P/G) functionalized graphene and compared their performance for glycerol oxidation against that of Au/C (Fig. 2.8).[136] Au-P4P/G possessed the highest electro-catalytic activity and current density. Our results demonstrated that metal-support interactions changed the electronic properties of Au nanoparticles and this in turn altered its C3 selectivity. Au-P4P/G was notably more selectivity to glyceric acid than Au-PmAP/G and Au/C, regardless of the applied potential used for glycerol electro-oxidation. High C3 selectivity observed with Au-P4P/G was attributed to the electron enrichment experienced by Au due to its interaction with the strongly electron donating pyridine groups present in the P4P chains. Conversely, the weakly electron donating –N= groups in PmAP brought about weaker metal-support

interaction. Thus, electronic enhancement experienced by Au was less significant and PmAP was not as effective in tuning Au selectivity.

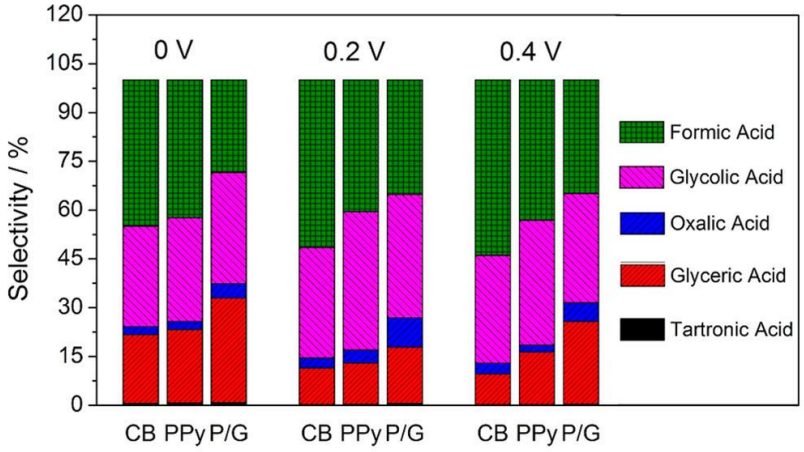

Fig. 2.8. Product selectivity of Pd NPs on different supports (CB, CNx, CNx/G) at various potentials. Reprinted with permission from ref 137. Copyright ACS Publications.

Next, Pd nanoparticles were supported on carbon nitride (Pd/CN_x) and carbon nitride modified graphene (Pd/CN_x-G). Catalytic performance of Pd/CN_x and Pd/CN_x-G for glycerol electro-oxidation were compared against Pd/C.[137] Metal-support interactions played a central role in governing the selectivity of Pd nanoparticles. Pd/CN_x-G gave rise to the highest C3 selectivity, owing to the comparatively smaller Pd nanoparticles (~4.4nm) present on the support (Fig. 2.8). On the other hand, despite its larger particle size, Pd/CN_x exhibited higher C3 selectivity than Pd/C. Interaction between Pd nanoparticles and nitrogen atoms present on CN_x likely altered the electronic properties[138, 139] of the former and weakened its absorption ability to C3 products, especially glyceric acid.

2.3.2.2. Advanced carbon materials as supports

Graphene[140-145] and carbon nanotubes[13, 146-149] (CNTS) based materials have emerged as a new class of carbon materials in recent years. Owing to their physicochemical and electrochemical properties par excellence, graphene and CNTS are widely applied as catalysts and supports.[150] As supports for glycerol oxidation[151, 152], graphene and carbon nanotubes (CNTS) based catalysts resulted in higher current densities and improved catalytic performance than when

supported on other types of carbon materials such as carbon black and activated carbon.[153-157]The superior electro-catalytic activity of the former is due to its good electrical conductivity and large electrochemical active surface areas which allows for better catalyst utilization. Furthermore, edges and defects on graphene and CNTS as well as their large surface areas enabled these supports to effectively anchor the metal nanoparticles and stabilize them. The as-prepared catalysts thus typically consist of small, uniformly dispersed nanoparticles which are highly active for glycerol oxidation.[158] The robust nature of these carbon supports also suggest that their high performance can be maintained even under harsh conditions, rendering them suitable for industrial applications.[159, 160]

Extensive research has also been carried out to modify graphene and CNTS to further improve catalytic performance. With respect to glycerol electro-oxidation, metal nanoparticles supported on multi-walled CNTS (MWCNTS) performed significantly when MWCNTS were functionalized with -COOH (MWCNT-COOH) rather than $–SO_3H$ (MWCNTS- SO_3H). Higher activity of MWCNT-COOH was due to its ability to form uniformly dispersed, small nanoparticles. MWCNT-COOH also possessed a higher electrochemically active surface area (EASA) than MWCNTS-SO_3H.[161]

San's and Shen's groups made use of the intrinsic properties of these carbon supports to immobilize CeO_2[162, 163] nanoclusters onto MWCNTS (CeO_2-MWCNTS)[164] and graphene nanosheets (CeO_2-GNS)[165] respectively. Immobilization helped stabilize the CeO_2 nanoclusters tend to agglomerate during preparation[166-168] and when subjected to electrochemical conditions[169-171]. Formation of CeO_2-MWCNTS and CeO_2-GNS enabled the subsequent deposition of small, uniformly dispersed Au and Pt nanoparticles respectively as the CeO_2 nanoclusters functioned as anchor site for the metal nanoparticles. Both Au/CeO_2-MWCNTS and Pt/CeO_2-graphene exhibited higher current density and significantly improved

durability when applied to glycerol electro-oxidation as compared to Au/MWCNTS and Pt/GNS respectively.

2.3.3. Effect of non-noble metals on Pt and Pd based catalysts

Co-catalysts are often used to improve the catalytic performance of noble metal catalysts for glycerol electro-oxidation. Employment of a co-catalyst, typically a non-noble metal, generally leads to significant improvements in electrochemical activity.[172, 173]

The promotional effect of Ni on the electrochemical activity of Pd and Pt has been previously reported. PdNi/C demonstrated improved reaction kinetics relative to Pd/C at low potentials.[174, 175] This was attributed to a bifunctional mechanism involving the transfer of OH^- species from the $Ni(OH)_2$ surface towards the adsorbed organic molecules close to the Pd surface where the reaction takes place. A larger forward peak current density and higher real surface activity, exchange current density, and i_f/i_r ratio was exhibited by Pt_2Ni/C relative to Pt/C. Enhanced electrochemical activities was attributed to the following characteristics in Pt_2Ni/C (1) modified lattice parameter of the Pt-Ni alloy might structurally favour the reaction (2) electronic modification with an increased Pt 5d band vacancy would electronically promote the reaction.[176]

On the other hand, when Pt was alloyed with Sb, the resulting PtSb/C catalyst was highly selectivity towards DHA (61.3% selectivity) at high conversion rates of 90.3% when the reaction was carried out under acidic conditions in an electro-catalytic reactor system.[177] In contrast, under the same conditions, Pt/C was highly selective to glyceraldehyde and glyceric acid. Little to no DHA was produced by Pt/C. PtSb/C was also significantly more active compared to Pt/C. Presence of Sb in Pt results in fewer intermediate residues accumulating on the catalyst surface during glycerol electro-oxidation. For Pt based catalysts, adsorption and accumulation of carbonaceous intermediates on the Pt surface is a common problem that eventually leads to catalyst deactivation. As such, presence of a co-catalyst not only altered the

reaction pathway but also prevented the active sites on Pt from being blocked. Similarly, the synergistic effect of Ru and Sn on PtRuSn ternary catalyst enabled complete oxidation of CO or CO-like poisonous species on Pt sites and prevented catalyst deactivation.[178] Addition of Ru and Sn also facilitated C-C bond cleavage and formic acid was the dominant product. Geometric environment of the fcc Pt crystallites was altered as a result of Ru and Sn addition. In particular, incorporation of larger Sn atoms into the PtRu lattice led to elongation of crystal structure, which in turn likely facilitated C–C and C–H cleavage. Additionally, Sn addition modifies the electronic environment of PtRuSn/C via electron transfer to Pt. This electronic modification weakens the bond between carbon atoms and surface Pt atoms. Furthermore, Sn oxides supply sufficient oxygen containing species of OH which facilitates removal of the adsorbed carbonaceous species.

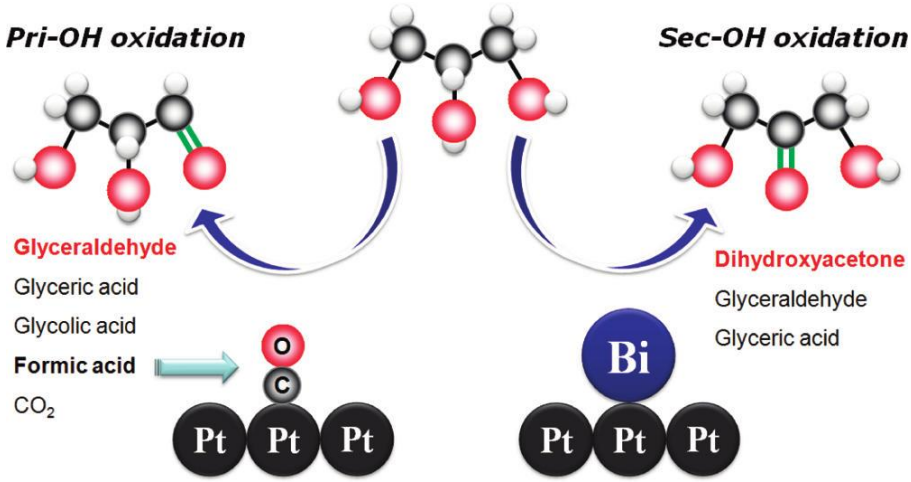

Fig. 2.9. Glycerol electro-oxidation over Pt (favours the primary oxidation pathway) and Pt containing reversibly adsorbed Bi (favours the secondary oxidation pathway). Reprinted with permission from ref 112. Copyright ACS Publications.

Inaya, Tsuto and their co-workers were the first to observe that the presence of Bi on the Pt nanoparticle surface greatly improved selectivity towards dihydroxyacetone (DHA).[179] When the reaction was carried out in a semi-batch reactor, a maximum of 20% DHA selectivity could be obtained with 1%Bi-5%Pt/C catalyst at 30% glycerol conversion. Conversely, 5%Pt/C only managed ~5% DHA selectivity at 40% conversion. The authors posited that the Bi adatoms function as site blockers on Pt(111) and their presence orientated the adsorbed glycerol

molecule in such a way that the secondary –OH group was positioned favourably for oxidation. In extension of this work, Koper and co-workers examined the relationship between Pt and Bi under electro-catalytic conditions (Fig. 2.9).[180] Specifically, they were interested in determining whether the irreversible or reversible adsorption of Bi onto Pt was more effective in achieving high DHA selectivity under acidic conditions. Reversibly adsorbed Bi on Pt/C was more effective in directing the reaction onto the secondary oxidation pathway, especially at low applied potentials; 100% selectivity to DHA was obtained at ~0.6V vs RHE (reversible hydrogen electrode). At higher applied potentials. Bi underwent oxidative desorption from the electrode. High Bi surface coverage was necessitated for enhanced selectivity to DHA, failing which a significant increase in glyceric acid selectivity was observed. The interaction between Bi and the two primary alcohol groups on glycerol might play a role in increasing DHA selectivity. However, the presence of Bi in solution for reversible adsorption lowered current density and activities relative to Pt/C.

Kim and co-workers also examined the catalytic performance of carbon supported PtBi alloys in an electro-catalytic reactor, under acidic conditions with heating.[177] They determined that product distribution was highly dependent on the electrode potential and nature of the catalyst. In particular, applied potential influenced the nature of the species present on the catalyst surface and altered its catalytic activity. PtBi/C was highly selective to DHA at low potentials. However, at higher applied potentials, selectivity to DHA decreased as Bi oxidized to form Bi oxide/hydroxide species, which are not selective to DHA.

Subsequently, Koper and co-workers extended their study to determine the effect of antimony (Sb), tin (Pb), lead (Sn) and indium (In) adatoms on Pt/C.[181] Irreversible adsorption of Sb onto Pt/C achieved 80% DHA selectivity at lower potentials (0.35–0.55V vs RHE). Yet despite its promising performance, Sb was still less efficient than Bi bringing about 100% DHA selectivity.

In contrast, Pb, Sn and In did not manage to steer the reaction pathway from primary to secondary oxidation. Glyceric acid was the main oxidation product obtained. Poor DHA selectivity was attributed to their incomplete adsorption onto Pt/C. As mentioned above, high surface coverage of the adatom is a necessary pre-condition for high activity.

2.3.4. Effect of non-noble metals on Au based catalysts

The promotional effect of co-catalysts on the catalytic performance of Au has also been reported. For instance, the effect of RuO_2 on Au was studied by dispersing Au onto preformed RuO_2/C.[182] However, there appears to be limited synergistic interaction between RuO_2 and Au. Although RuO_2 promoted Au catalyst was more stable than the un-promoted catalyst, RuO_2 reduced the electrochemically active surface area of Au and decreased maximum current density. Furthermore, presence of RuO_2 also did not alter the product distribution and glycerol conversion values of Au/C.

In comparison, C-C-C bond breakage was favoured when Au was alloyed with Au (AgAu/C). favoured the formation of formic acid.[183, 184] The impact of Ag on the glycerol electro-oxidation over AuAg/C was likely driven by electronic modifications and Ag segregation on the catalysts surface. Presence of Ag also enhanced the electrochemical activity of Au/C, resulting in decreased onset potential and higher current density during chronoamperometry.[184]

2.3.5. Glycerol electro-oxidation in alkaline membrane fuel cells

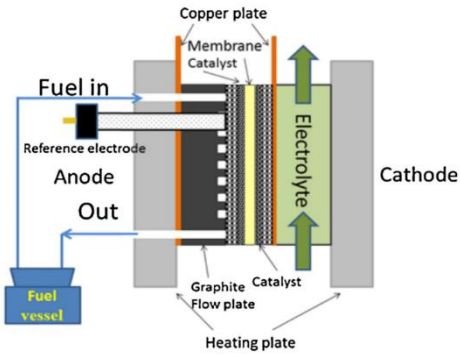

Fig. 2.10. Schematic illustration of the anion exchange membrane-based fuel electro-catalytic flow reactor. Reprinted with permission from ref 116. Copyright Elsevier Publications.

Catalytic performance of supported Au[185-187], Pd[188] and Pt[119] based catalysts for glycerol oxidation in direct alcohol alkaline membrane fuel cells (DAFC) was extensively investigated by Li and co-workers (Fig. 2.10). Catalytic performance is generally dependent on the following (1) applied potential (2) catalyst loading (3) concentration of base (4) concentration of glycerol (5) catalyst preparation method. Most importantly, high selectivity to either mesoxalic acid[160] or tartronic acid[185] could be achieved by when glycerol oxidation was carried out in DAFCs. For example, 69.3% selectivity to tartronic acid could be attained at 89.2% glycerol conversion when glycerol oxidation is carried out over Au/C catalysts in DAFC for 12 h. 1527 J of energy was released during this process.

Selectivity to mesoxalic acid and tartronic acid could be further optimized by tuning the applied potential. Furthemore, a thick electrode layer is particularly favourable for the generation of TA and MA. Electrode thickness alters the rate at which reactants and products diffuse out of the catalyst layer. This in turn affects the concentration profiles of reactants and reaction intermediates available inside the electrocatalytically active region. Thicker porous electrodes likely facilitate deeper oxidation of the intermediates by holding them within the confined electrolyte volume for longer periods of time. At the same time, glycerol is held outside of the electrocatalytically active region. Electrode thickness can be tuned by adjusting the metal loading or by changing the catalyst amount. Notably, Au/C catalysts with loadings of 5mg cm^{-2} afforded 46% selectivity to mesoxalic acid at an applied potential of 0.3 V (anode overpotential of 0.531 V). In comparison, when catalyst loading was reduced to 1mg cm^{-2}, Au/C was more selective to tartronic acid (39% selectivity) but less selective to mesoxalic acid (19% selectivity), at the same applied potential. These results are significant because despite strong commercial interest, mesoxalic acid has never been reported as a major product from the direct oxidation of glycerol, when the reaction was carried out in half cells or semi-batch reactors.[189-191] Currently, the most effective way to derive MA from glycerol is via a 2 step

oxidation method using 2 different catalysts. Glycerol is first converted to TA before it is further oxidized to MA, typically using a conventional Pt-Bi based catalyst. As such, DAFCs thus represent a highly promising route to sustainable electro-catalytic conversion of biorenewable intermediates to chemicals along with electricity cogeneration.

2.4. Summary of chapter 2

	Platinum group catalysts	
Advantages	1. Active under base free conditions ⇨ Oxidation products do not need to undergo additional neutralization and acidification steps to obtain the free acid 2. With the use of Bi promoters in conjunction with Pt nanoparticles, DHA can be produced with extremely high selectivity.	
Disadvantages	1. High temperatures and a low partial pressure of oxygen required in order to stabilize the catalytically active Pt^0 species and prevent oxygen poisoning 2. Highly susceptible to poisoning by by-products or adventitious species 3. Strongly coordinated products generated in-situ may lead to reversible metal dissolution–precipitation	
Size dependency	- $\geqslant$ 6 nm : less active but more selective to glyceric acid - $\leqslant$ 6 nm : more active but less selective to glyceric acid	
Basic conditions	- Activity is significantly higher under alkaline conditions - Glycerate as the primary product	
Base free or acidic conditions	- Active under acidic conditions but reaction occurs rather sluggishly - Glyceraldehyde is the major product	
Selectivity is dependent on applied voltage	- Between 0.4 and 1.0 V (vs. RHE): glyceraldehyde as the dominant product without apparent C–C bond cleavage - Above 1 V: PtO_x activates C-C bond cleavage to form mainly glycolic acid, formic acid and CO_2	
Effect of non-noble metal dopants on selectivity	Bi	- Incorporation or irreversible adsorption of Bi onto Pt/C significantly improves selectivity of Pt/C to DHA. ⇨ Bi blocks primary oxidation pathway and provides a specific Pt−Bi surface site poised for secondary alcohol oxidation.
	Sb, Sn, Pb, In	- Depending on mode of adsorption (reversible or irreversible), Sn, Pb and In either blocks the glycerol oxidation pathway or has no effect in altering the oxidation pathway from primary to secondary. - Irreversible adsorption of Sb onto Pt/C improves DHA selectivity and electro-catalytic activity. ⇨ Selectivity is surface coverage dependent. A constant and high adatom surface coverage is required to maintain high DHA selectivity over time

Effect of alloying Pt with non-noble metals	Ni	Significantly improves electro-catalytic activity due to 1) modified lattice parameter which might structurally favour the reaction (2) electronic modification with an increased Pt 5d band vacancy
	Cu	- Improves conversion and glyceric acid selectivity under base free conditions - Increased resistance to oxygen and by-product poisoning compared to Pt/C - Cu presumably helps facilitate the initial dehydrogenation step of glycerol oxidation
	Sb and Bi	- Sb homogenously entered into the lattice of Pt whilst Pt nanoparticles are wrapped by a layer of $B_{i2}O_2CO_3$ - Overall, PtSb/MWCNTs is more selective for DHA compared to PtBi/MWCNTs ⇨ (1) Sb acts as a semiconductor which may be an appropriate promoter of Pt that hinders further oxidation of DHA (2) Sb atom is a more efficient site blocker compared to Bi (3) Homogenously dispersed PtSb is less active for the further oxidation of dihydroxyacetone. At the same time, higher selectivity of PtSb/MWCNTs to Glyceric acid may contribute to higher DHA selectivity. Glyceric acid favours inhibition of active sites which are predominantly responsible for the further oxidation of DHA.
	Sn	- Improved conversion and TOF; glyceric acid is the major product ⇨ Enhancement of activity attributed to activation of oxygen molecules and/or deprotonation of hydroxyl group by surface SnO species - Besides improved electro-catalytic activity, synergistic effect of both Ru and Sn in PtRuSn/C enables efficient removal of CO or CO-like carbonaceous intermediate species and prevent poisoning of active Pt sites.

	Gold based catalysts
Advantages	1. Highly active under basic conditions 2. More stable and more resistant to oxidation compared to Pt group catalysts due to the inert nature of Au 3. Higher tolerance towards poisoning chemical groups such as aliphatic and aromatic amines 4. When used in direct glycerol alkaline membrane fuel cells, deactivation caused by ternary ammoniums can be reduced by optimizing the types of quaternary ammonium functional groups present in the anion exchange membrane. Poisoning ternary ammonium groups can also be easily removed via washing. 5. More selective than Pt/Pd based catalysts due to ability to discriminate between different chemical groups and geometrical positions 6. Au electrodes exhibit higher current density than Pt electrodes at higher applied potentials. Higher activity of Au is due to its delayed surface oxidation compared to Pt, which thus allows for the application of higher effective overpotentials.
Disadvantages	1. OH^- ions are necessary for activity. DFT calculations also show that OH^- catalyses the rate determining, primary H-abstraction, step during the reaction. Thus, it remains unclear whether OH^- ions or Au are the 'true' catalyst. 2. OH^- catalyses C-C bond breakage and the generation of C1 and C2 side products are inevitable 3. Oxidation products need to undergo additional neutralization and acidification steps to obtain the free acid after the reaction.
Size dependency	- In general, larger Au nanoparticles (average diameter $\geqslant$ 20 nm) are more selective for glyceric acid but smaller Au nanoparticles (average diameter < 20 nm) are more active for glycerol oxidation. - Carbon based supports: optimal particle size between 7 to 8 nm due to shielding effect of smaller nanoparticles by the support. - Oxide supports: activity increases with decreasing particle size
Basic conditions	- Most active under basic conditions. - Glycerate generally obtained as the primary product. - No evidence that Au nanoparticles can generate secondary oxidation products.
Base free conditions	- Generally inactive under base free conditions - Exceptions: 1. Au/H-mordenite, which shows some activity (5% conversion) under base free conditions. Activity is further improved when Au is alloyed with Pt.
Selectivity dependent on	- High applied potentials (after 0.85 V vs RHE) favours C-C bond cleavage and an increase in glycolic acid and formic acid selectivity.

applied potentials	- Mild applied potentials (between 0.4 – 0.8 V vs RHE) favours glyceric acid
Effect of catalyst preparation method	Advantages of sol immobilization over deposition precipitation: 1. Smaller nanoparticles, narrower size dispersion, good surface exposition and high dispersion. 2. Resulting nanoparticles exhibit greater tolerance towards poisoning amine groups 3. Reducing reaction temperature and tuning the ethanol:water ratio of the solvent system can produce ultra-small gold nanoparticles which demonstrate extremely high activity for glycerol oxidation Effect of PVA protecting agent: 1. Amount of PVA to Au precursor influences size and dispersion ⇨ Higher PVA to Au precursor ratio results in smaller particle sizes and narrower particle distribution ⇨ However, with excess PVA, immobilization of the Au nanoparticles onto the support is more difficult, leading to partial aggregation and coalescence of Au.
Effect of promoters	- Oxides (Co_3O_4, NiO, Mn_3O_4, MgO) promote glycerol oxidation over Au by negatively shifting the onset potential - But their effect on selectivity of Au and electrochemical activity remains unclear
Impact of non-noble catalysts on Au	- Effect of alloying Au with non-noble metals has been less extensively studied compared to alloying Au with Pd and Pt - There is little to no synergistic effect between Au and Ru_2O - AuCu alloys also showed little to no synergistic effect when supported on Nb_2O_5 - AuAg is highly selective to formic acid and glycolic acid although these catalysts tend to suffer from very poor electrochemical performance
Carbon based supports	- In general, carbon supported nanoparticles are more active than oxide supported nanoparticles for glycerol oxidation - On carbon, glycerol oxidation is optimized for nanoparticles around 8nm in diameter as smaller nanoparticles are partially shielded within the pores of the support. Nature of carbon support affects catalytic performance. Key properties which influence catalytic performance are: 1. Degree of graphitization 2. Degree of crystallinity 3. Fraction and structure of micropores
Oxide supports	Tune catalytic performance by tuning acidity/basicity of supports

	1. Acidic supports give rise to higher C3 activity than basic supports and favour formation of glyceraldehyde ⇨ Higher activity favoured with more acidic supports whilst selectivity was enhanced with weakly acidic supports ⇨ Only Bronsted acid sites contribute towards total acid strength 2. Basic supports promote sequential oxidation of glyceraldehyde to glyceric acid, tartronic acid and other C2 and C1 side products. ⇨ Reduce over-oxidation to CO_2 by doping strongly basic sites with weaker base 3. Basic supports result in higher activity compared to acidic supports especially under base free conditions, due to their ability to enhance the β-hydride abstraction, rate limiting step
Optimizing catalytic performance	Glycerol oxidation over Au based catalysts can be optimized by tuning the following reaction conditions: 1. NaOH : glycerol ratio 2. Catalyst loading: high catalyst loading (i.e. high catalyst to glycerol ratio) facilitates deeper oxidation instead of C-C bond cleavage 3. Use of alkaline earth oxides, BaO and CaO, as pH modifiers improves selectivity to glyceric acid which is stabilized by the formation of glyceric acid hemicalcium salts 4. Controlling applied potential: deeper oxidation products such as mesoxalic acid and tartronic acid are optimized when reaction occurs under a mild potential range (0.4–0.7 V vs. SHE)

	Copper based catalysts
	- Cu based catalysts like Cu nanoparticles, CuNiAl hydrotalcites and CuMgAl demonstrated high catalytic performance for glycerol oxidation - CuNiAl hydrotalcites and CuMgAl were also highly selective for glyceric acid - Cu based catalysts have yet to be tested for glycerol electro-oxidation

	Bimetallic catalysts (supported AuPd and AuPt catalysts)
Advantages over monometallic catalysts	1. Enhanced glycerol conversion 2. Improved selectivity to glyceric acid 3. Improved catalyst stability 4. Alloying Pd and Pt with Au increases their resistance to oxygen poisoning 5. MgO and H-mordenite supported AuPt catalyst possess the ability to carry out glycerol oxidation under base-free conditions

From the literature review conducted, it was determined that:

1. Au based catalysts catalyse glycerol (electro)-oxidation more effectively than platinum group based catalysts. The former leads to improved catalytic performance and greater resistance to oxidative poisoning compared to the latter.
2. For Au based catalysts, support effect, size effect, effect of reaction conditions, effect of preparation methods, effect of alloying with platinum group metals are 5 key areas which have been extensively researched on.
3. Effect of non-noble metal promoters has been relatively well studied for Pt group catalysts. Bi is arguably the most effective promoter for Pt. Bi adatoms function as site blockers on Pt (111) and their presence orientates the adsorbed glycerol molecule in such a way that the secondary –OH group is positioned favourably for oxidation. With respect to glycerol electro-oxidation, reversible adsorption of Bi on Pt/C enabled 100% selectivity to DHA at low applied potential. Importantly, the authors determined that high surface coverage was necessitated for high DHA selectivity. At higher applied potentials, Bi underwent oxidative desorption from the electrode and this resulted in a significant increase in glyceric acid selectivity.
4. In comparison, the effect of non-noble metals on the catalytic performance of Au/CB has received far less attention. Non-noble metals can interact with Au/C when alloyed together or as promoters. Addition of oxides (Co_3O_4, NiO, Mn_3O_4 and MgO) to Au/C promoted its catalytic activity and stability by negatively shifting onset potential during glycerol electro-oxidation.[192] However, the effect oxide addition on Au/C's selectivity and electrochemical activity over a wider range of applied potentials was not determined.

As such, this thesis will focus on understanding how non-noble metal promoters (Cu, Ni an Ag) affect the catalytic performance of Au/C for glycerol electro-oxidation. Au-promoter

interaction was examined by irreversibly adsorbing the promoters onto Au/C via in-situ electro-deposition. This method was chosen as it best ensures a constant and full surface coverage during our long reaction time of 2 h. Following this, the resulting catalyst is then tested for glycerol electro-oxidation in alkaline medium under a range of applied potentials.

Chapter 3

Cu modified carbon supported Au nanoparticles as highly selective catalysts for glycerol electro-oxidation in alkaline solution

3.1. Introduction

Several strategies have been developed to improve catalytic selectivity during glycerol oxidation. One approach is via the use mediators and adatoms. For instance, when Ciriminna and co-workers employed radical TEMPO catalyst (2,2,6,6- tetramethylpiperidine-1-oxyl) for glycerol oxidation under different conditions, moderate DHA selectivity[193] and high MA selectivity[6] could be independently obtained. On the other hand, Kwon and co-workers investigated the ability of adatoms – Bi,[180] Sn, Sb, In, As, Pb[181] – to mediate the selectivity of Pt/C catalysts for glycerol oxidation. Reversibly adsorbed Bi on Pt/C was most effective in completely blocking the active sites for primary alcohol oxidation. Presence of reversibly adsorbed Bi in conjunction with electrochemical control, resulted in 100% DHA selectivity over Pt/C.

Another approach is via tuning the nature of support.[98-100, 106, 114] Nature of support influences the metal-support interaction which in turn affects catalytic performance. For example, our group observed that Pd nanoparticles generated on carbon nitride/graphene support (Pd-CN_x/G) showed improved C3 selectivity relative to Pd/C and Pd-CN_x due to smaller Pd particle sizes obtained during synthesis. Additionally, strong interaction between Pd and nitride groups on the CN_x surface likely altered the electronic properties of Pd and weakened its adsorption ability toward C3 products, especially glyceric acid.[137]

The use of bimetallic nanocomposites is also a commonly employed strategy to improve the performance of Au nanoparticles.[52, 53] In particular, synergistic interaction between Au and Cu or Cu oxides has resulted in catalysts that are highly activity and/or selective for glycerol oxidation.[115, 127, 129] However, in those reports, glycerol oxidation was carried out in autoclave reactors under high pressure and temperature.

Herein, we demonstrate that the C3 selectivity of carbon supported Au nanoparticles (Au/C) for glycerol electro-oxidation under alkaline conditions is enhanced by the presence of electro-deposited Cu species on the Au surface. To the best of our knowledge, this is the first article showing that the selectivity of Au nanoparticles for glycerol electro-oxidation can be improved by its interaction with electro-deposited metal and/or metal oxide species present on the Au surface. C3 selectivity could be further tuned by optimizing Cu electro-deposition potential and time.

3.2. Experimental

3.2.1. Synthesis of 4nm Au nanoparticles supported on carbon black

1 ml 1% $HAuCl_4 \cdot 3H_2O$ was added to 100 ml DI water and the solution was stirred vigorously for 1 min before adding 1 ml 1% sodium citrate solution. After an additional 1 min of vigorous stirring, 1 ml freshly prepared, ice cold 0.075% $NaBH_4$ in 1% sodium citrate was quickly added and the solution stirred for another 5 min before storage at 4 ^oC. Then, an appropriate amount of aqueous carbon black dispersion and Au nanoparticle solution were mixed under ultrasonication for 1 h and stirred overnight. After 24 h, pH of the solution was adjusted to below 2 by using 0.2 M HCl and the further stirred for another hour. Finally, the product was filtered, washed three times with copious amounts of DI water and methanol then dried below 80 ^oC.

3.2.2. Electrochemical Characterization

All electrochemical tests were carried out at room temperature in a conventional three-electrode cell using a Princeton Applied Research VMP2 multichannel potentiostat. Our three electrodes cell consisted of Pt wire counter electrode, Ag/AgCl (sat KCl) reference electrode and carbon cloth (CC, 1.5 × 1.5 cm^2, Gashub) working electrode. All applied potentials are reported with respect to the Ag/AgCl reference electrode.

3.2.3. Preparation of CC working electrode

~2.4 mg of the catalyst was dispersed in 1 mL of ethanol and 0.5 mL of 0.05 wt.% Nafion solution via ultrasonication. This dispersion was drop cast onto CC to prepare a sample with a loading of ~1.07 mg cm^{-2}. The electrodes were dried overnight under ambient conditions.

3.2.4. Cu electro-deposition process

Au/C was first cycled 20 times in 0.2 M NaOH to improve wettability of the hydrophobic carbon cloth. The electrodes were then immersed in a stock solution containing 50 mM $CuSO_4.5H_2O$ in 0.1 M Na_2SO_4 and held under constant potential. The electrodes were then rinsed thoroughly in DI water before being cycled 30 times in 0.2 M NaOH solution to ensure catalytic stability. The as-prepared electrodes were tested for glycerol electro-oxidation by placing them in 26 mL of 0.5 M NaOH + 0.5 M glycerol solution under constant potential for 2 h. Subsequently, 1 mL of the solution was collected for high-performance liquid chromatography (HPLC) analysis.

3.2.5. Characterization with XPS and XRD

X-ray photoelectron spectroscopy (XPS) data were collected with a Theta Probe electron spectrometer (ESCA-Lab-200i-XL, Thermo Scientific). X-ray diffraction (XRD) patterns were collected by Bruker D2 Phaser. The as prepared carbon cloth electrodes were directly utilized for XPS and XRD analysis without further modification

3.2.6. Chromatographic Analysis of Products

The obtained products were analysed using a Biorad HPX-87H Aminex column for high-performance liquid chromatography (HPLC, Agilent 1260 Infinity). The eluent was 4 mM sulfuric acid. During the test, 20 μL of the sample was injected into the column which was maintained at 65 °C. Eluent flow rate was 0.2 mL min^{-1}. Both refractive index (RID) and UV-VIS detectors were used to analyse the results. Standard solutions of the various oxidation products were also analysed under the same conditions to produce the calibration

3.3. Results and Discussion

3.3.1. TEM Characterization

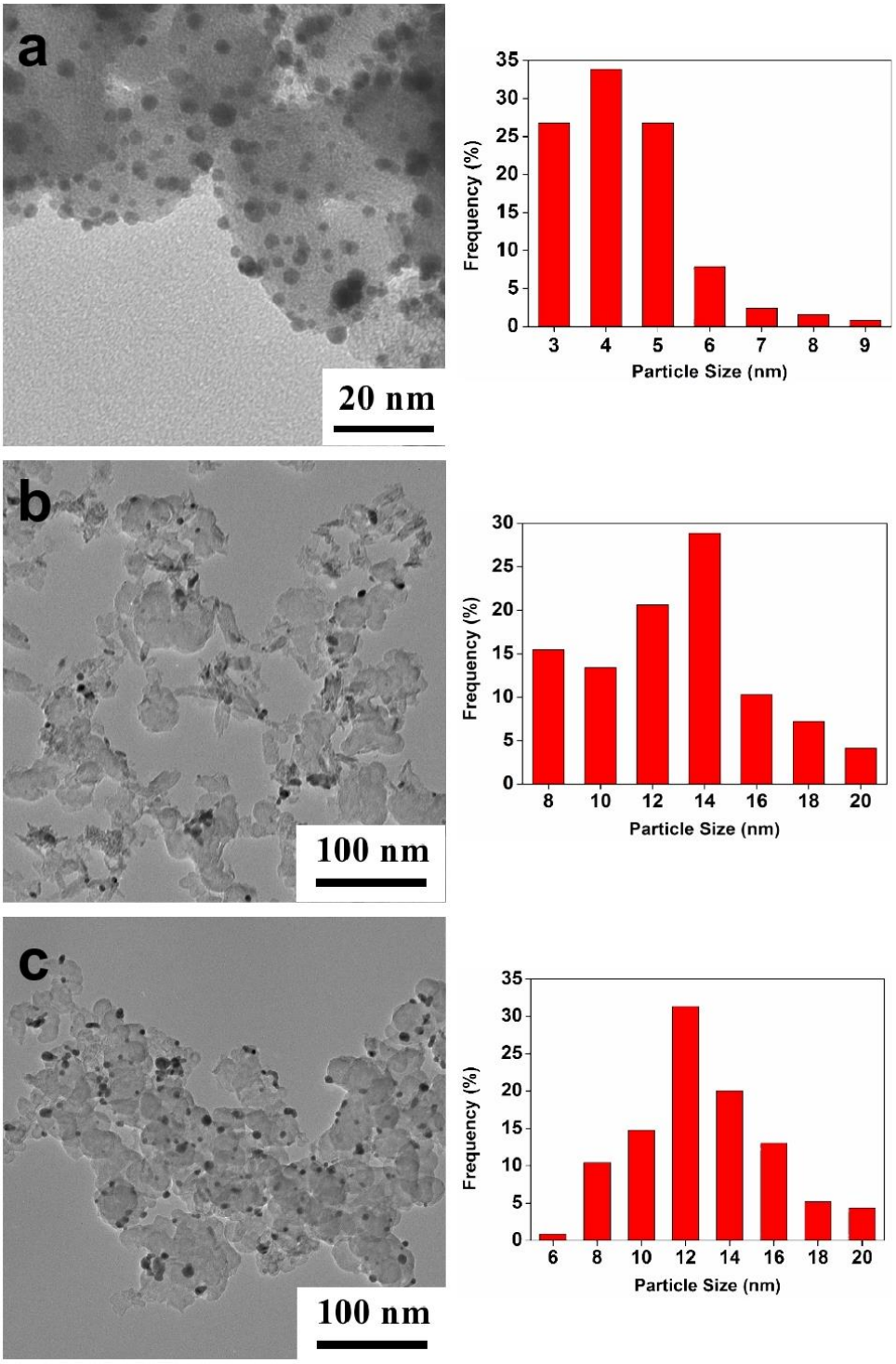

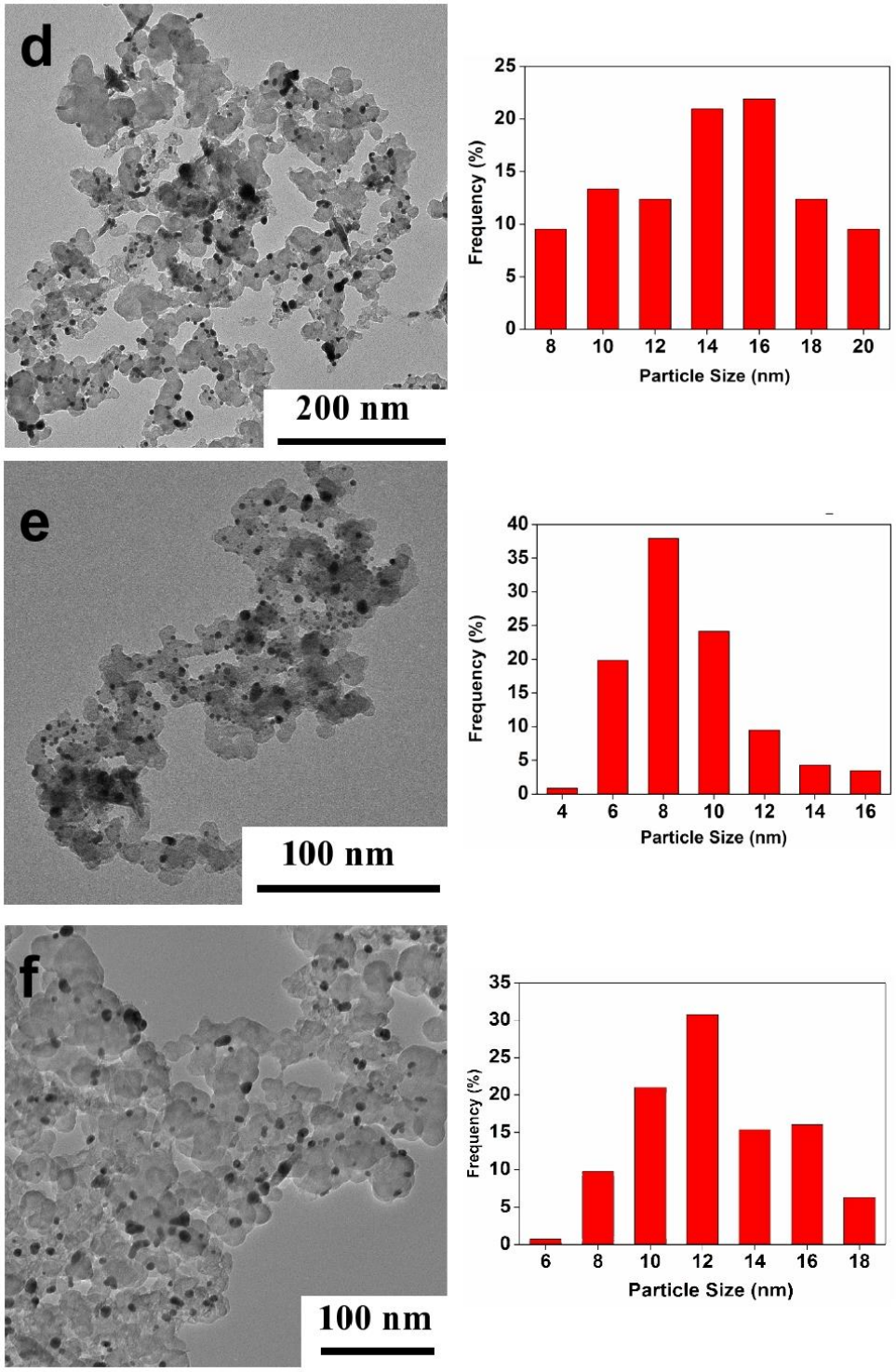

Fig. 3.1. TEM images of a) Au/C b) $Cu_{-0.1V,\ 30min}$-Au/C c) $Cu_{+0.015V,\ 30min}$-Au/C d) $Cu_{-0.015V,\ 90min}$-Au/C e) $Cu_{+0.1V,\ 30min}$-Au/C f) $Cu_{+0.3V,\ 30min}$-Au/C and their corresponding size distribution.

Fig. 3.1 shows the TEM images of the various catalysts after Cu electro-deposition was carried out at various potentials and for different time lengths. The Cu-Au/C catalysts are all larger than Au/C and this indicates that Cu species have been successfully deposited onto Au/C.

However, there is no discernible trend in size distribution possibly due to Cu species not being evenly coated onto the Au/C surface. Having said that, our catalytic results (see below) demonstrated that size effect did not influence resulting catalytic selectivity.

3.3.2. XRD Characterization

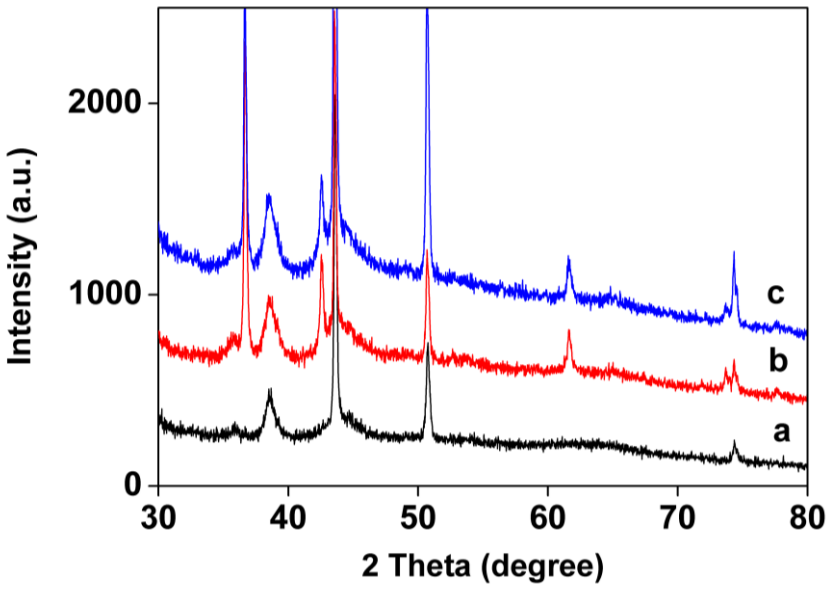

Fig. 3.2. XRD pattern of a) $Cu_{+0.015V,\ 30min}$-Au/C b) $Cu_{+0.015V,\ 60min}$-Au/C c) $Cu_{+0.015V,\ 90min}$-Au/C.

XRD data derived after Au/C nanoparticles underwent Cu electro-deposition at +0.015 V for varying time lengths is shown in Fig. 3.2. The catalysts are denoted as $Cu_{+0.015V,\ tmin}$-Au/C, where t represents the length of electro-deposition process. Au is present in all samples, as observed from the sharp diffraction peak at ~38.5 º, which is assigned to the (111) plane of the Au phase (JCPDS 65-2870). Length of the Cu deposition process influenced the type of Cu species deposited. $Cu_{+0.015V,\ 30min}$-Au/C contained only Cu (0), as determined by the diffraction peaks at ~43.7 º and ~50.7 º and ~74.4 º, which are assigned to the (111), (200) and (220) planes of the Cu (0) phase (JCPDS 04-0836) respectively. Cu (111) diffraction peak also coincided with the Au (200) peak which occurs in the same region. However, when Cu electro-deposition occurred for at least 60 min, both Cu (0) and Cu_2O are observed. $Cu_{+0.015V,\ 60min}$-Au/C and $Cu_{+0.015V,\ 90min}$-Au/C displayed additional diffraction peaks at ~36.7 º and ~42.6 º and ~61.6 º,

which are assigned to the (111), (200) and (220) planes of the Cu_2O phase (JCPDS 78-2076) respectively.

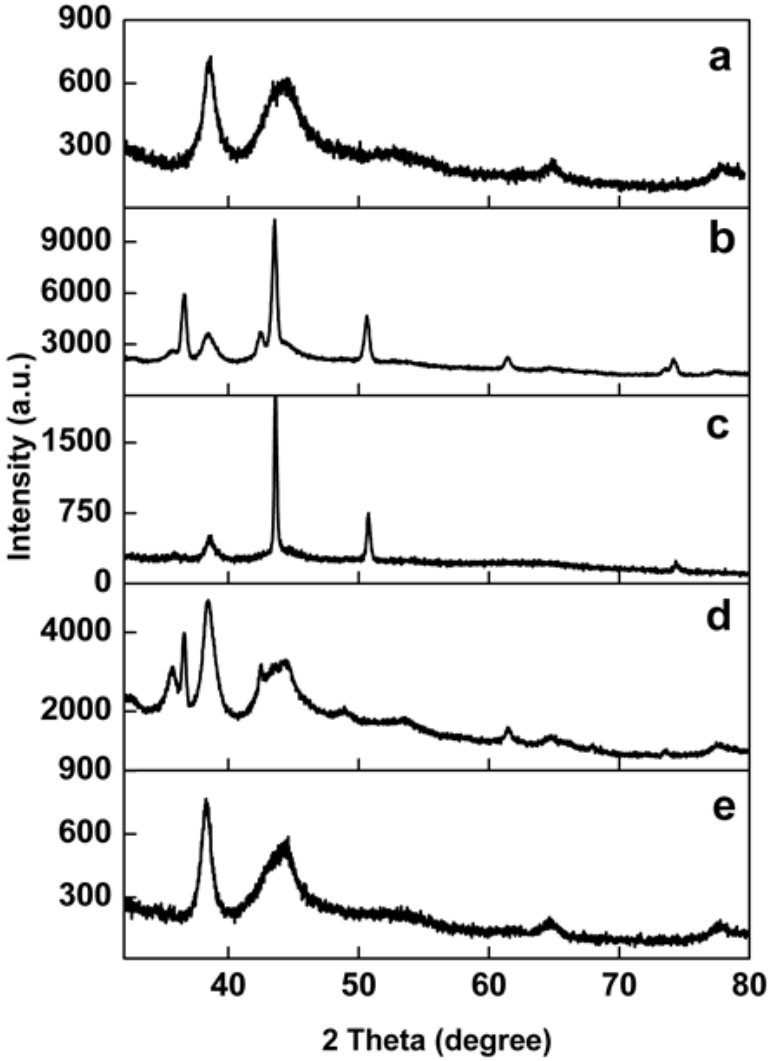

Fig. 3.3. XRD pattern of a) Au/C b) $Cu_{-0.1V,\ 30min}$-Au/C c) $Cu_{+0.015V,\ 30min}$-Au/C d) $Cu_{+0.1V,\ 30min}$-Au/C e) $Cu_{+0.3V,\ 30min}$-Au/C. Carbon peak at ~26^o was eliminated for greater clarity.

Fig. 3.3 shows the XRD patterns derived after Cu electro-deposition was carried out over Au/C for 30 min at various applied potentials. The resulting catalysts are denoted as $Cu_{V,\ 30min}$-Au/C where by V indicates the Cu electro-deposition potential. Au was present in all the samples investigated. Besides the Au (111) peak, $Cu_{+0.1V,\ 30min}$-Au/C and $Cu_{+0.3V,\ 30min}$-Au/C displayed additional peaks at ~44.1 ^{o}, ~64.5 ^{o} and ~77.5 ^{o}, which are assigned to the (200), (220) and (311) planes of the Au phase respectively. Moreover, in comparison to $Cu_{+0.015V,\ 30min}$-Au/C, $Cu_{+0.1V,\ 30min}$-Au/C contained both CuO and Cu_2O. $Cu_{+0.1V,\ 30min}$-Au/C displayed additional

diffraction peaks at ~35.6 º, ~48.8 º, ~53.2 º and ~61.3 º, which are assigned to the (111), (-202), (020) and (-113) planes of the CuO phase (JCPDS 48-1548) respectively.

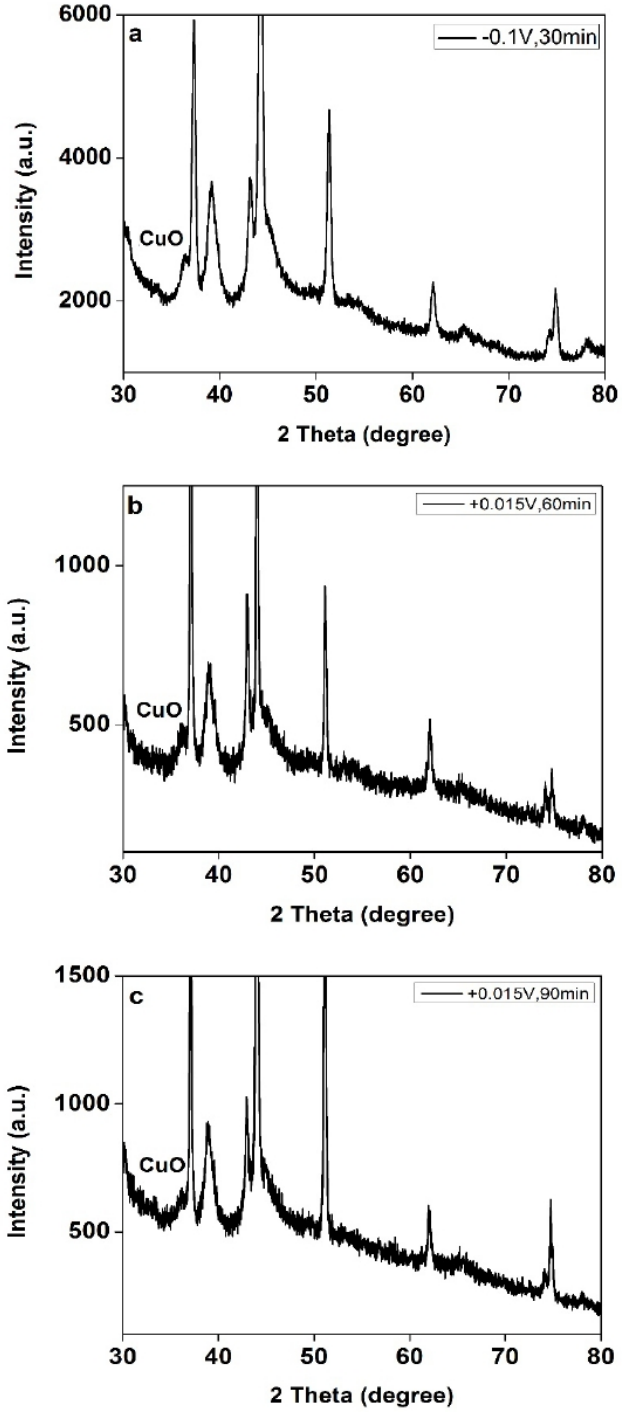

Fig. 3.4. Expanded XRD patterns derived after Cu electro-deposition at a) $Cu_{-0.1V,\ 30min}$ -Au/C b) $Cu_{+0.015V,\ 60min}$-Au/C and c) $Cu_{+0.015V,\ 90min}$-Au/C.

Table 3.1. Nernst potential calculated for the respective Cu electro-deposition potentials**.**

Cu electro-deposition potential (V) vs. Ag/AgCl	Calculated Nernst potential (V) vs. RHE
+0.3	+0.498
+0.1	+0.298
+0.015	+0.213
-0.1	+0.098
-0.3	-0.102

Nernst Equation was used to take into account differences in reaction conditions: $E = E° + 0.0592(pH_{solution})$

Table 3.2. Possible electrochemical reactions in the reaction system.

Eq	Electrochemical reaction	Nernst Potential (V) (vs. RHE)
1	$CuSO_4 + 2e^- \rightleftharpoons Cu + SO_4^{2-}$	+0.34
2	$Cu_2O + 2e^- \rightleftharpoons 2\ Cu + 2\ OH^-$	+0.054
3	$Cu^{2+} + H_2O + 2e^- \rightleftharpoons Cu_2O + 2\ H^+$	+0.61
4a	$CuO(\alpha) + 2\ H^+ + 2\ e^- \rightleftharpoons Cu_2O + H_2O$	+0.25
4b	$CuO(\beta) + 2\ H^+ + 2\ e^- \rightleftharpoons Cu_2O + H_2O$	+0.33
5	$Au^+ + e^- \rightleftharpoons Au$	+2.11

Various Cu species were obtained from the different electrochemical reactions that occurred at different applied potentials. $Cu_{-0.1V,\ 30min}$-Au/C contained mainly Cu (0) and Cu_2O, as its XRD spectra is similar to that of $Cu_{+0.015V,\ 90min}$-Au/C (Fig. 3.2). Overall, Cu^{2+} reduction (from $CuSO_4$ stock solution) to Cu was the dominant reaction. As the reaction proceeded, electro-deposited Cu was then oxidized to Cu_2O owing to low reduction potential of the reaction (Eq 2, Table 3.2). This accounts for the presence of Cu_2O in all the samples except for $Cu_{+0.3V,\ 30min}$-Au/C. Furthermore, when Cu electro-deposition occurred at +0.1 V (E=+0.289 V vs. RHE, Table 3.1), the applied potential was sufficiently high such that Cu_2O underwent further oxidation to CuO. As such, both Cu_2O and CuO was observed in $Cu_{+0.1V,\ 30min}$-Au/C (Fig. 3.3d). These observations are in line with previous reports which examined the Cu electro-deposition

process with X-ray and UV-photoelectron spectroscopy (XPS and UPS) and X-ray reflectivity measurements.[194, 195] Small amounts of CuO were also observed in XRD spectra of $Cu_{+0.015V, 60min}$-Au/C, $Cu_{+0.015V, 90min}$-Au/C and $Cu_{-0.1V, 30min}$-Au/C. As with $Cu_{+0.1V, 30min}$-Au/C, CuO (-111) peak in these samples existed as a shoulder peak alongside Cu_2O (111) at ~36.2 ^{0} (Fig. 3.3). Yoneda-XAFS and theoretical calculations showed that a duplex type structure consisting of an outer CuO and an inner Cu_2O layer were formed on top of metallic Cu thin films after its exposure to air.[196] Hence, surface oxidation of Cu_2O also accounts for the presence of CuO. Lastly, high applied potential of +0.3 V (E=+0.498 V vs. RHE, Table 3.1), meant that only miniscule amounts of Cu was deposited onto Au/C (Fig. 3.5a). XRD spectra of $Cu_{+0.3V, 30min}$-Au/C is essentially identical to Au/C (Fig. 3.3e).

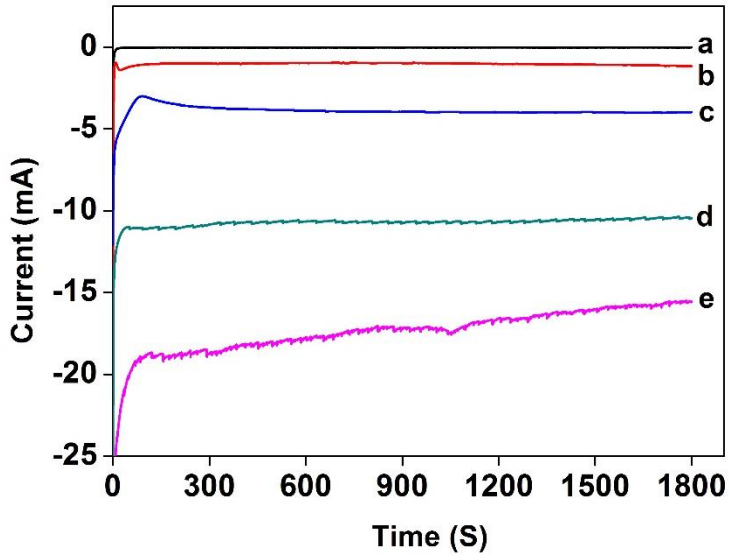

Fig. 3.5. Chronoamperograms for a) Cu+0.3V, 30mins-Au/C b) Cu+0.1V, 30mins-Au/C c) Cu+0.015V, 30mins-Au/C d) Cu-0.1V, 30mins-Au/C e) Cu-0.3V, 30mins-Au/C.

3.3.3. XPS Characterization

Table 3.3. Relative chemical composition of catalysts prepared at different Cu electro-deposition potentials. Elemental concentrations are expressed as atomic percentage (at. %).

Sample	Au4f (element concentration, at. %)		Cu2p (element concentration, at. %)		Au/Cu_xO_y atomic ratio
	Au^0	Au^+	Cu^+/ Cu	Cu^{2+}	
$Cu_{-0.1V,\ 30min}$-Au/C	89.33	10.67	81.38	18.62	2.65/97.35
$Cu_{+0.015V,\ 30min}$-Au/C	90.51	9.49	60.77	39.23	3.84/96.16
$Cu_{+0.015V,\ 90min}$-Au/C	72.48	27.52	61.02	38.98	2.24/97.76
$Cu_{+0.1V,\ 30min}$-Au/C	96.18	3.82	63.68	36.32	3.13/96.87
$Cu_{+0.3V,\ 30min}$-Au/C	100	0	100	0	54.03/45.97

X-ray photoelectron spectroscopic (XPS) was used to analyse surface composition of the catalysts prepared at different Cu electro-deposition potential and time. Table 3.3 summarizes their respective elemental surface compositions (atom%). All binding energies were referenced to the adventitious C1s line at 284.8 eV. $Au4f_{7/2}$ peak for all 5 samples was located at a BE of 84.4 eV (Fig. 3.6), which is typical of pure metallic Au(0) species.[197-199] Our samples are thus composed of binary nanocomposites instead of Au-Cu alloys since alloy formation is typically accompanied by a shift of the Au4f peak relative to pure Au nanoparticles.[200]

An additional Au4f peak at 85.7 eV was present when Cu electro-deposition was carried out between -0.1 V and +0.1 V (Fig. 3.6b-e respectively). This peak is assigned to the Au^+ species.[197, 201] Au^+ content was highest in $Cu_{+0.015V,\ 90min}$-Au/C (27.52%) after an extended oxidation period of 90 min and lowest in $Cu_{+0.1V,\ 30min}$-Au/C (3.82%). When Cu electro-deposition occurred at +0.1 V, its Nernst potential at +0.298 V (Table 3.1) was very close to the equilibrium potential of Cu^{2+} reduction reaction. Hence, smaller amounts of Cu species were deposited onto Au/C at +0.1 V (Fig. 3.5b). This in turn decreased Au-Cu oxide interaction

and reduced the amount of Au^+ species generated. Au^+ was generated via electron transfer from Au to the electro-deposited Cu_2O present on its surface. Consequently, Cu_2O was reduced to Cu. This redox process is thermodynamically favourable and spontaneous owing to the relatively large difference in their reduction potentials (ΔE=+2.06 V).[202] Au^+ has also been observed in other types of Cu_2O-Au nanocomposites such as heterodimers, core-shell particles and hollow spheres.[203] Additionally, Au nanoparticles supported on CeO_2 (Au/CeO_2) and Au nanoparticles partially covered with very small NiO_x (NiO_x@Au) segments also reported the presence of Au^+ species after electron transfer occurred between Au(0) and CeO_2[204-206] and Ni_2O_3[207] respectively. In comparison, CuO is more stable due to its higher reduction potential and Au^+ species are not commonly observed in Au-CuO nanocomposites.[208-210]

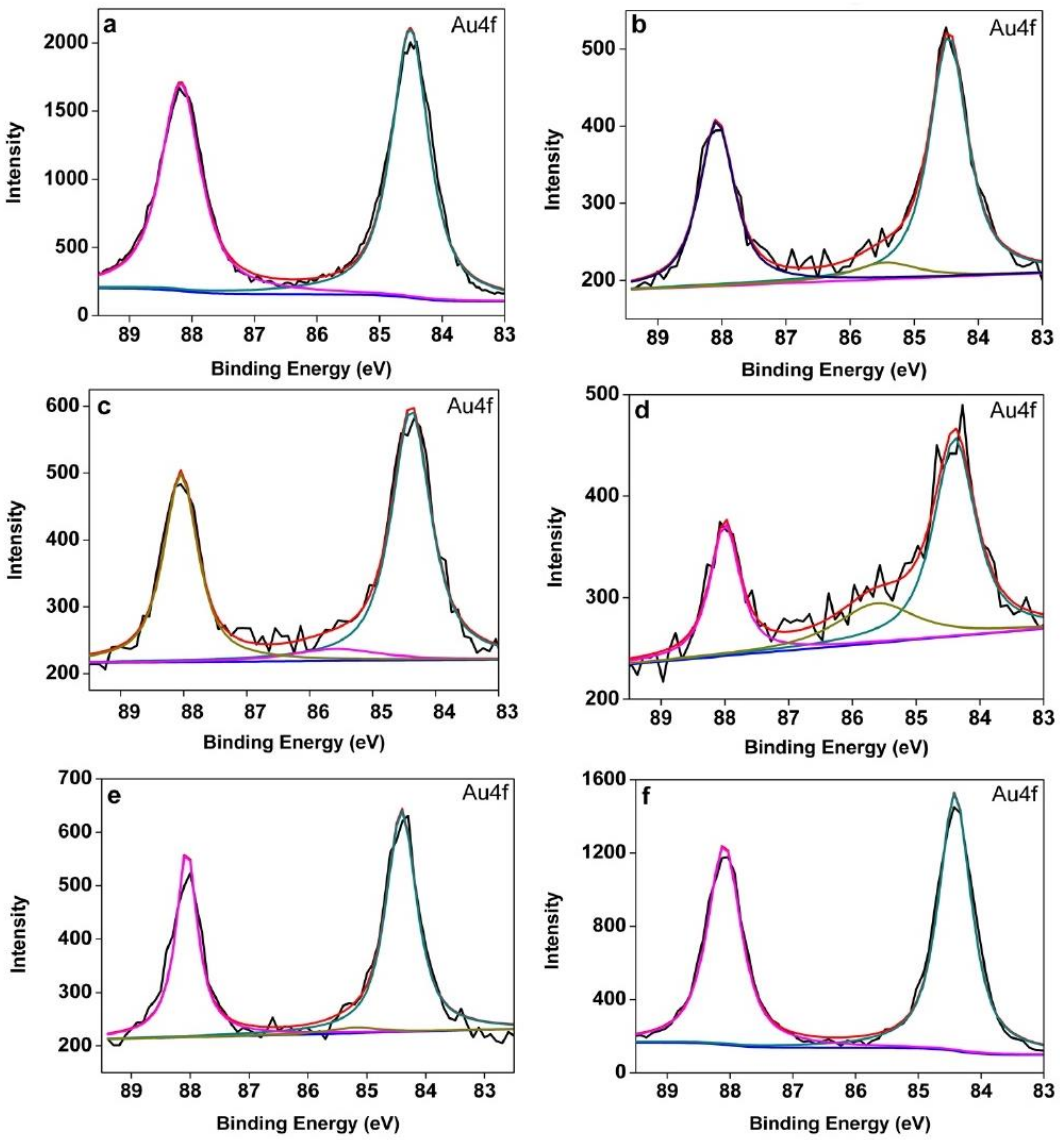

Fig. 3.6. XPS curve fitting of the Au4f photoelectron peak for a) Au/C b) $Cu_{-0.1V,\ 30min}$-Au/C c) $Cu_{+0.015V,\ 30min}$-Au/C d) $Cu_{+0.015V,\ 90min}$-Au/C e) $Cu_{+0.1V,\ 30min}$-Au/C f) $Cu_{+0.3V,\ 30min}$-Au/C.

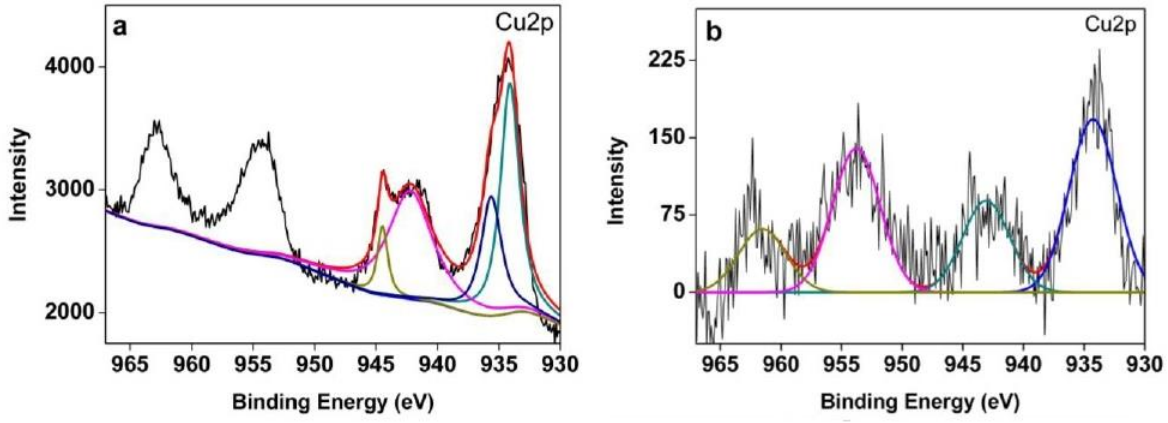

Fig. 3.7. a) Typical XPS Cu2p photoelectron peak after deconvolution b) XPS Cu2p peak for $Cu_{+0.3V,\ 30min}$-Au/C.

A typical Cu2p XPS spectra is shown in Fig. 3.7a. $Cu2p_{3/2}$ BE cannot be used to distinguish between Cu^+ and Cu^0 as they are essentially identical. Nevertheless, XPS shows that Cu^+/Cu and/or Cu^{2+} are present in all samples. Cu2p spectra typically shows 2 major components at BE ~934 eV and ~935 eV, which correspond to Cu^+ and/or Cu and Cu^{2+} respectively.[211-214] In line with XRD results, Cu^+/Cu are the dominant species. Cu^+ generally contributes between 60-80 atom% while Cu^{2+} contributes between 40-20 atom% (Table 3.3). As mentioned previously, the presence of CuO is due, in part, to surface oxidation of Cu_2O.

Discrepancy exists between the XRD and XPS analysis of $Cu_{+0.015V,\ 30min}$-Au/C. Namely that metallic Cu was the sole species observed in the XRD spectrum but XPS also identified the minor presence of Cu^{2+}. A similar inconsistency was reported when comparing the XRD and XPS spectra of Cu_2O nanoplatelets supported on few layer graphene.[215] Only Cu and Cu_2O diffraction peaks were present in their XRD spectrum. However, both Cu^+ and Cu^{2+} were identified in the XPS Cu2p spectra, with the latter being dominant. Different natures of both techniques can account for the inconstancies observed. XPS exclusively probes the outermost layers of nanoparticles while XRD provides phase identification of the sample and determines its average bulk composition. As such, different contents of the same species are observed in XRD and XPS.

XPS also confirmed that Au is the major species on the surface of $Cu_{+0.3V,\ 30min}$-Au/C (Table 3.3.). Moreover, the atomic proportion of Au on $Cu_{+0.3V,\ 30min}$-Au/C is about 18% more than the other samples. XPS also evidenced the presence of Cu species in $Cu_{+0.3V,\ 30min}$-Au/C which were not observed in XRD (Fig. 3.7b). Cu^+ was the sole Cu species observed. As expected, the intensity of its Cu2p peaks were significantly lower than those obtained for other samples. The notably lesser amount of Cu_2O deposited resulted in little to no CuO being observed in the XPS spectra.

3.3.4. Voltammetric characterization of catalysts

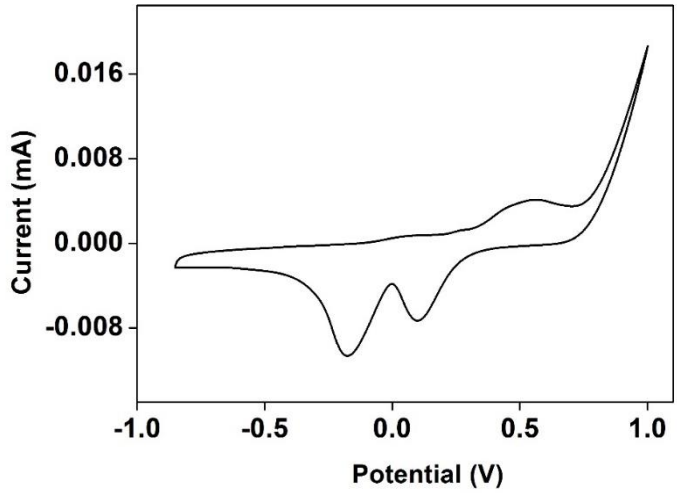

Fig. 3.8. Cyclic voltammogram (CV) of Au-C on carbon cloth electrode in 0.1 M NaOH at a scan rate of 50mV/s.

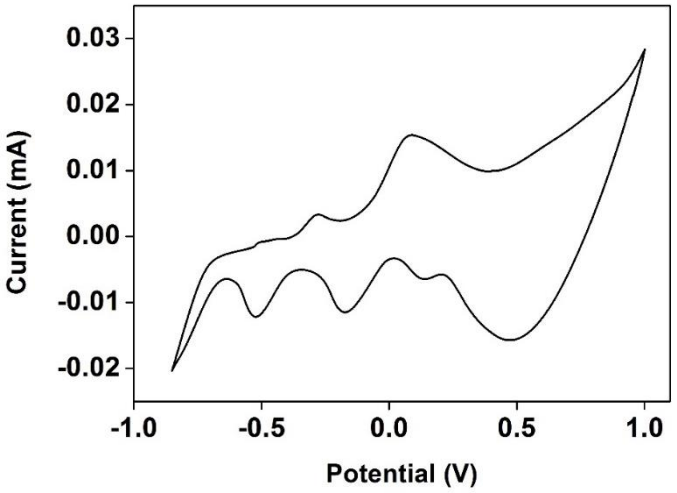

Fig. 3.9. A typical cyclic voltammogram (CV) of Au/C post Cu electro-deposition for 30 mins in 0.1 M NaOH at a scan rate of 50mV/s.

Due to high catalyst loading of 2mg/cm^2, catalytic activity was observed to be more sluggish. Au peaks were not observed after Cu electro-deposition likely due to the presence of Cu species on the surface of Au/C.

3.3.5. Catalytic activity for glycerol electro-oxidation

Table 3.4. Glycerol electro-oxidation in alkaline medium using catalysts prepared at different Cu electro-deposition potentials.

Catalyst	Tartronate (%)	Glycerate (%)	Oxalate (%)	Glycolate (%)	Formate (%)	C3 Selectivity (%)
Au/C	7.68	22.06	3.08	43.98	23.20	29.74
$Cu_{+0.3V,\ 30min}$-Au/C	17.56	28.89	16.00	12.69	24.87	46.45
$Cu_{+0.1V,\ 30min}$-Au/C	11.93	27.07	8.23	20.73	32.04	39.00
$Cu_{+0.015V,\ 30min}$-Au/C	14.55	39.03	3.77	17.59	25.06	53.58
$Cu_{-0.1V,\ 30min}$-Au/C	12.35	34.73	7.65	20.07	25.21	47.07
$Cu_{-0.3V,\ 30min}$-Au/C	7.95	26.86	4.51	25.85	34.83	34.81

Carbon cloth electrodes containing Au/C underwent Cu electro-deposition at various potentials for 30 min. The as-prepared catalysts were then investigated for glycerol electro-oxidation which was carried out at 0.1 V for 2 h in alkaline medium. Extensive DFT calculations carried out for CO oxidation over Cu modified Au surfaces indicate that a monoatomic layer of Cu on the Au slab performed very well for O_2 adsorption/activation and CO_2 formation from coadsorbed CO and O (Fig. 3.10).[216] The configuration consisting of a top layer of Cu atoms and three layers of Au atoms beneath it, gives rise to the highest increase in O_2 adsorption energy and bond activation as a consequence of charge donation from metal surfaces to O_2 antibonding molecular orbital. Subsequently, this surface performs best for CO oxidation. CO also adsorbs preferably on the top configuration of Cu−Au (100) catalytic surface and the adsorption energy released is more than two times that on Au (100). Additionally, the Au−Cu

surface is superior and more active than pure Cu toward CO oxidation. It offers less activation barrier and higher thermodynamic favour, which serves as a driving force for the reaction on the catalytic surface. Given the results of DFT studies, it is expected that the as-prepared Cu modified Au nanoparticles will exhibit improved catalytic performance relative to Au/CB.

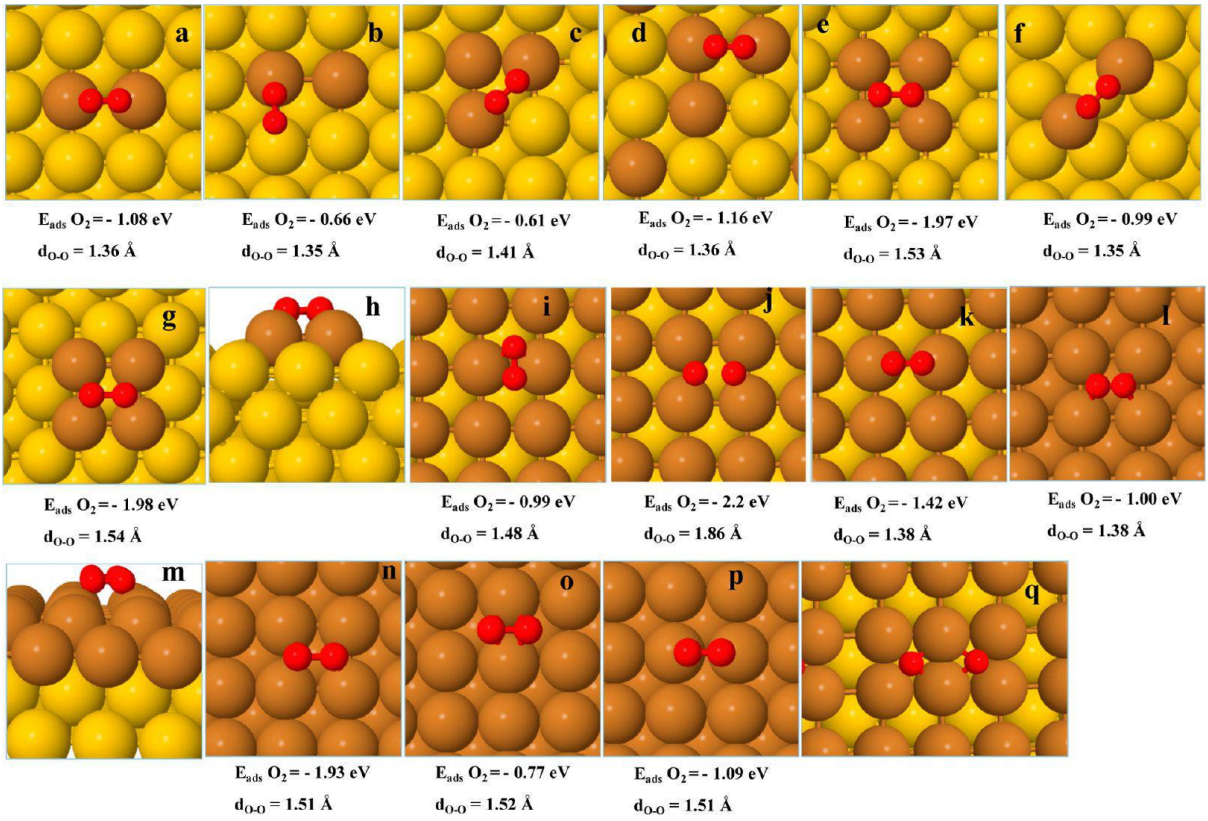

Fig. 3.10. Molecular O_2 adsorption on the different positions of various Au−Cu bimetallic and pure Cu surfaces. The substitution of Cu atoms in the top row has been increased until the replacement of the whole top Au layer by Cu atoms. Panels f−h correspond to the adsorption on Cu add atoms on the four layers Au slab. Panels n−p represent the O_2 adsorption upon pure Cu slab models. The adsorption energy and bond length of O2 has been given in each case below the corresponding panel. Panel q shows the most stable configuration for the dissociated coadsorbed O atoms. The adsorption energies reported are calculated as Eads(O_2) = Eslab-O_2 − Eslab − EO_2(gas). Reprinted with permission from ref 216. Copyright 2013, ACS Publications.

Table 3.4 evidences that the presence of electro-deposited Cu species improved the innate C3 selectivity (glycerate and tartronate) of Au/C. C3 selectivity of all Cu-Au/C samples were higher than that of pure Au/C. Presence of electro-deposited Cu species increased C3 selectivity while simultaneously supressing C-C bond breaking, as observed from the

significantly lower glycolate selectivity exhibited by the Cu-Au/C samples. Having said that, type of Cu species present on Au/C does affect the extent to which its C3 selectivity was improved. Highest improvement in C3 selectivity occurred when Cu electro-deposition took place at +0.015 V. $Cu_{+0.015V,\ 30min}$-Au/C increased C3 selectivity by ~24% relative to Au/C. C3 selectivity obtained by $Cu_{-0.1V,\ 30min}$-Au/C was relatively similar to that of $Cu_{+0.015V,\ 30min}$-Au/C selectivity due to their similar Au^+ content (~10%). As mentioned above, Au^+ is commonly observed in Au/CeO_2 catalysts. Furthermore, when Au/CeO_2 was applied to CO oxidation,[217] water-gas shift reaction,[218, 219] and formaldehyde oxidation,[220, 221] Au^+ was identified as the dominant catalytic species as catalysts containing higher amounts of Au^+ exhibited higher activity. Similarly, we posit that presence of Au^+ was the main driving force for increased selectivity to glycerate and tartronate. Yet, C3 selectivity of $Cu_{-0.1V,\ 30min}$-Au/C was still ~6% lower than that of $Cu_{+0.015V,\ 30min}$-Au/C. Slightly elevated C-C bond breakage occurred over the former and resulted in higher selectivity to glycolate and oxalate. As observed from XPS analysis, $Cu_{-0.1V,\ 30min}$-Au/C contains ~20% more Cu^+ species on its surface as compared to $Cu_{+0.015V,\ 30min}$-Au/C (Table 3.3). The higher composition of Cu_2O species likely generated a catalyst that favoured C-C bond breaking over deeper oxidation. Additionally, when Cu electro-deposition occurred at -0.1 V, more Cu species were deposited onto Au/C. The slightly thicker Cu coating would have hindered diffusion of the oxidation products away from the catalyst layer, thus leading to slight decrease in C3 selectivity.

C3 selectivity generally decreased when Cu electro-deposition was carried out at applied potentials more positive than +0.015 V. C3 selectivity of $Cu_{+0.1V,\ 30min}$-Au/C decreased by about 14% compared to $Cu_{+0.015V,\ 30min}$-Au/C due to its comparatively lower Au^+ content (Table 3.3). Nonetheless, C3 selectivity of $Cu_{+0.1V,\ 30min}$-Au/C was still about 10% higher than that of Au/C. Although no Au^+ was observed in $Cu_{+0.3V,\ 30min}$-Au/C, its C3 selectivity was slightly higher than that of $Cu_{+0.1V,\ 30min}$-Au/C. This was mainly contributed by an increase in tartronate selectivity.

Since only Cu_2O was deposited onto Au/C, the Cu_2O species present likely interacted with Au in such a way that deeper oxidation of glycerate to tartronate was favoured.

C3 selectivity of $Cu_{-0.3V,\ 30min}$-Au/C showed the smallest increment (~5%) relative to Au/C. Correspondingly, $Cu_{-0.3V,\ 30min}$-Au/C was the most selective to formate. When Cu electro-deposition occurred at +0.3 V, the Nernst potential of the reaction was -1.02 V (Table 3.1). The highly negative applied potential provided a very large driving force for $CuSO_4$ reduction to Cu and likely precluded further oxidation of Cu to Cu_2O. As such, Au^+ was not present in the system. Furthermore, the rapid reduction of Cu^{2+} onto Au/C also means that considerably more Cu was deposited at -0.3 V (Fig. 3.4). The thicker Cu coating on Au/C hindered the diffusion of glycerate and tartronate away from the catalyst layer after being formed. The intermediates thus remained trapped within the catalyst layer and continued to undergo further oxidation until they were released as formate or carbon dioxide. In the same vein, Li and co-workers determined that a thick electrode layer facilitated deeper oxidation of glycerate to tartronate or mesoxalate as the former was held within the confined electrolyte volume for longer periods of time. This was observed when glycerol electro-oxidation was carried out in a direct alcohol alkaline membrane fuel cell.[160, 187]

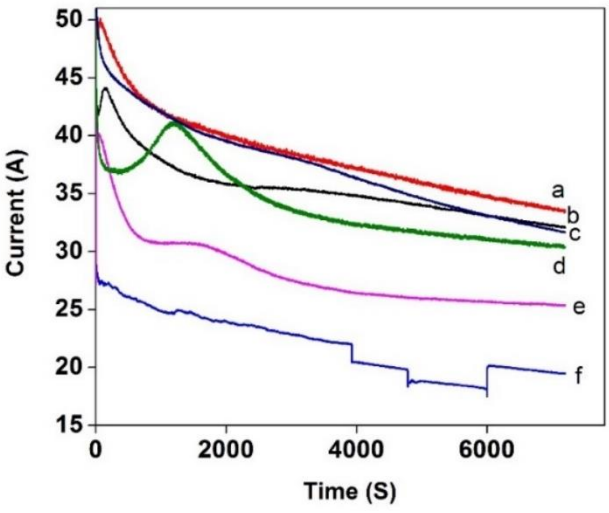

Fig. 3.11. Chronoamperograms obtained from a) $Cu_{+0.1V,\ 30min}$-Au/C b) $Cu_{+0.015V,\ 30min}$-Au/C c) Au/C d) $Cu_{-0.3V,\ 30min}$-Au/C e) $Cu_{-0.1V,\ 30min}$-Au/C f) $Cu_{+0.3V,\ 30min}$-Au/C after glycerol oxidation was carried out at +0.1 V for 2 h.

Cu electro-deposition did not significantly affect the electro-chemical activity of Au/C for glycerol electro-oxidation (Fig. 3.10). These results are indicative that Cu itself is a good promoter of glycerol electro-oxidation.

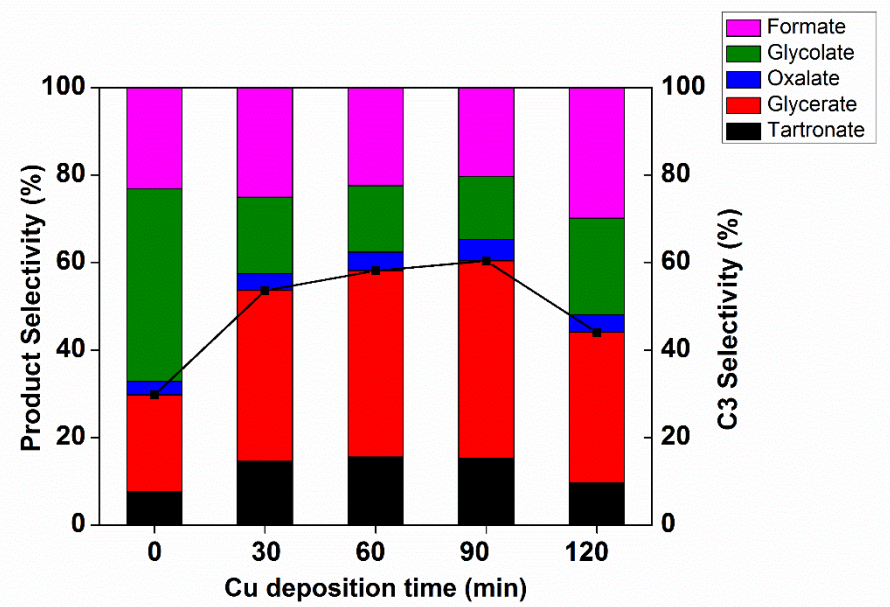

Fig. 3.12. Product selectivity during glycerol electro-oxidation over catalysts prepared at +0.015 V, with different time lengths.

Using +0.015 V as the optimal applied potential, we then investigated how electro-deposition time influenced catalytic selectivity. The catalysts were denoted as $Cu_{+0.015V,\ tmin}$-Au/C where t indicates the length of the electro-deposition process. C3 selectivity of the as-prepared catalysts for glycerol electro-oxidation at +0.1 V is summarized in Fig. 3.11. C3 selectivity increased with increasing deposition time until it reached a maximum at 90 min. $Cu_{+0.015V,\ 90min}$-Au/C achieved C3 selectivity of ~60%, which was double that of Au/C. Herein, $Cu_{+0.015V,\ 90min}$-Au/C doubled selectivity to both glycerate and tartronate whilst C-C bond breakage to glycolate and formate was suppressed to the largest extent. As established previously, presence of Au^{+} species generated from Au-Cu_2O interaction is the main contributing factor towards the relatively higher C3 selectivity of this group of catalysts. Importantly, XPS analysis shows that when Cu electro-deposition was extended to 90 min, the proportion of Au^{+} present in $Cu_{+0.015V,\ 90min}$-Au/C (27.5%) was almost 3 times higher than that in $Cu_{+0.015V,\ 30min}$-Au/C (9.5%) (Table

3.3). The significantly higher proportion of Au^+ species accounts for the superior C3 selectivity exhibited by $Cu_{+0.015V, 90min}$-Au/C. However, when Cu electro-deposition was extended to 120 min, C3 selectivity observed a sharp decrease ~16% relative to $Cu_{+0.015V, 90min}$-Au/C. The longer deposition time resulted in more Cu species being deposited onto Au/C. As with $Cu_{-0.3V, 30min}$-Au/C, a thicker catalyst layer is detrimental for C3 selectivity. Nevertheless, C3 selectivity of $Cu_{+0.015V, 120min}$-Au/C was still ~15% higher than that of Au/C. This again evidences the synergistic relationship between Au and Cu and/or Cu_2O.

Finally, we investigated how selectivity of $Cu_{+0.015V, 90min}$-Au/C was affected by the applied potential at which glycerol electro-oxidation occurred. Fig. 3.12 shows that C3 selectivity obtained by $Cu_{+0.015V, 90min}$-Au/C was higher than that of Au/C across the entire potential range tested. Highest C3 selectivity achieved by $Cu_{+0.015V, 90min}$-Au/C was ~60% and this was obtained when glycerol electro-oxidation was carried out at 0 V and 0.1 V. Moreover, at 0 V and 0.1 V, C3 selectivity of $Cu_{+0.015V, 90min}$-Au/C was about 1.7 and 2 times higher than that of Au/C respectively. In line with previous reports, C3 selectivity decreased with increasing applied potential.[136, 159, 160] C-C bond breaking is accelerated at higher potentials and glycerate is converted to glycolate and formate with greater ease. As such, C3 selectivity of $Cu_{+0.015V, 90min}$-Au/C decreased when glycerol electro-oxidation occurred at applied potentials higher than 0.1 V. For example, when glycerol electro-oxidation took place at 0.3 V instead of 0.1 V, C3 selectivity obtained by $Cu_{+0.015V, 90min}$-Au/C decreased by more than half from ~60% to ~26%.

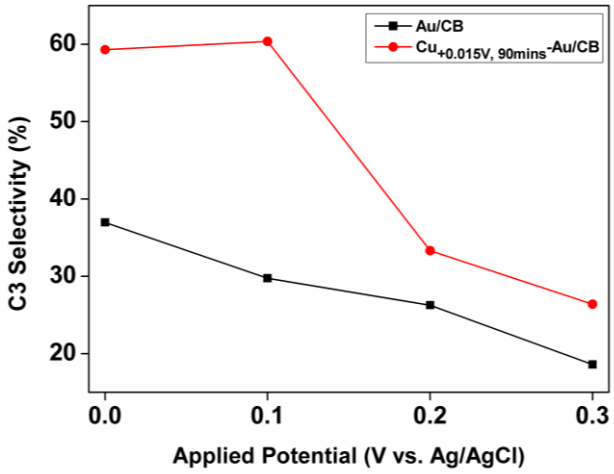

Fig. 3.13. Comparing C3 selectivity of $Cu_{+0.015V,\ 90min}$-Au/C with that of pure Au/C over a range of potentials.

3.4. Conclusion

Herein, we have demonstrated that electro-deposition of Cu species onto Au/C significantly enhanced C3 selectivity of Au nanoparticles during glycerol electro-oxidation. Cu electro-deposition at -0.1 V and +0.015 V resulted in the most selective catalysts. High selectivity was attributed to the presence of an Au^+ species which was generated as a result of Au interaction with electrodeposited Cu_2O. Extending electro-deposition time to 90 min at +0.015 V, further increased Au^+ content by three times. As such, $Cu_{+0.015V,\ 90min}$-Au/C displayed the highest C3 selectivity amongst all the catalysts investigated. Beyond these optimal conditions, little to no Au^+ species were observed and C3 selectivity decreased. Furthermore, longer deposition times (120 min) and too negative deposition potentials (-0.3 V) were detrimental to catalytic selectivity. Under these conditions, thick Cu and/or Cu oxide layers built up over Au/C and impeded diffusion of intermediates from the catalyst surface after oxidation. Glycerate and tartronate were thus trapped at the catalyst layer for longer periods of time and C-C bond breaking to glycolate and formate was enhanced.

Chapter 4

Ni modified carbon supported Au nanoparticles as highly selective C3 catalysts for glycerol electro-oxidation

4.1. Introduction

In the previous chapter, we examined the ability of electro-deposited Cu species to influence the selectivity of Au/C catalysts for glycerol electro-oxidation. Au and electro-deposited Cu shared a synergistic relationship such that the resulting catalysts exhibited enhanced C3 selectivities. In particular, an Au^+ species was observed in the most selective catalysts. Au^+ was likely generated as a result of electron transfer between Au and Cu_2O. Given these positive results, we then extended our investigation to the electro-deposited Ni species on the C3 selectivity of carbon black supported Au nanoparticles (Au/C) for glycerol electro-oxidation.

Ni was chosen based on reports evidencing the high electro-catalytic activity of pure nickel catalysts for glycerol electro-oxidation under alkaline conditions.[112, 222-226] Cyclic voltammetry (CV) studies identified NiOOH as the active catalytic species as glycerol electro-oxidation occurred in tandem with the conversion of β-$Ni(OH)_2$ to NiOOH. Subsequently glycerol was oxidized at the NiOOH surface, while NiOOH was simultaneously reduced and reformed β-$Ni(OH)_2$. However, HPLC analysis of bulk solution revealed that formic acid and glycolate were the major products generated.

4.2. Experimental

4.2.1. Ni electro-deposition process

Au/C was prepared and treated using the same experimental procedure listed in Chapter 3.

The electrodes were then immersed in a stock solution containing 50 mM nickel (II) nitrate hexahydrate ($Ni(NO_3)_2.6H_2O$) and held under constant potential. Following that, the electrodes were rinsed thoroughly in DI water before being cycled 30 times in 0.2 M NaOH solution. The as-prepared electrodes were then tested for glycerol electro-oxidation by placing them in 26

mL of 0.5 M NaOH + 0.5 M glycerol solution and holding under constant potential for 2 h. Subsequently, 1 mL of the solution was collected for high-performance liquid chromatography (HPLC) analysis.

4.3. Results and Discussion

4.3.1. XPS characterization

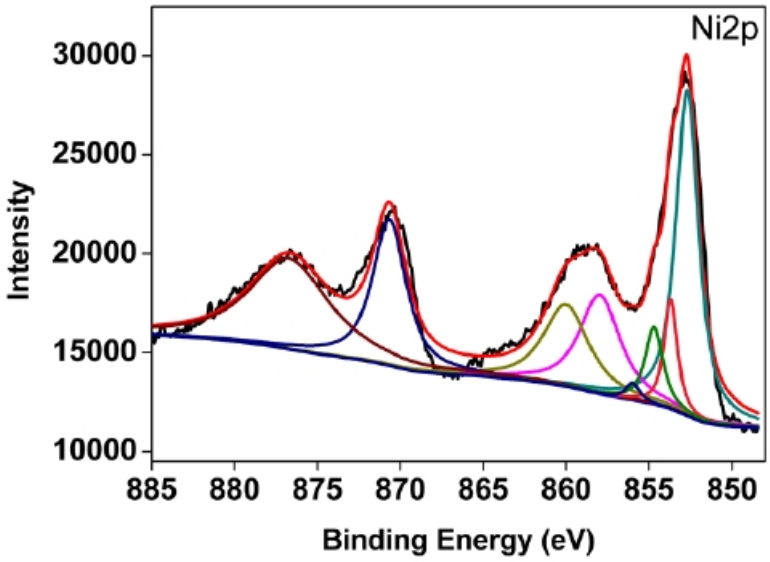

Fig. 4.1. Typical XPS Ni2p photoelectron peak after deconvolution.

Table 4.1. Relative Au composition of catalysts prepared at different Ni electro-deposition potentials. Elemental concentrations are expressed as atomic percentage (at.%).

Sample	Au4f (element concentration, at. %)		Au/Ni_xO_y atomic ratio (%)
	Au^0	Au^+	
$Ni_{-0.3V,40min}$-Au/C	89.95	10.05	7.29/92.71
$Ni_{-0.6V,40min}$-Au/C	0	0	0/100
$Ni_{-0.8V,40min}$-Au/C	0	0	0/100
$Ni_{-1.2V,40min}$-Au/C	0	0	0/100

Table 4.2. Binding energies of Au4f and Ni2p peaks and their corresponding species.

Sample	Au4f (eV)	Ni2p (eV)
$Ni_{-0.3V}$-Au/C	84.41 (Au^0) 85.00 (Au^+)	852.58 (Ni^0) 853.40 (NiO) 854.30 (NiOOH) 856.77 ($Ni(OH)_2$)
$Ni_{-0.6V}$-Au/C	0	852.70 (Ni^0) 853.75 (NiO) 854.70 (NiOOH) 856.00 ($Ni(OH)_2$)
$Ni_{-0.8V}$-Au/C	0	852.60 (Ni^0) 854.60 (NiOOH) 856.60 ($Ni(OH)_2$)
$Ni_{-1.2V}$-Au/C	0	852.35 (Ni^0) 854.50 (NiOOH) 856.60 ($Ni(OH)_2$)

X-ray photoelectron spectroscopy (XPS) was used to analyse surface composition of the samples prepared with different Ni electro-deposition potentials. Each sample was held at the indicated potential for 40 min and the samples are denoted as $Ni_{V,40min}$-Au/C whereby V represents the applied potential at which Ni electro-deposition took place. Table 4.1 summarizes their respective elemental surface compositions (atom%) while the individual binding energies of the deconvoluted peaks are listed in Table 4.2. All binding energies are referenced to the adventitious C1s line at 284.8 eV.

Fig. 4.1 depicts the typical Ni2p spectra obtained from each sample after deconvolution. Overall, Ni^{2+} reduction to metallic Ni was the dominant electrochemical reaction across the entire applied potential range tested (Table 4.4) In line with this, the Ni^0 peak at ~852 eV was the dominant peak. Furthermore, additional peaks at ~853 eV, ~854 eV and ~856.02 eV were

also identified in the Ni2p spectra. These peaks can be ascribed to the NiO,[227, 228] $Ni(OH)_2$,[229-231] and NiOOH species[232-235] which were generated post electro-deposition, when the carbon cloth electrodes were cycled between -0.8 V to 1.0 V for 30 cycles in 0.2 M NaOH solution. As previously reported, when carbon supported Ni catalysts (Ni/C) were cycled in alkaline media, surface oxidation of Ni/C occurs in two or more steps as illustrated by the following equations:[223, 236-238]

1) Ni^0 is first oxidized to α-$Ni(OH)_2$ at lower potentials ($-0.61 \leq E \leq -0.11$ V vs. Ag/AgCl):

$$Ni + 2OH^- \rightleftharpoons \alpha\text{–}Ni(OH)_2 + 2e^- \qquad (1)$$

2) At higher potentials ($-0.11 \leq E \leq 0.79$ V vs. Ag/AgCl), α-$Ni(OH)_2$ is converted to β-$Ni(OH)_2$ which is the less hydrated, more stable and thermodynamically favored Ni hydroxide species.

$$\alpha\text{–}Ni(OH)_2 \rightleftharpoons \beta\text{–}Ni(OH)_2 \qquad (2)$$

3) When $E > 0.79$ V vs. Ag/AgCl, β-$Ni(OH)_2$ is further oxidized to the β-NiOOH

$$\beta\text{–}Ni(OH)_2 + OH^- \rightleftharpoons \beta\text{–}NiOOH + H_2O + 2e^- \qquad (3)$$

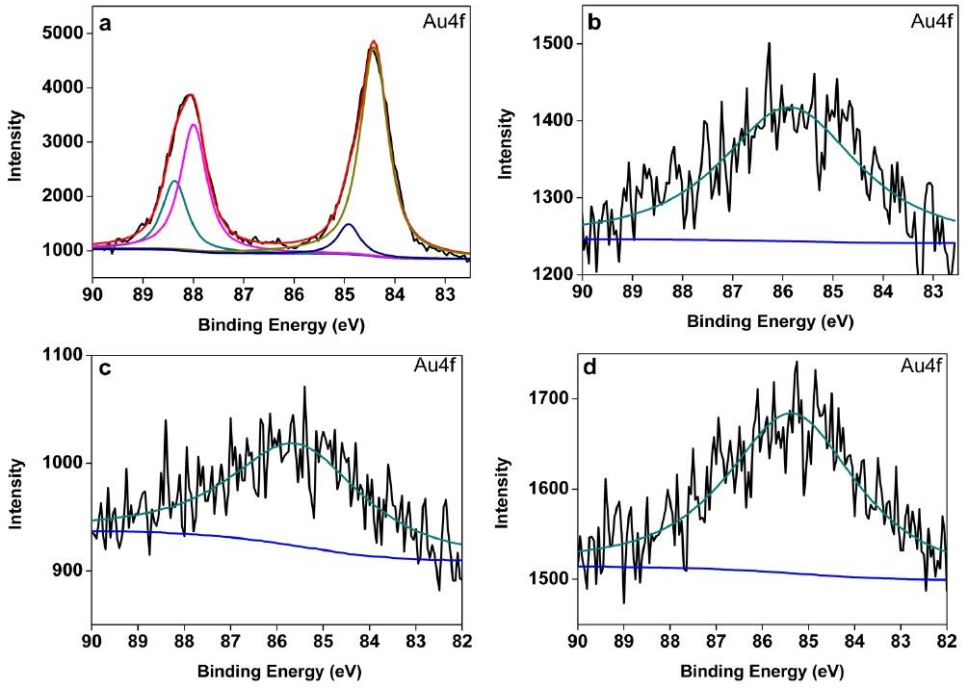

Fig. 4.2. XPS spectra of Au4f in (a) Ni-0.3V, 40min-Au/C (b) Ni-0.6V, 40min-Au/C (c) Ni-0.8V, 40min-Au/C (d) Ni-1.2V, 40min-Au/C.

Fig. 4.2 shows the Au4f XPS spectra of the 4 samples. Au4f spectra of $Ni_{-0.3V,\ 40min}$-Au/C was fitted well to double groups of peaks, corresponding to $Au4f_{7/2}$ and $Au4f_{5/2}$. Additionally, its $Au4f_{7/2}$ peak consisted of 2 components at 84.41 and 85.0 eV, which correspond to Au^0 (89.95%) and Au^+ (10.05%) respectively. Au^+ was generated when electron transfer occurred between Au nanoparticles and the highly oxidized NiOOH species.[207, 239-241] In contrast, the characteristic doublet peak pattern of Au4f was not observed in the spectra of $Ni_{-0.6V,\ 40min}$-Au/C, $Ni_{-0.8V,\ 40min}$-Au/C and $Ni_{-1.2V,\ 40min}$-Au/C. Instead, these 3 samples only exhibited one broad, low intensity peak centred around 85 eV. When Ni electro-deposition occurred at applied potentials more negative than -0.3 V, large amounts of Ni and Ni (hydro)oxide species were deposited onto Au/C. The thick Ni layer in turn obscured detection of Au during XPS analysis. Similarly, the C1s peaks of $Ni_{-0.6V,\ 40min}$-Au/C, $Ni_{-0.8V,\ 40min}$-Au/C and $Ni_{-1.2V,\ 40min}$-Au/C (Fig. 4.3) could not be observed as well. These results indicate that the surface of the $Ni_{-0.6V,\ 40min}$-Au/C, $Ni_{-0.8V,\ 40min}$-Au/C and $Ni_{-1.2V,\ 40min}$-Au/C are composed mainly of Ni species and little to no Au is exposed.

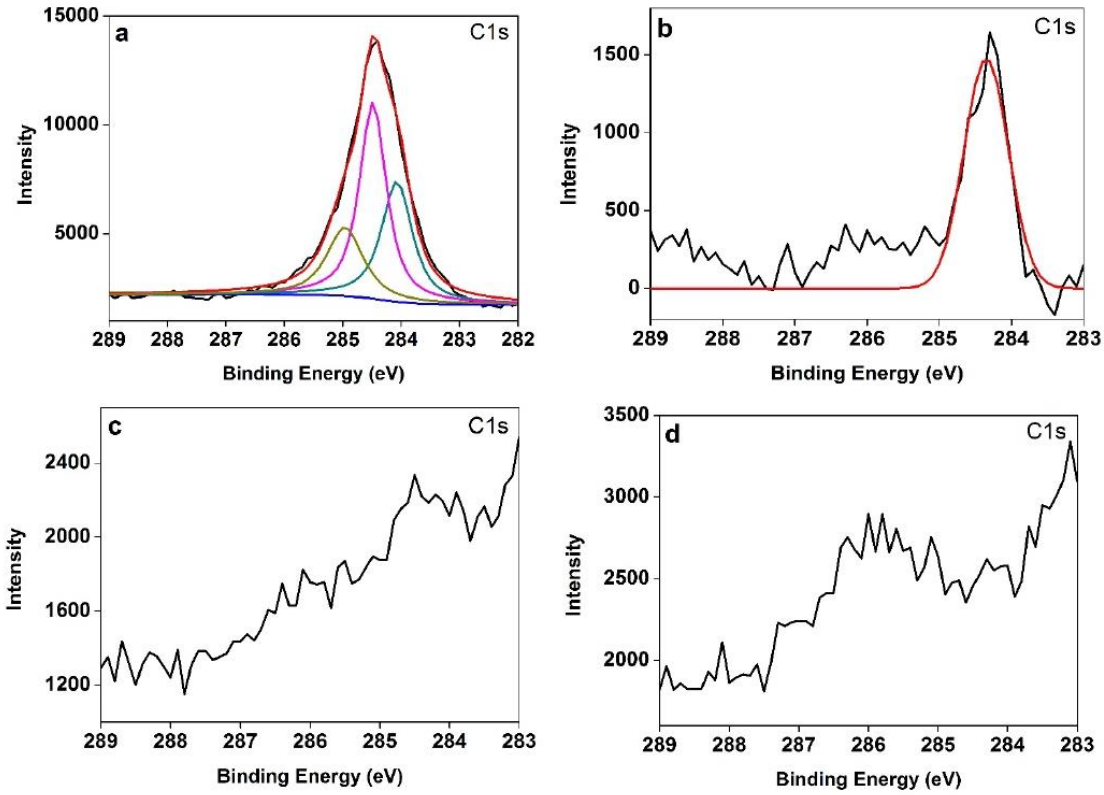

Fig. 4.3. C1s spectra obtained after Ni electro-deposition was carried out at (a) -0.3V (b) -0.6V (c) -0.8V (d) -1.2V.

4.3.2. TEM characterization

Fig. 4.4 shows the TEM images obtained from pure Au/C, $Ni_{-0.3V,\ 40min}$-Au/C, $Ni_{-0.6V,\ 40min}$-Au/C and $Ni_{-1.2V,\ 40min}$-Au/C. Pure Au/C consisted of spherical particles which are well dispersed on the C support (Fig. 4.4a). An analysis of 200 particles determined that the Au nanoparticles exhibited a narrow size distribution centred around 3 nm. Au nanoparticles continued to maintain their spherical shape even after undergoing Ni electro-deposition. Interestingly, thin crumpled Ni oxide sheets were observed in the TEM images of $Ni_{-0.6V,\ 40min}$-Au/C and $Ni_{-1.2V,\ 40min}$-Au/C (Fig. 4.4c and d), with the latter possessing a significantly greater quantity of these sheet like structures. Furthermore, the carbon support cannot be clearly seen in the TEM image of $Ni_{-1.2V,\ 40min}$-Au/C, which thus indicates that an extremely thick Ni layer was deposited onto Au/C when the applied potential was -1.2 V. This observation is further confirmed by the fact that the C1s XPS peak of $Ni_{-1.2V,\ 40min}$-Au/C was not detected during measurement (Fig. 4.3d).

$Ni(OH)_2$ sheet like structures possessing rough and wrinkled surface features were previously synthesized when Ni electro-deposition was carried out over zinc oxide nanorods (ZnO).[242, 243]

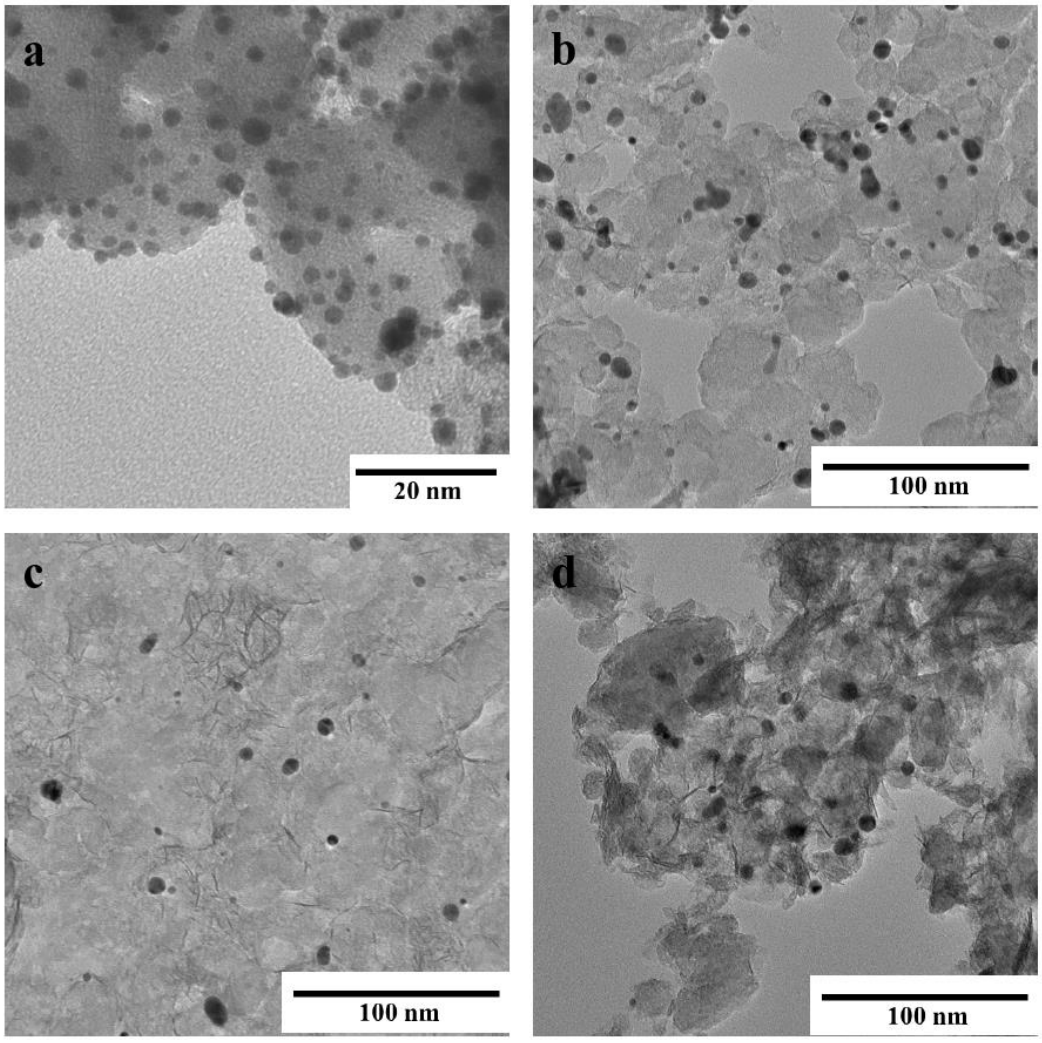

Fig. 4.4. TEM images obtained from (a) Au/C (b) $Ni_{-0.3V,\ 40min}$-Au/C (c) $Ni_{-0.6V,\ 40min}$-Au/C (d) $Ni_{-1.2V,\ 40min}$-Au/C.

4.4. Catalytic activity for glycerol electro-oxidation

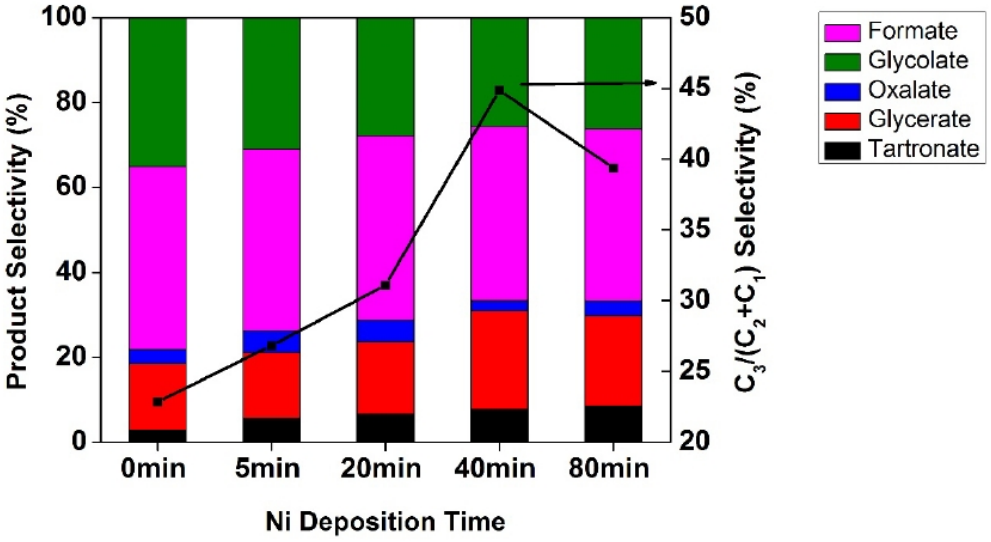

Fig. 4.5. Product and C3 selectivity achieved when glycerol electro-oxidation was carried out over (a) Au/C (b) $Ni_{-0.3V,\ 40min}$-Au/C (c) $Ni_{-0.6V,\ 40min}$-Au/C (d) $Ni_{-0.8V,\ 40min}$-Au/C (e) $Ni_{-1.2V,\ 40min}$-Au/C.

Carbon cloth electrodes containing Au/C underwent Ni electro-deposition at various applied potentials for 40 min. The as-prepared catalysts were then investigated for glycerol electro-oxidation, which was carried out at +0.3 V for 2 hours in 0.5 M glycerol + 0.5 M NaOH solution. Fig. 4.5 shows the relative product distribution and overall C3 selectivity obtained by each catalyst. Highest improvement in C3 selectivity occurred when Ni electro-deposition took place at -0.3 V. C3 selectivity achieved by $Ni_{-0.3V,\ 40min}$-Au/C (~45%) was about twice as high as that of pure Au/C (~23%). $Ni_{-0.3V,\ 40min}$-Au/C enabled enhanced conversion to glycerate and tartronate whilst simultaneously suppressing formate production. Au^+ species present in $Ni_{-0.3V,\ 40min}$-Au/C likely contributed to its enhanced C3 selectivity. In the same vein, Au^+ species are commonly generated in CeO_2 supported Au nanoparticles (Au/CeO_2). Furthermore, Au^+ was determined to be the active species in these catalysts. When Au/CeO_2 was applied to CO oxidation[217], water-gas shift[218, 219] and formaldehye oxidation[220] reactions, catalysts with higher Au^+ content gave rise to higher activity. The presence of a relatively thin Ni layer also facilitated ease of diffusion of the oxidation products away from the catalyst layer and thus

limited the extent of over-oxidation.[160, 187] In contrast, when Ni electro-deposition occurred at applied potentials more negative than -0.3 V, C3 selectivity of the resulting catalysts experienced a marked decrease relative to $Ni_{-0.3V,\ 40min}$-Au/C. C3 selectivity attained by $Ni_{-0.6V,\ 40min}$-Au/C, $Ni_{-0.8V,\ 40min}$-Au/C and $Ni_{-1.2V,\ 40min}$-Au/C ranged between 23-26% which is relatively similar to that obtained by pure Au/C (Fig. 4.5). The poorer C3 selectivity exhibited by this group of catalysts is due to their significantly higher Ni surface coverage, which in turn shielded the active Au species from the reactant media and severely limited their activity. On the other hand, the highly oxidized NiOOH was previously identified as the active species when carbon supported nickel nanoparticle catalysts (Ni/C) were tested for glycerol,[224, 225] sugar[244, 245] and alcohol[246, 247] (methanol and ethanol) electro-oxidation in alkaline media. However, in our system, it is apparent that the NiOOH catalytic sites were significantly less active than the catalytic sites present on Au nanoparticles. The thicker Ni surface coverage also hindered diffusion of the oxidation products away from the catalyst layer and thus encouraged over-oxidation to C1 and C2 side products.

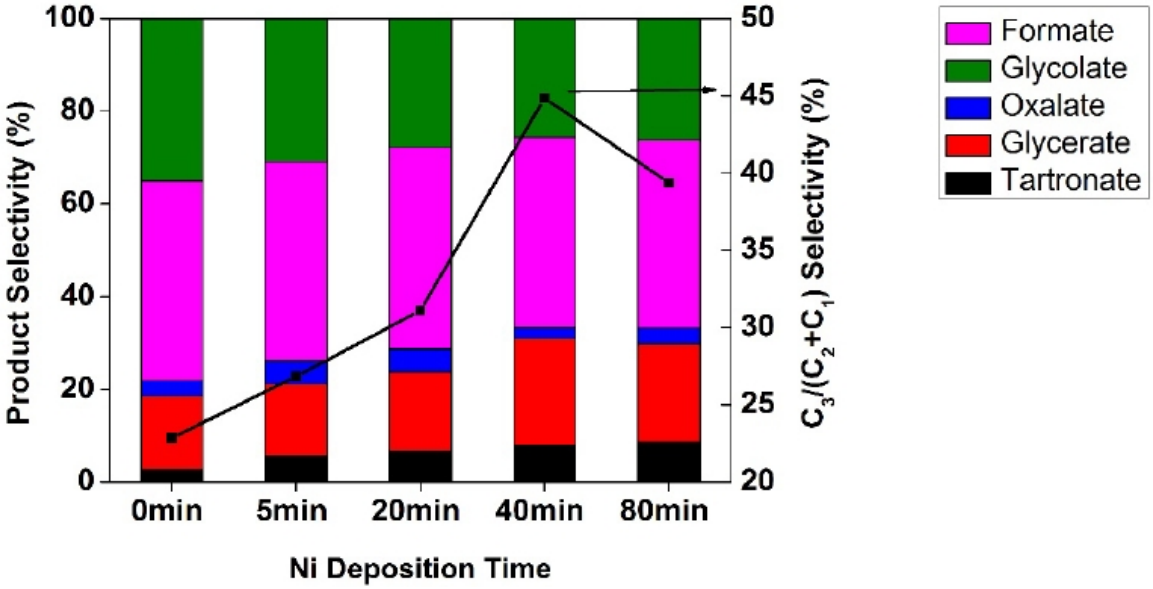

Fig. 4.6. Product and C3 selectivity achieved when glycerol electro-oxidation was carried out (a) Au/C (b) $Ni_{-0.3V,\ 5min}$-Au/C (c) $Ni_{-0.3V,\ 20min}$-Au/C (d) $Ni_{-0.3V,\ 40min}$-Au/C (e) $Ni_{-0.3V,\ 80min}$-Au/C.

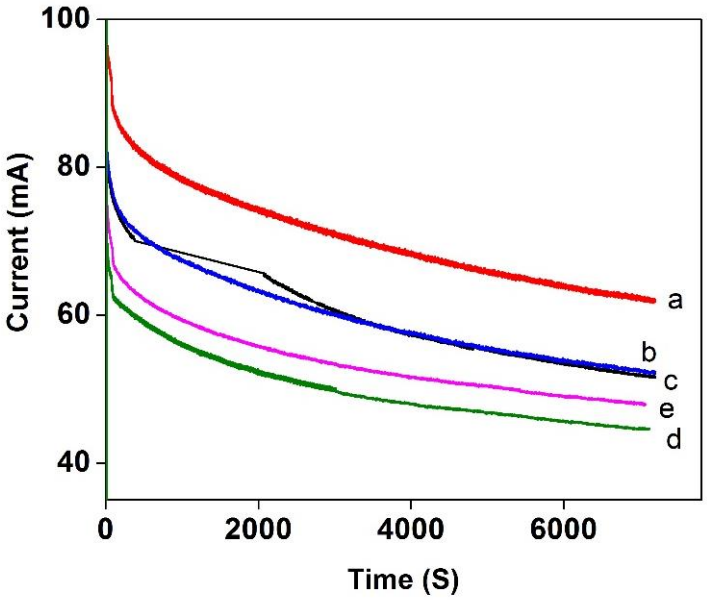

Fig. 4.7. Chronoamperograms obtained by a) $Ni_{-0.3V,\ 5min}$-Au/CB b) $Ni_{-0.3V,\ 20min}$-Au/CB c) Au/CB d) $Ni_{-0.3V,\ 40min}$-Au/CB e) $Ni_{-0.3V,\ 80min}$-Au/CB

Using -0.3 V as the optimal applied potential, deposition time was then varied between 5 and 80 min to determine its effect on the C3 selectivity. The resulting catalysts are denoted as $Ni_{-0.3V,\ tmin}$-Au/C where t represents the length of time which electro-deposition was carried out for. C3 selectivity with increased with increasing deposition time until it reached a maximum of 45% after Ni electro-deposition occurred for 40 min (Fig. 4.6). However, when Ni electro-deposition was carried out for an additional 40 min, C3 selectivity of $Ni_{-0.3V,\ 80min}$-Au/C decreased slightly to 39%. The longer electro-deposition time resulted in a thicker Ni layer on Au/C which was detrimental to C3 selectivity. Nonetheless, C3 selectivity of Au/C improved post Ni deposition and this is indicative of the synergistic effect between Au and the electro-deposited Ni species. Additionally, Ni electro-deposition did not significantly affect the electrochemical activity of Au/CB. Current obtained post deposition was relatively similar to that of Au/CB (Fig 4.7).

Table 4.3. Comparing C3 selectivity obtained from Au/C and $Ni_{-0.3V,\ 40min}$-Au/C when glycerol electro-oxidation was carried out at different applied potentials.

Applied Potential (V)	Sample	Product Selectivity (%)					$C_3/(C_2+C_1)$ selectivity (%)
		Tartronate (%)	Glycerate (%)	Oxalate (%)	Glycolate (%)	Formate	
0.1	Au/C	6.33	20.36	6.36	28.66	38.29	36.41
	$Ni_{-0.3V,\ 40min}$-Au/C	15.87	27.88	4.20	35.23	16.82	77.78
0.2	Au/C	4.20	16.84	5.52	33.34	40.11	26.65
	$Ni_{-0.3V,\ 40min}$-Au/C	7.97	25.49	2.85	25.36	38.34	50.28
0.3	Au/C	2.72	15.87	3.27	43.12	35.02	22.84
	$Ni_{-0.3V,\ 40min}$-Au/C	7.82	23.15	2.36	41.04	25.63	44.86
0.4	Au/C	1.55	14.36	2.10	43.84	38.16	18.92
	$Ni_{-0.3V,\ 40min}$-Au/C	6.05	17.51	2.36	42.91	31.17	30.82

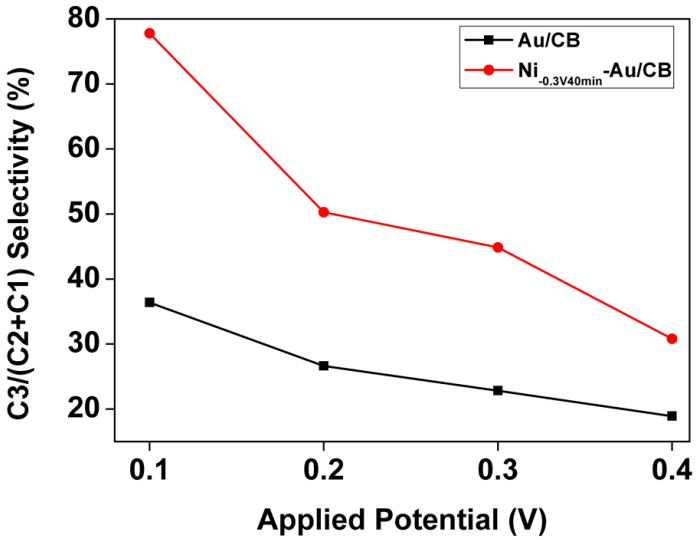

Fig. 4.8. Comparing the C3 selectivity of $Ni_{-0.3V,\ 40min}$-Au/C with that of pure Au/C over a range of potentials.

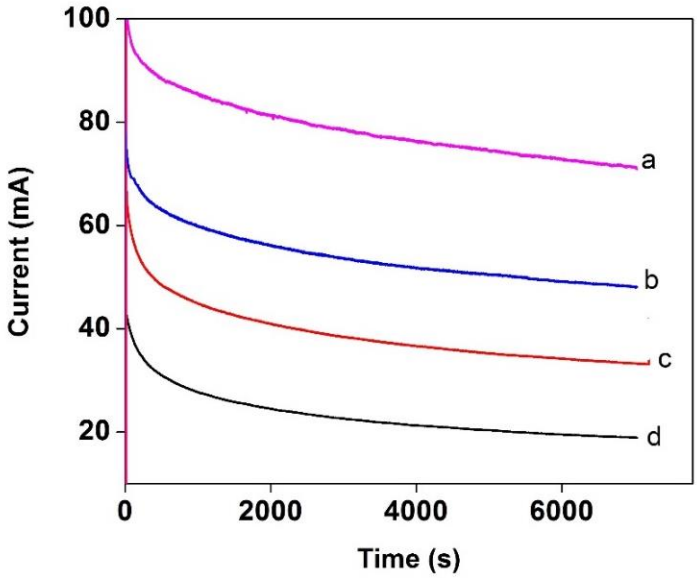

Fig. 4.9. Glycerol electro-oxidation chronoamperograms obtained by $Ni_{-0.3V,\ 40min}$-Au/CB at a) +0.4 V b) +0.3 V c) +0.2 V d) +0.1 V.

Lastly, C3 selectivity of $Ni_{-0.3V,\ 40min}$-Au/C was determined when glycerol electro-oxidation was carried out at different applied potentials. Table 4.3 lists the product distribution and C3 selectivity obtained by Au/C and $Ni_{-0.3V,\ 40min}$-Au/C at each applied potential tested. In general, selectivity decreased with increasing applied potential due to accelerated C-C bond cleavage at higher potentials (Fig. 4.7). Nevertheless, C3 selectivity of $Ni_{-0.3V,\ 40min}$-Au/C was higher than that of Au/C across the entire potential range tested. C3 selectivity of $Ni_{-0.3V,\ 40min}$-Au/C was highest when glycerol oxidation was carried out at 0.1 V. At this potential, C3 selectivity of $Ni_{-0.3V,\ 40min}$-Au/C was 78% and was about twice as high as that obtained by Au/C (36.41%). Notably, C3 selectivity obtained by $Ni_{-0.3V,\ 40min}$-Au/C continued to be twice as high as that of Au/C over the entire potential range tested (Table 4.3).

4.5. Conclusion

Electro-deposition of Ni species onto Au/C enhanced its C3 selectivity for glycerol electro-oxidation. Optimal C3 selectivity was obtained when Ni electro-deposition was carried out for 40 min at -0.3 V. Au^{+} species generated under these conditions likely contributed to the higher selectivity of this catalyst. Furthermore, at this potential, the Ni layer derived was sufficiently

thin such that the oxidation products could easily diffuse away from the catalyst layer after being generated. In contrast, when Ni electro-deposition occurred at applied potentials more negative than -0.3V, significantly larger amounts of Ni were deposited onto Au/C. The thicker Ni surface coverage partially shielded the Au nanoparticles from the glycerol solution and thus severely limited their activity. C3 selectivity of the Ni-Au/C catalysts prepared under these conditions were relatively similar to that of pure Au/C. Any possible synergistic effect between Au and Ni was thus nullified by the thick Ni surface coverage.

Chapter 5

Ag containing porous Au structures as highly selective catalysts for glycolate and formate

5.1. Introduction

Formic acid is an important chemical feedstock that is mostly used as a synthetic precursor or as a commercial product in the leather, agriculture and dye industries.[248] Formic acid is also a potential starting material for hydrogen production and also has the potential to power fuel cells to generate electricity.[249, 250] Formic acid is currently produced from toxic carbon monoxide and water through the carbonylation of NaOH at elevated pressures and temperatures. Production of formic acid from glycerol thus represents an environmentally friendly and cost efficient way to generate formic acid.

A small number of studies have demonstrated that the presence of silver (Ag) facilitates C-C-C bond breaking of glycerol and favours the formation of formic acid. When glycerol electro-oxidation was carried out over polycrystalline Ag electrode in alkaline medium, glycerate, glycolate and formate were the main products.[251] However, glycerol oxidation was hindered at electrode potentials higher than 1.13 V vs RHE after the first monolayer of Ag_2O forms on the electrode surface. Surface Ag_2O prevents adsorption of glycerol and OH^- species and the subsequent oxidation of glycerol.

In comparison, Tremiliosi-Filho and co-workers carried out glycerol electro-oxidation over carbon supported AuAg alloys (AuAg/C) in alkaline medium.[183, 252] FTIR studies confirmed that C-C-C bond breaking was favoured and formate was formed selectively. Notably, AuAg/C exhibited an onset potential that was 120 mV lower than that of Au/C. Improved electrochemical activity was attributed to the ligand effect as presence of Ag altered the electronic properties of Au by reducing the Au density of states close to the Fermi level. This in turn tuned the adsorption strength of adsorbates on the Au surface and increased energy

efficiency during catalysis. On the other hand, current density obtained by AuAg/C during glycerol electro-oxidation was nearly 10 times lower than that of Au/C. This is due to the segregation of Ag on the surface of the alloys which reduced the amount of available Au for catalysis. In fact, Ag/C nanoparticles were independently shown to be very poor catalysts for promoting glycerol oxidation while Au was the active species in the alloy that dictated the rate of reaction. Hence, in order to take advantage of high formic acid selectivity that Au-Ag based catalysts afford whilst maintaining high catalytic and electrochemical activity, it is important to design Ag containing catalysts which possess Au rich surfaces.

We carried out preliminary studies to determine the effect of electro-deposited Ag on the catalytic performance of Au/C. In agreement with previous reports, presence of Ag resulted in elevated levels of C-C bond cleavage and high selectivity to formate and glycolate was achieved. However, the thick layer of electro-deposited Ag present caused the resulting catalysts to suffer from poorer electrochemical activity relative to Au/C. Our preliminary studies also indicated that only a very small amount of Ag was required to tune the reaction pathway. High selectivity to formate and glycolate was observed regardless of electro-deposition time and applied voltage.

To circumvent the problem of poor electrochemical activity, the catalyst should be designed such that it possesses an Au rich surface and contain small amounts of Ag. The Au rich surface ensures high electrochemical activity whilst Ag directs C-C bond cleavage. Following this, the ability of residual Ag containing, porous Au structures to tune the glycerol oxidation pathway towards formate and glycolate whilst maintaining high electro-catalytic activity was examined. 3D porous Au structures were obtained by etching alloyed AuAg sheets in concentrated nitric acid solution. However, dealloying did not completely remove Ag and residual amounts remained embedded within the 3D framework. Our catalyst thus consisted of a porous Au rich framework that possessed residual amounts of Ag within its pores. When tested for glycerol

oxidation, the Ag containing porous Au catalyst exhibited high selectivity towards formate as well as high electrochemical activity. Catalytic performance of surface Ag rich porous structures was also examined. Surface Ag content was altered by annealing the porous Au structures at various temperatures. Annealing caused residual Ag to diffuse and precipitate onto the surface of the framework and the porous structures became increasingly Ag rich as annealing temperatures increased. Surface Ag rich structures exhibited significantly poorer electrochemical activity compared to surface Au rich structures however selectivity to formate improved.

5.2. Preliminary Studies

Preliminary studies were carried out to determine the effect of electro-deposited Ag on Au/CB. Preparation of Au/CB saturated carbon cloth working electrode was carried out in the same manner as detailed in detailed in our previous works (Chapter 3.2 and Chapter 4.2).

Ag electro-deposition process

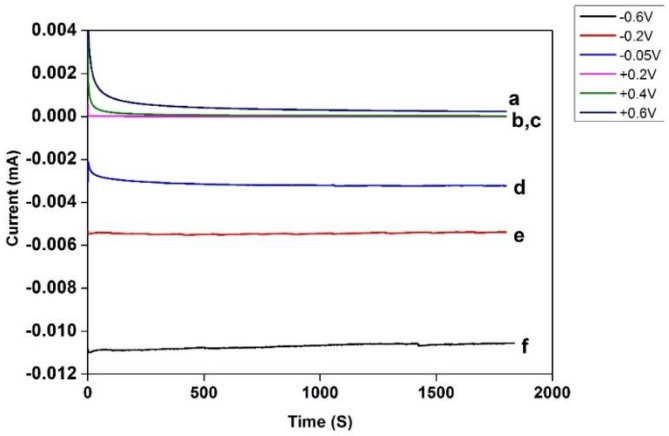

Fig. 5.1. Chronoamperomgrams for 30 min Ag electro-deposition over Au/CB at a) +0.6 V b) +0.4 V c) +0.2 V d) -0.05 V e) -0.2 V f) -0.6 V.

The carbon cloth working electrodes were immersed in a stock solution containing 50 mM silver nitrate ($AgNO_3$) dissolved in 50 mM ammonium hydroxide (NH_4OH) and held under constant potential for 30 min.[253, 254] Following that, the electrodes were rinsed thoroughly in DI water before being tested for glycerol electro-oxidation.

Ag electro-deposition over Au/CB was carried out over a range of potentials between +0.6 V to -0.6 V (Fig 5.1). The samples are labelled with the general formula $Ag_{V,\ 30min}$ -Au/CB whereby V denotes the Ag electro-deposition potential.

Formate and glycolate are the major products obtained, regardless of electro-deposition potential (Fig 5.2). Similar trends in product selectivity were also observed when Ag electro-deposition was carried out at -0.2 V for 30, 60 and 120 min respectively (Fig 5.3). These results are indicative that a small amount of Ag was sufficient to steer the catalytic pathway towards C-C bond cleavage.

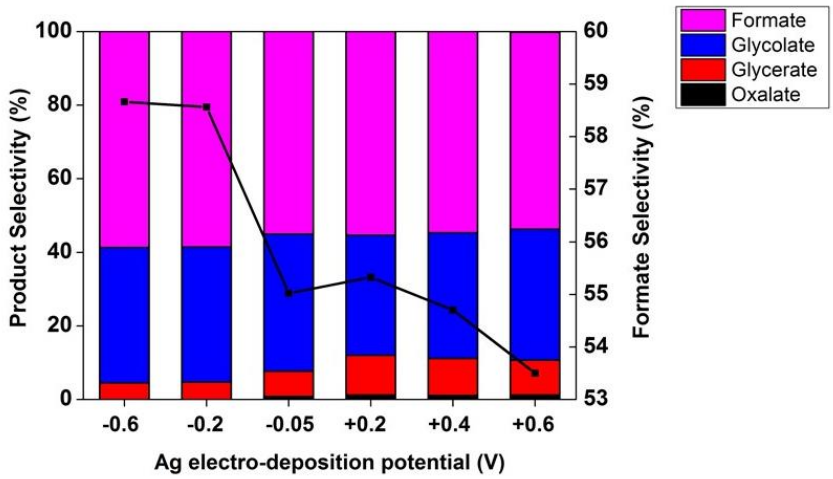

Fig. 5.2. Product and formate selectivity obtained when Ag electro-deposition was carried out at different potentials.

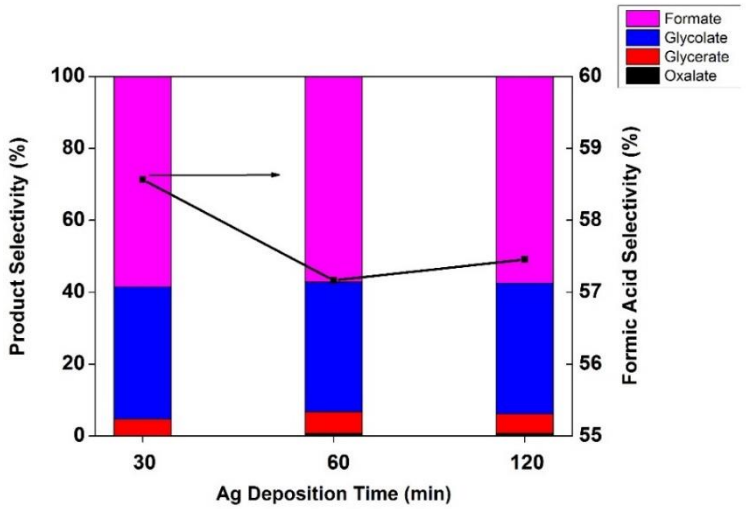

Fig. 5.3. Product and formate selectivity obtained when Ag electro-deposition was carried out at -0.2 V for 30, 60 and 120 min respectively.

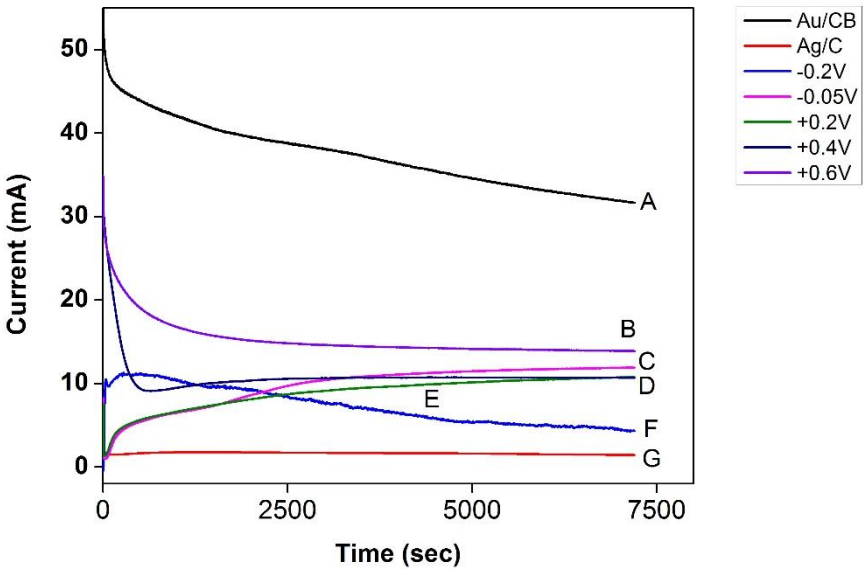

Fig. 5.4. Chronoamperograms obtained from a) Au/CB b) $Ag_{+0.6V,\ 30min}$-Au/CB c) $Ag_{-0.05V,\ 30min}$-Au/CB d) $Ag_{+0.4V,\ 30min}$-Au/CB e) $Ag_{+0.2V,\ 30min}$-Au/CB f) $Ag_{-0.2V,\ 30min}$-Au/CB g) Ag/C.

In line with reports on Ag based catalysts, our results also show that electrochemical activity of Au/CB for glycerol electro-oxidation suffers after Ag electro-deposition. Current obtained after Ag electro-deposition is significantly lower than that of pure Au/CB. Furthermore, Ag/C exhibited the lowest current (Fig 5.4). Given these findings, it was then determined that the catalyst should be designed such that it possesses an Au rich surface and contain small amounts of Ag. The Au rich surface ensures high electrochemical activity whilst Ag directs C-C bond cleavage. Following this, the ability of residual Ag containing, porous Au structures to tune the glycerol oxidation pathway towards formate and glycolate whilst maintaining high electro-catalytic activity was examined.

5.3. Experimental

5.3.1. Materials

Alloyed silver-gold (AuAg) sheets were purchased from Changhong Metals Ptd Ltd, China. The sheets were 0.1 mm thick, with both gold and silver possessing 99.99% purity. 1g of alloy was composed of 42 wt% Au and 58 wt% Ag.

All electrochemical reactions were conducted in a three electrodes cell which comprised of a stainless steel working electrode, Pt wire counter electrode and Ag/AgCl reference electrode. All potentials are reported with respect to the Ag/AgCl reference electrode.

5.3.2. Methods

5.3.2.1. Preparation of Au porous structures

The etching process consisted of floating the AuAg sheets (~0.5 cm x 1 cm) in concentrated nitric acid (69%) for a given amount of time. The sheets were then removed from the nitric acid solution (HNO_3) and thoroughly rinsed with DI water before oven drying at 80 ^oC for 30 min.

Following this, the dealloyed sheets were annealed for 2 h under argon atmosphere at a prescribed temperature. The as prepared catalysts were then tested for glycerol electro-oxidation by placing them in 15 ml of 0.5 M NaOH + 0.5 M glycerol solution under constant potential for 2 h. Subsequently, 2 mL of the solution was collected for high-performance liquid chromatography (HPLC) analysis.

5.3.2.2. Preparation of Ag/C reference catalyst

Ag/C was prepared via direct electro-deposition of Ag onto carbon cloth electrode (1.5 cm x 1.5 cm). The carbon cloth electrodes were immersed into stock solution containing 50 mM $AgNO_3$ dissolved in 1 M NH_4OH (28% NH_3 in H_2O). Ag electro-deposition was carried out at -0.2 V for 30 min. Following which the electrodes were rinsed thoroughly with water and tested for glycerol oxidation under the conditions mentioned above.

5.3.2.3. Preparation of Au/CB reference catalyst

4 nm Au nanoparticles supported on carbon black (Au/CB) were prepared as follows: $HAuCl_4 \cdot 3H_2O$ (1%; 1 mL) was added to deionised (DI) water (100 mL), and the solution was stirred vigorously for 1 min before the addition of 1% sodium citrate solution (1 mL). After an additional 1 min of vigorous stirring, freshly prepared, ice-cold 0.075 % NaBH4 in 1 % sodium

citrate (1 mL) was added quickly, and the solution was stirred for another 5 min before storage at 4 ^{o}C. Then, an appropriate amount of aqueous carbon black dispersion and Au nanoparticles solution were mixed under ultra-sonication for 1 h and stirred overnight. After 24 h, the pH of the solution was adjusted to below 2 by using 0.2 M HCl and stirred for another hour. Finally, the product was collected by filtration, washed three times with copious amounts of DI water and methanol then dried below 80 ^{o}C.

Preparation of carbon cloth working electrode: ~2.4 mg of Au/CB was dispersed in ethanol (1 mL) and 0.05 wt% Nafion solution (0.5 mL) by ultrasonication. This dispersion was then drop-cast onto CC to prepare a sample with a loading of around 1.07 mg cm^{-2}. The electrodes were dried overnight under ambient conditions before testing for glycerol electro-oxidation.

5.4. Results and discussion

5.4.1. Effect of catalyst pre-treatment and etching time on morphology

The most common way to generate porous structures with different porosities is to vary etching time.[255-257] Etching usually occurs by simply soaking the AuAg sheets in concentrated HNO_3 solution. However, long etching times result in coarsened structures due to fast diffusion of gold in the electrolyte. Hence, in order to fabricate porous Au structures with ligament sizes less than 6 nm, AuAg sheets are etched in concentrated HNO_3 under applied anodic potential.[258] Erlebacher and co-workers report that Ag is completely removed from the alloyed sheet after etching for 5 mins and the resulting framework contains pores centred around 8 nm. Furthermore, 15 mins of etching generated 15-20 nm sized pores while continued immersion caused the porosity length scale to approach the thickness of their original membrane (about 100 nm).[255] However, longer immersion times led to significant coarsening and the eventual collapse of the 3D structure into a 2D one. The porous framework also became more brittle.

Alternatively, porous Au structures with varying porosities can be attained by annealing the sheets under argon atmosphere after etching.[259-261] Li and Sieradzki reported that heating the

dealloyed samples between 100-900 ^{o}C resulted in a more than 2 orders of magnitude spread in the length scales of the microstructures. Furthermore, heat treatment before dealloying may also help to relieve the AuAg sheets of residual stresses developed during the cutting operation.[260, 262, 263]

Preliminary studies were conducted to determine the effect of treatment method on the morphology of the resulting porous structures. Influence of heat treatment prior to the etching process was examined by annealing the samples either at 800 ^{o}C for 2 h or at 900 ^{o}C for 12 h under argon atmosphere. Following this, the AuAg sheets were then etched in concentrated HNO_3 for either 5 or 60 mins to further determine if there was any effect of etching time on morphology and catalytic performance. The resultant catalysts were then dried and tested for glycerol electro-oxidation. FESEM images of the spent catalysts which were subjected to the treatment methods described above are shown in Fig. 5.5. The typical random porous 3D structure is observed in all the samples. As such, annealing the AuAg sheets prior to etching does not have a significant effect on the resultant morphology. Fig. 5.6a and c show the samples which were dealloyed for 5 min but annealed prior at 800 ^{o}C for 2 h and 900 ^{o}C for 12 h respectively. Both samples contained pores which were up to 4 nm in length. Pore size increased with etching time. The extent of increase was also influenced by annealing conditions. Pores were mainly between 10-20 nm when the samples were annealed at 800 ^{o}C for 2 h followed by etching for 60 min (Fig. 5.6b). On the other hand, when the AuAg sheets were pre-heated at 900 ^{o}C for 12 h before being etched for 60 min, the resulting sample consisted of interconnected, elongated pores which were tens of nm in length, with some pores reaching up to 100 nm. However, long etching times in both cases caused the samples to become extremely brittle and fragmented easily upon handling. Hence, tuning porosity by varying etching time and is not a feasible way to generate samples that can be easily handled for catalytic testing.

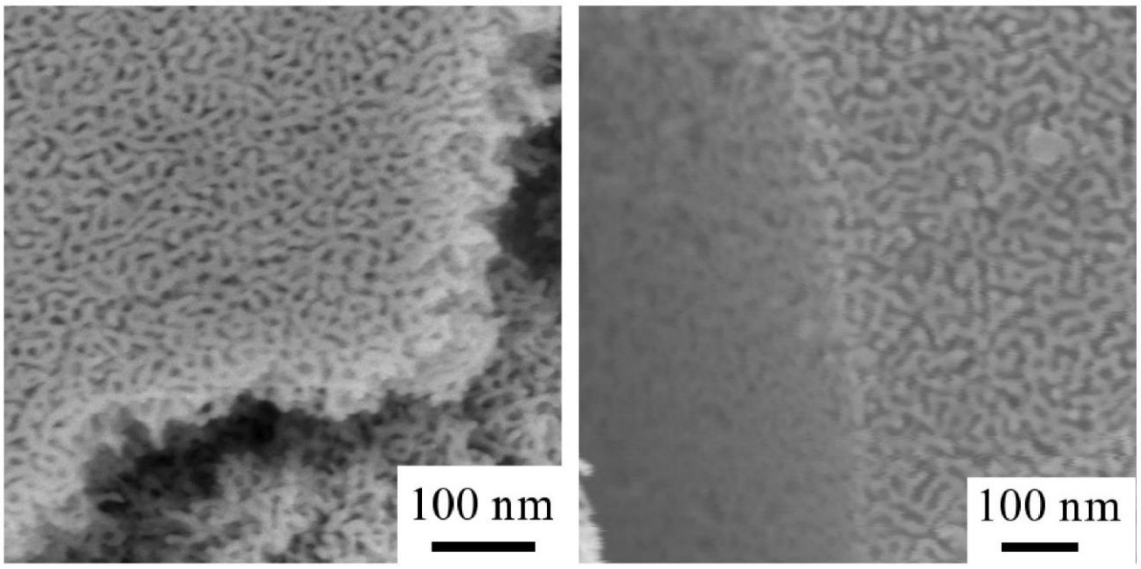

Fig. 5.5. FESEM images of porous Au samples annealed at 900 ^{o}C for 12 h before dealloying for 60 min.

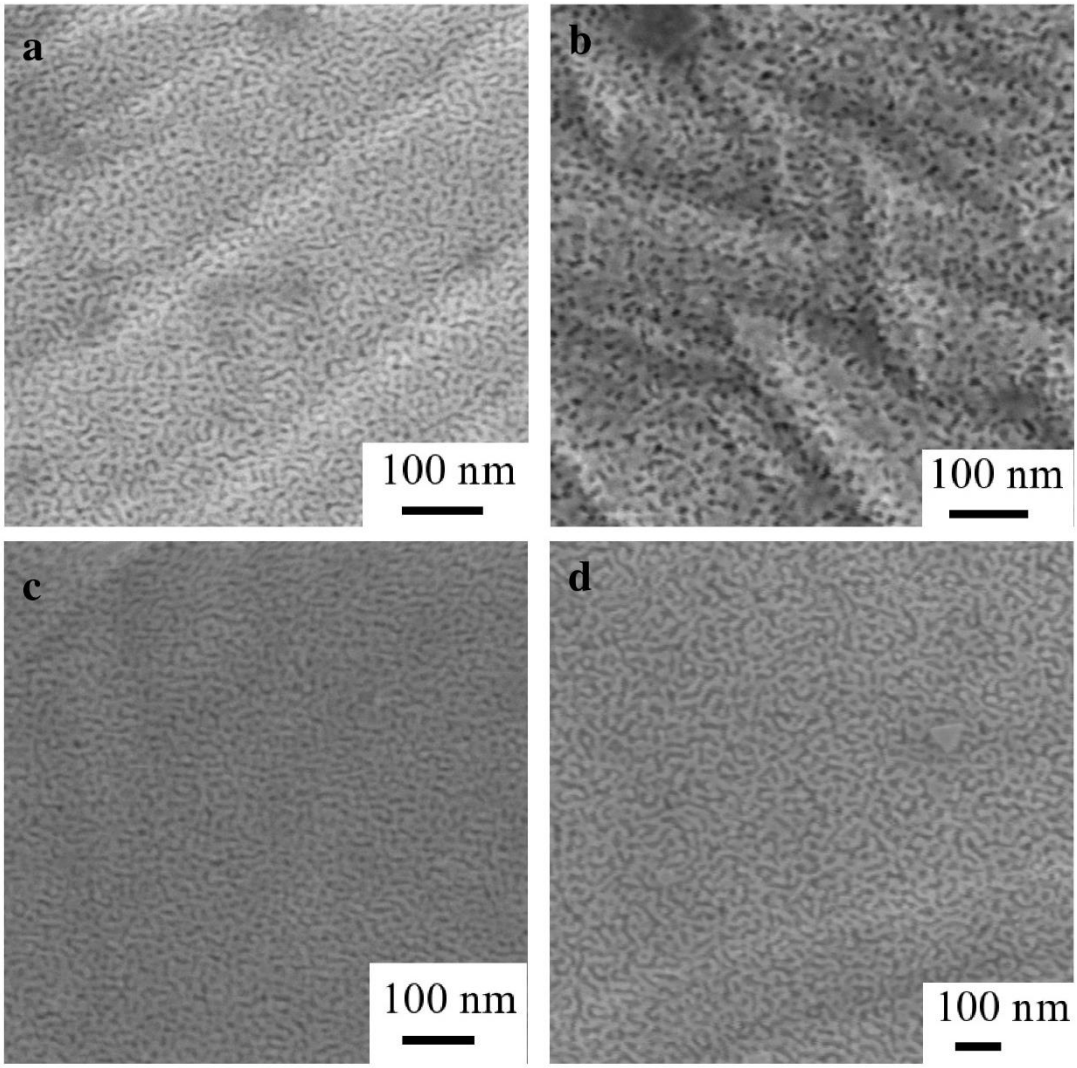

Fig. 5.6. FESEM images of porous Au samples that were heat treated at 800 ^{o}C for 2 h before dealloying for a) 5 min b) 60 min. FESEM images of porous Au samples that were heat treated at 900 ^{o}C for 2 h before dealloying for c) 5 min d) 60 min.

5.4.2. Effect of etching-annealing method on morphology and catalytic performance

Next, we attempted to vary porosity using the etching – annealing method. Etching time was initially kept at 5 min and subsequent annealing took place at either 100 ^{o}C or 600 ^{o}C for 2 h, under argon atmosphere. The as-prepared samples were then tested for glycerol electro-oxidation. Fig. 5.7 shows the FESEM images of spent catalysts prepared under the conditions described above. The silver coloured AuAg alloyed sheets became copper coloured after floating in concentrated HNO_3 solution. As observed in fig 5.3b, 5 min of dealloying followed by annealing at 100 ^{o}C for 2 h generated pores in the range of 20-30 nm. In comparison, the

samples which were only etched for 5 min possessed pores that reached a maximum of 4 nm. Elevating annealing temperature to 600 ^{o}C caused extensive morphological changes in the sample. The 3D random porous structure that was observed in all the previous samples was noticeably absent. Instead of being perforated with numerous small pores, the surface of 3D structure was largely flat but divided by deep gorges and a few large pores. (Fig. 5.8). This was likely due to extensive fusion of the Au ligaments during heating at such high temperatures. Pores generated at 600 ^{o}C were significantly larger than those generated at 100 ^{o}C; the 4 pores featured in fig 5.3c range between 300-450 nm. On another note, samples prepared by this etching-annealing method became more ductile instead of brittle after treatment. Consequently, the sheets did not easily fragment even when handled with tweezers. Given the ease of product handling and the ease of generating samples with varying porosity, we carried out further variations of this method to optimize our results.

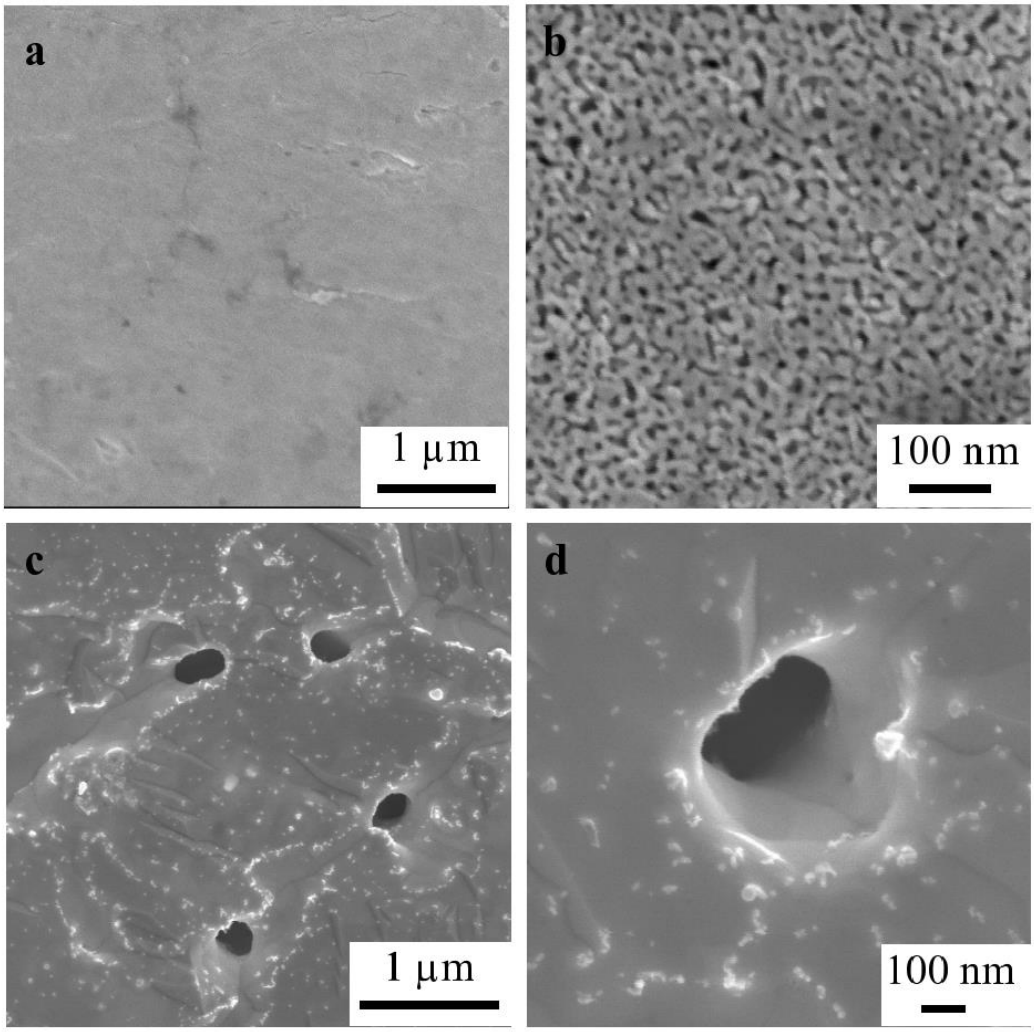

Fig. 5.7. FESEM images of the porous Au structure that was etched for 5 min followed by heating at a-b) 100 ºC and c-d) 600 ºC.

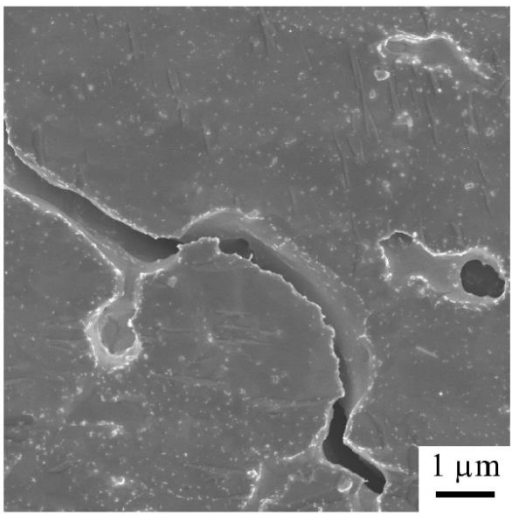

Fig. 5.8. FESEM image evidencing the deep gorge present in the sample that was prepared by etched for 5 min followed by annealing at 600 ºC for 2 h.

Subsequently, etching was carried out for 15 min followed by annealing at 100 ^{o}C or 600 ^{o}C. These catalysts were then tested for glycerol electro-oxidation and their catalytic performance was compared vis-à-vis samples that were dealloyed for 5 min but annealed at the same temperature. FESEM results of catalysts prepared under these conditions are presented and discussed below. The samples are labelled with the general formula Au(t)_tempt where t indicates the etching time and tempt represents the annealing temperature.

HPLC studies show that formic acid was the dominant product generated in all cases (Fig. 5.9). Given that catalysts prepared under different annealing conditions have distinctly different morphologies, these results are indicative that product selectivity is not controlled by the morphology or porosity. Notably, increasing annealing temperature from 100 ^{o}C to 600 ^{o}C resulted in almost 100% conversion to glycolic acid and formic acid. On the other hand, electrochemical activity was strongly influenced by annealing temperature and thus catalyst morphology (Fig. 5.10). Samples which were annealed at 100 ^{o}C exhibited markedly higher electrochemical activities compared to those annealed at 600 ^{o}C. For example, the glycerol oxidation current obtained by Au15_100 (53.2 mA) was nearly 10 times higher than that generated by Au15_600 (5.53 mA). Furthermore, samples which were etched for 15 min were generally more active than those which were only etched for 5 min. Taken together, these 2 results indicate that glycerol electro-oxidation activity is dependent on Au content and surface area of exposed Au. Samples with higher Au content (longer etching time) and greater exposed Au surface area (lower annealing temperature) are more active for glycerol electro-oxidation. Hence for our subsequent investigations, we fixed etching time at 15 min whilst varying annealing temperature to further optimize our results.

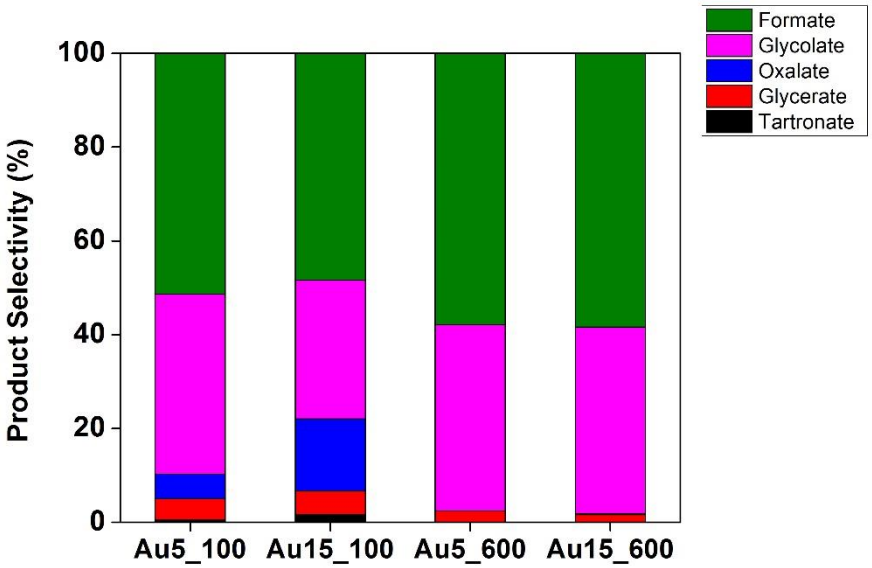

Fig. 5.9. Glycerol electro-oxidation in alkaline medium using catalysts prepared at different conditions.

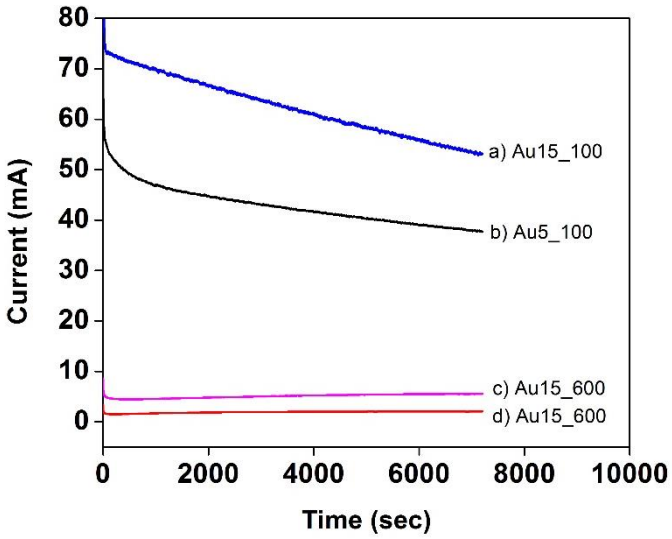

Fig. 5.10. Chronoamperograms of samples of a) Au15_100 b) Au5_100 c) Au15_600 d) Au5_600.

5.4.3. Effect of annealing temperature on morphology

For the samples discussed herein, etching time was fixed at 15 min whilst annealing temperature was varied between 100-900 ^{o}C to further investigate the effect of annealing temperature on catalytic performance. Annealing was carried out for 2 h under argon atmosphere. FESEM images of freshly prepared catalysts are presented in Fig. 5.11.

3D random porous structure was generated after 15 min of etching and most pores fall in the range of 10-20 nm (Fig. 5.11a). After etching the initially silver coloured AuAg sheets became

copper coloured and this is in line with the observations made by Erlebacher and co-workers.[255] There were no significant changes in pore size when the sample was annealed at 100 ^{o}C and pores remained in the range of 10-20 nm (Fig. 5.11b). Further increasing annealing temperature to 300 ^{o}C caused pore size to increase significantly and most pores were few hundreds of nm in length. Additionally, small, well dispersed particles were observed on the surface of the porous framework (Fig. 5.11c, indicated by red arrows). The copper coloured dealloyed sheets reverted back to being silver coloured after annealing occurred at 600 ^{o}C and 900 ^{o}C. FESEM shows that annealing at 600 ^{o}C caused extensive fusion of the Au ligaments in the porous framework (Fig. 5.11f). The sample appeared to be devoid of the 3D random porous architecture observed in the 15 min dealloyed sample. Instead, it consisted of very large Au ligaments with pores in the micrometre length scale. Notably, the 3D structure was maintained even after annealing at such high temperatures. Similar to the 300 ^{o}C annealed sample, the surface of the 600 ^{o}C annealed sample was also covered with numerous, small particles (Fig. 511f). These surface irregularities (pimples) have been attributed to a pinning effect on the surface diffusion of gold atoms when nanoporous Au is annealed at medium temperature range (between 400 ^{o}C to 600 ^{o}C) after dealloying. The pinning effect may be caused by residual acid or silver nitrate on the nanoporous Au surface.[261]

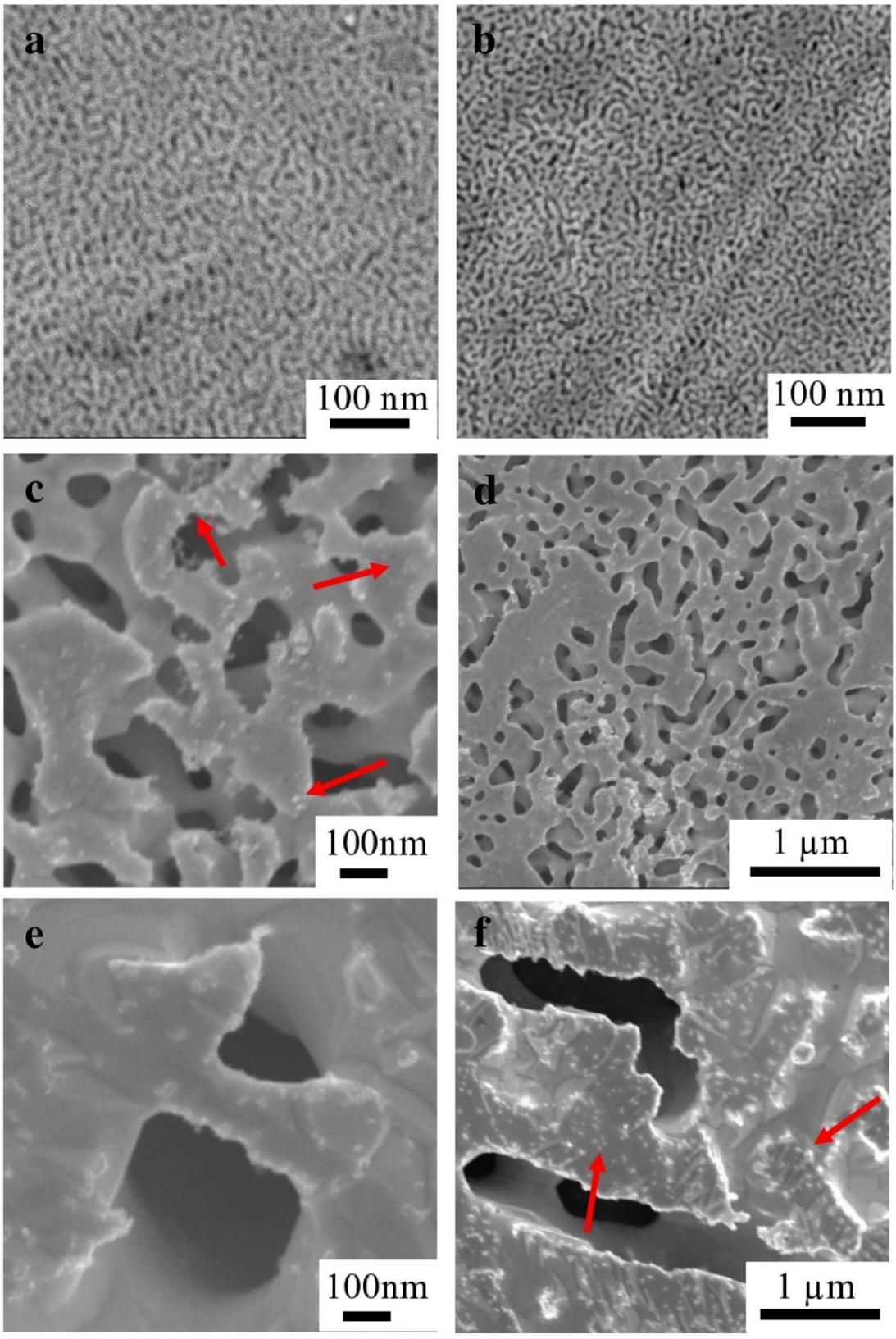

Fig. 5.11. FESEM images of the samples obtained after etching for 15 min in concentrated nitric acid and subsequent annealing at a) no annealing b) 100 ^{o}C c-d) 300 ^{o}C e-f) 600 ^{o}C.

5.4.4. EDX and XPS Analysis

Energy dispersive x-ray spectroscopy (EDX) was used to analyze the bulk composition of the spent catalyst. Table 5.2 to 5.5 and their corresponding SEM figures present the average Ag and Au atomic and mass ratios for each sample. Averaged atomic and mass ratios for each sample is recorded in table 5.1. The samples are notated in the form Au(t)_tempt, where t represents the dealloying time in mins and tempt represents the annealing temperature in degrees celsius.

1 g of AuAg alloy consisted of 42.0 wt% Au and 58.0 wt% Ag, as specified by the manufacturer. Au content increased significantly after the AuAg sheet was etched for 15 min in concentrated HNO_3 and relative mass of Au increased to 92.9% in Au15. Additionally, surface Au content of Au15 decreased with increasing annealing temperature whilst surface Ag content increased (Table 5.1). These 2 trends reflect the fact that etching in concentrated HNO_3 did not completely remove Ag and some amounts of residual Ag remained confined within the nanoporous structure.[264] In fact, nanoporous Au can be considered as an Au-rich Ag−Au alloy as Ag is never completely removed during the leaching process.[265] As such, when Au15 was annealed, residual Ag, driven by a chemical potential gradient, diffused onto the surface of the porous structure and precipitated there. Thus, an apparent increase in Ag content from 7.06% in Au15 to 37.47% in Au15_600 was observed.

Table. 5.1. Average mass (%) and atomic (%) ratios of the different samples by EDX, derived from an average of 5 different areas.

Sample	Mass (%)		Atom (%)	
	Ag	Au	Ag	Au
Au15	7.06	92.94	12.12	87.88
Au15_100	14.81	85.19	24.06	75.94
Au15_300	23.07	76.93	35.34	64.66
Au15_600	37.47	62.53	52.14	47.86

X-ray photoelectron spectroscopy (XPS) was utilized to analyse surface composition of the catalysts prepared under different conditions. Fig. 5.16 presents the deconvoluted Ag and Au peaks for the respective samples. All binding energies were referenced to the adventitious C1s line at 284.8 eV. $Au4f_{7/2}$ peak for all 5 samples, including the AuAg alloy, could be deconvoluted into 2 peaks located at binding energy (BE) of 84.0 eV and 84.8 eV. These 2 peaks are assigned to Au (0) and Au(I) species respectively. On the other hand, the Ag $3d_{5/2}$ peak for is located at 368.2 eV for all the samples and this is typical of pure metallic Ag (0) species. Additionally, an oxidized Ag(I) species was generated after the annealing process and an additional peak around 368.8 eV was observed in Au15_100, Au15_300 and Au15_600 (Fig. 5.16 e, g and i respectively). Ag(I) elemental concentration was between 10-14% in the 3 samples (Table 5.5). Presence of Ag(I) is attributed to the adsorption of O atoms on undercoordinated surface Ag atoms when the samples were exposed to air.[266] Oxidation of Ag(0) to Ag(I) did not occur during annealing due to the low thermal stability of Ag_2O, which thermally reduces back to Ag(0) at high temperatures.[267] Furthermore, annealing was carried out under argon gas which precludes the oxidation of Ag.

More importantly, our XPS and EDX results agree with each other. XPS also shows that the sample surface becomes more Ag rich as annealing temperature increases. Table 5.5 summarizes the respective elemental surface compositions (atom%) of each sample. Ag/Au atomic ratio of the AuAg alloy was 1.92. After etching, the Ag/Au atomic ratio for Au15 decreased significantly to 0.26. Thus, Au15 is composed of an Au rich surface, with small amounts of residual Ag. However, Ag/Au atomic ratio of the annealed samples increased with increasing annealing temperature. Ag/Au atomic ratio of Au15_100 increased slightly to 0.51 while the atomic ratio for Au15_600 was 1.68. This indicates that Au15_100 still possessed a relatively Au rich surface even though some amounts of Ag had deposited onto the sample

surface during low temperature annealing. In comparison, Au15_600 was overwhelmingly Ag rich and its Ag/Au atomic ratio was relatively close to that of AuAg alloy.

Taken together, our EDX and XPS results evidence that residual Ag which was initially embedded within the porous structure melted during annealing and precipitated onto the surface of the porous framework. As annealing temperature increased, more Ag precipitated onto the surface of the framework and resulted in higher Ag/Au atomic ratios.

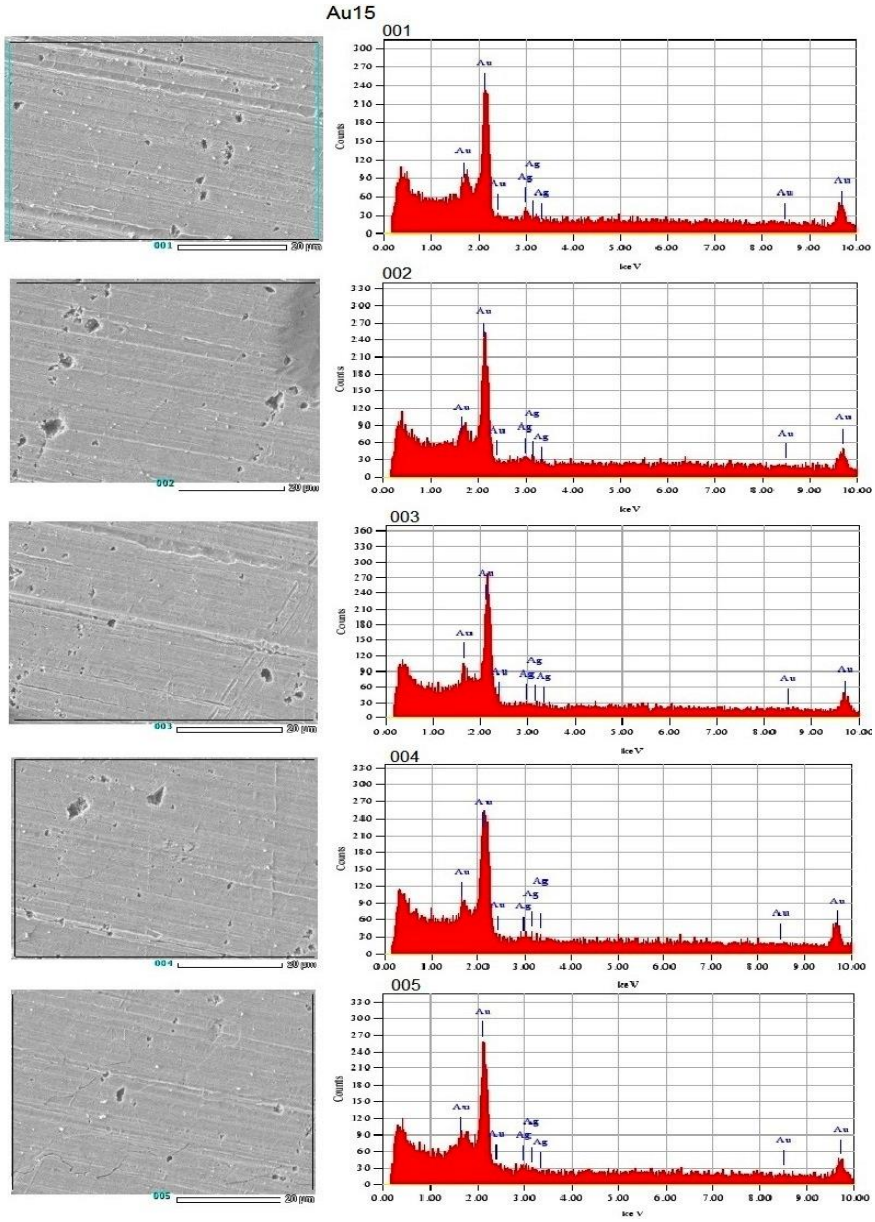

Fig. 5.12. SEM-EDX obtained from 5 different areas on Au15.

Table 5.2. Mass (%) and atomic (%) ratios of Au15.

Au15	**Mass (%)**		**Atom (%)**	
	Ag L	**Au M**	**Ag L**	**Au M**
1	7.32	92.68	12.60	87.40
2	10.34	89.66	17.40	82.60
3	7.05	92.95	12.16	87.84
4	3.93	96.07	6.95	93.05
5	6.64	93.36	11.50	88.50
Average	7.06	92.94	12.12	87.88

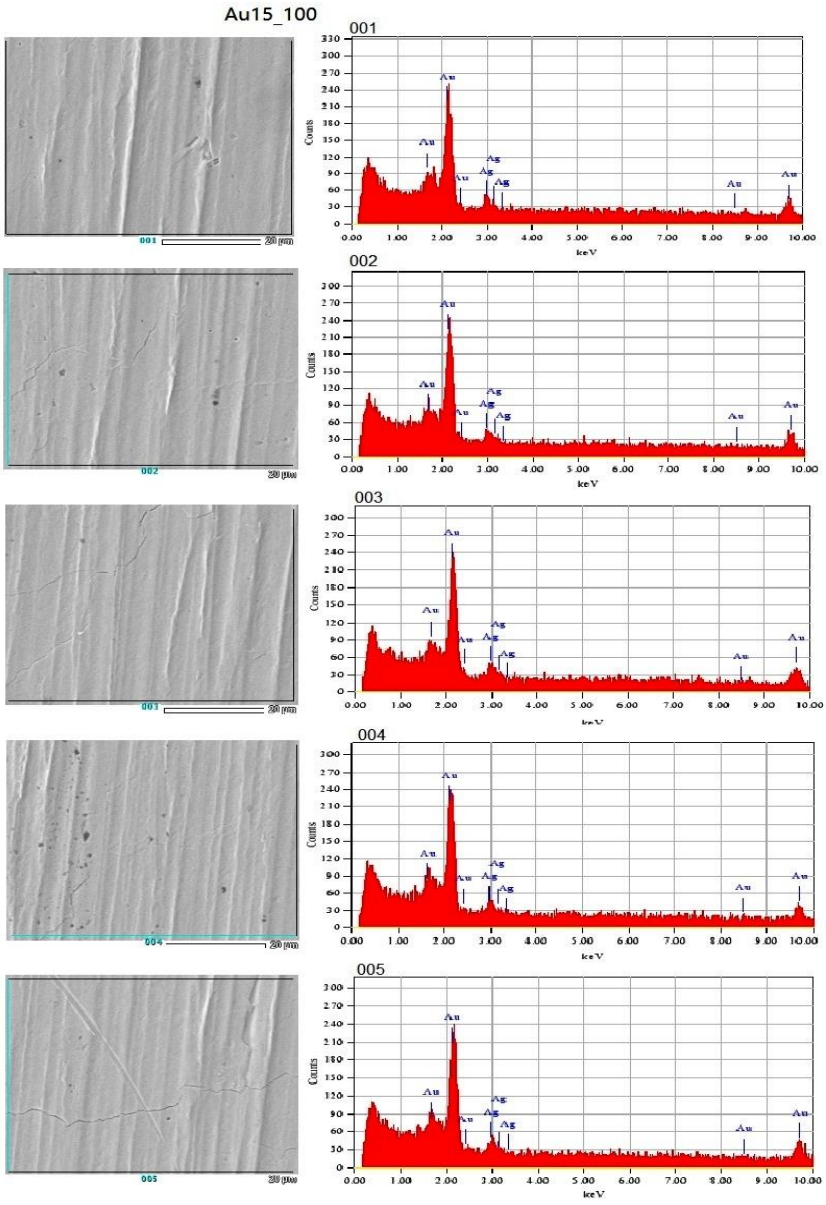

Fig. 5.13. SEM-EDX for Au15_100.

Table 5.3. Mass (%) and atomic (%) ratios of Au15_100.

Au15_100	Mass (%)		Atom (%)	
	Ag L	Au M	Ag L	Au M
1	16.51	83.49	26.53	73.47
2	13.90	86.10	22.76	77.24
3	16.26	83.74	26.18	73.82
4	15.46	84.54	25.03	74.97
5	11.90	88.10	19.78	80.22
Average	14.81	85.19	24.06	75.94

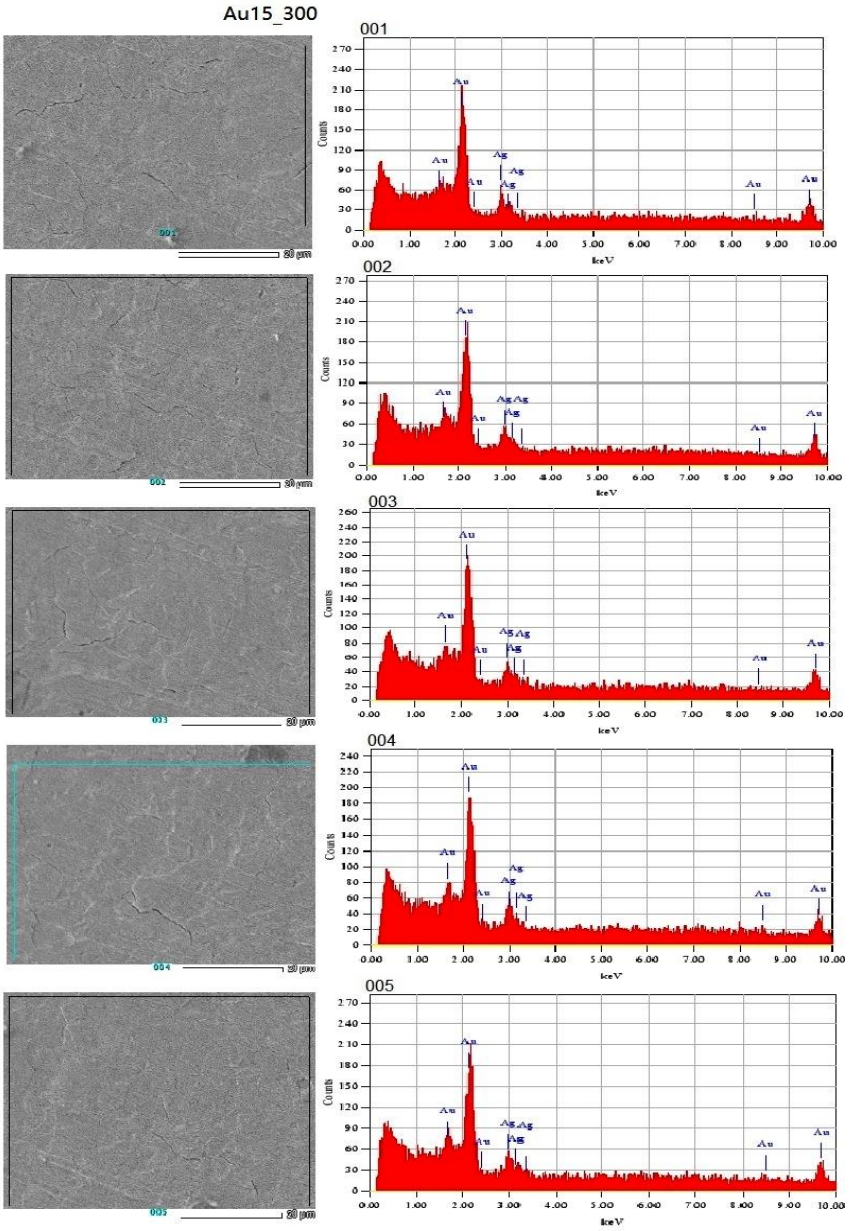

Fig. 5.14. SEM-EDX for Au15_300.

Table 5.4. Mass (%) and atomic (%) ratios of Au15_300.

Au15_300	Mass (%)		Atom (%)	
	Ag L	Au M	Ag L	Au M
1	23.45	76.55	35.87	64.13
2	24.60	75.40	37.34	62.66
3	19.11	80.89	30.13	69.87
4	25.58	74.42	38.56	61.44
5	22.62	77.38	34.81	65.19
Average	23.07	76.93	35.34	64.66

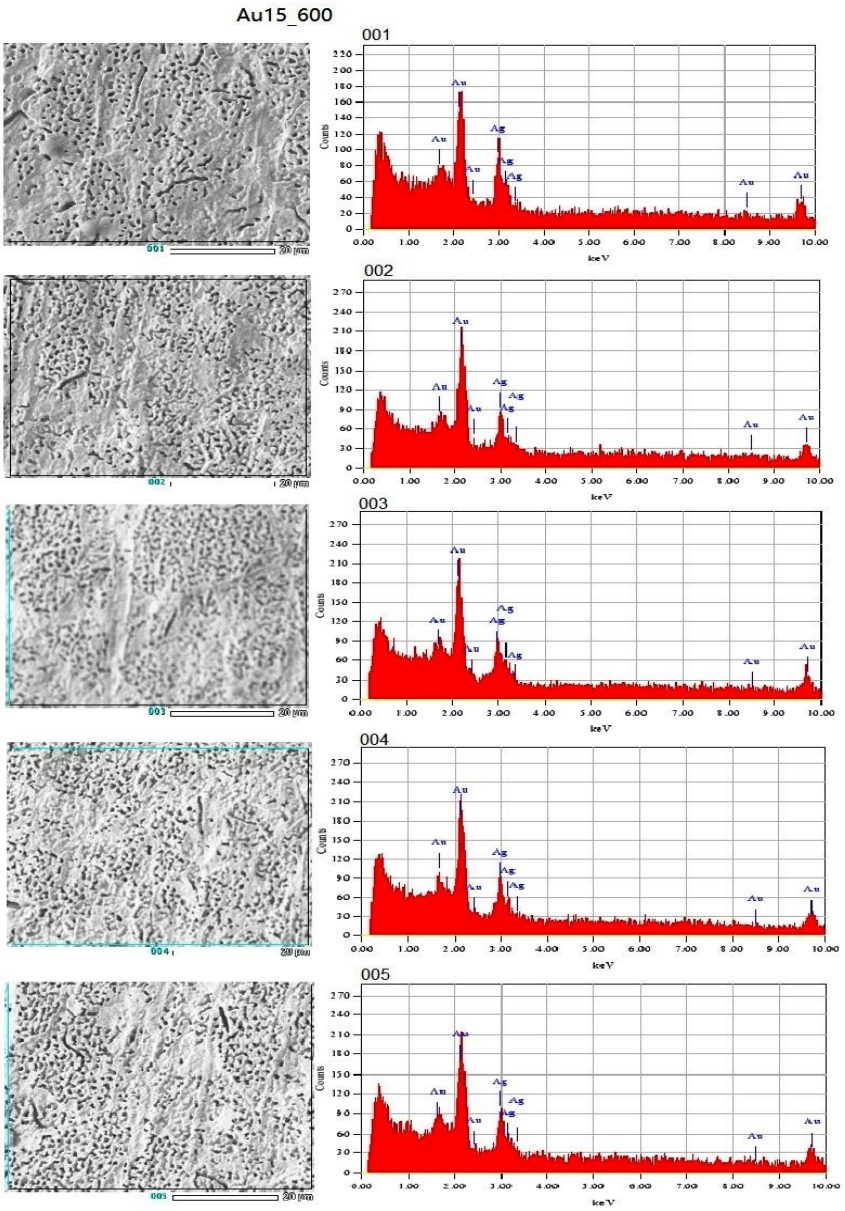

Fig. 5.15. SEM-EDX for Au15_600.

Table 5.5. Mass (%) and atomic (%) ratios of Au15_600.

Au15_600	Mass (%)		Atom (%)	
	Ag L	Au M	Ag L	Au M
1	40.17	59.83	55.07	44.93
2	39.04	60.96	53.90	46.10
3	30.42	69.58	44.39	55.61
4	41.20	58.80	56.13	43.87
5	36.51	63.49	51.22	48.78
Average	37.47	62.53	52.14	47.86

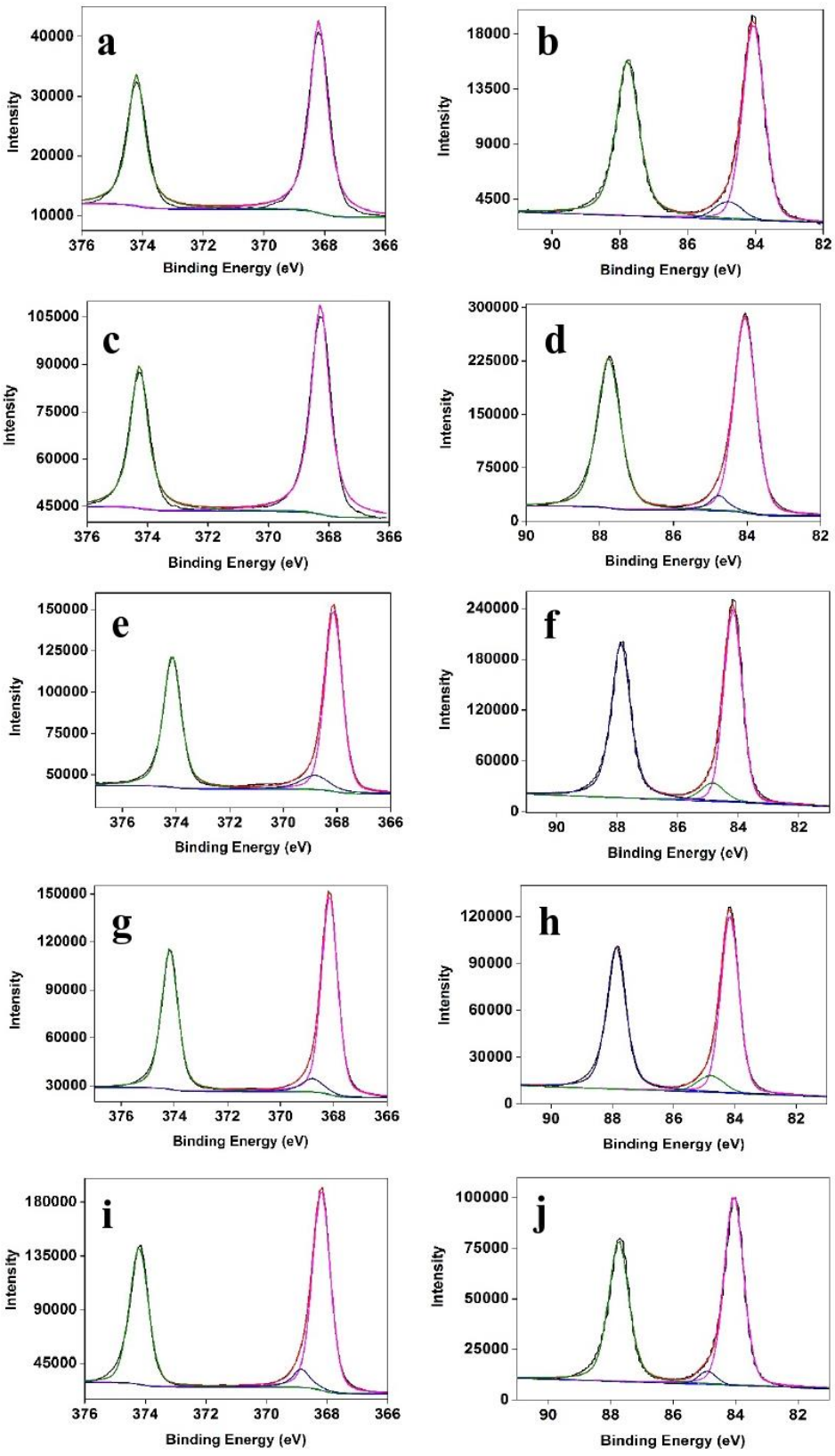

Fig. 5.16. XPS data. Ag $3d_{5/2}$ spectra for a) AuAg c) Au15 e) Au15_100 g) Au15_300 i) Au15_600; Au $4f_{7/2}$ spectra for b) AuAg d) Au15 f) Au15_100 h) Au15_300 j) Au15_600.

Table 5.6. Relative Au and Ag concentrations for samples prepared under different conditions. Elemental concentrations are expressed as atomic percentage (at.%).

Sample	Ag (element concentration, at. %)		Au (element concentration, at. %)		Ag/Au atomic ratio (%)
	Ag^0	Ag^+	Au^0	Au^+	
AuAg	100	0	90.46	9.54	1.92
Au15	100	0	92.46	7.54	0.26
Au15_100	86.20	13.80	87.93	12.07	0.51
Au15_300	90.41	9.59	88.59	11.41	1.07
Au15_600	90.06	9.94	94.49	5.51	1.68

5.4.5 Voltammetric characterization of porous Au-Ag alloys

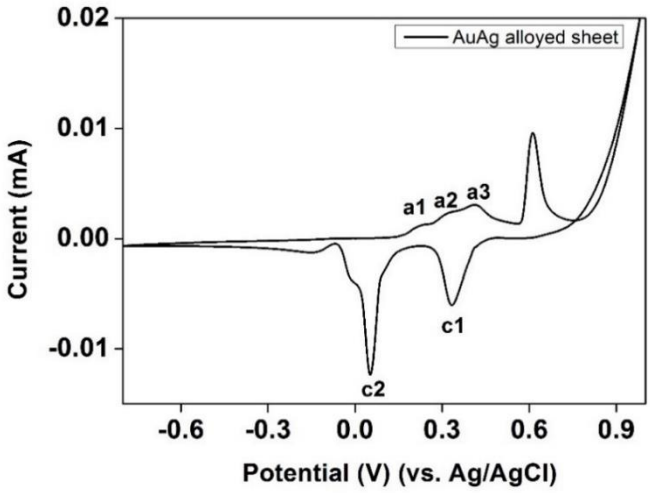

Fig. 5.17. CV obtained when the AuAg alloyed sheet was cycled in 1 M NaOH.

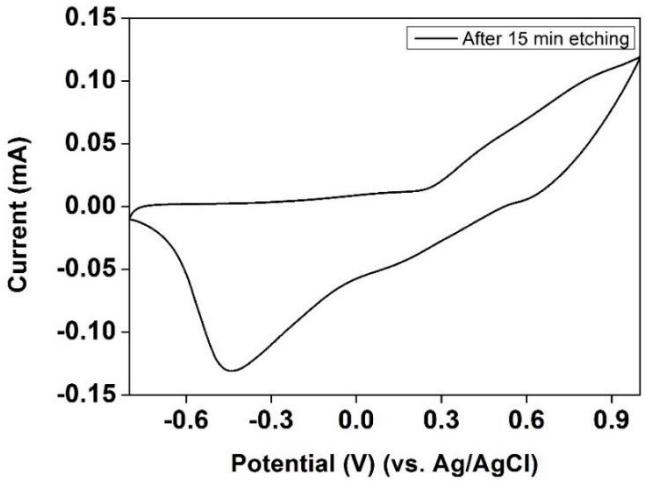

Fig. 5.18. CV obtained after the AuAg sheet was etched for 15 min. The sample was cycled in 1 M NaOH.

Fig. 5.17 shows the characteristic voltammetric behaviour of the AuAg sheet when cycled in 1 M NaOH. Shape of the cyclic voltammogram (CV) is similar to that reported for polycrystalline Ag electrodes[251, 268] and supported Ag nanoparticles[269] when cycled under alkaline conditions. Two main pairs of redox peaks (a1 and c1; a3 and c2) are observed in the CV. These peak pairs arise due to successive surface oxidation of the Ag electrode from Ag (0) to Ag (II) during the anodic scan, with oxidation to Ag(I) oxides represented by the intermediate peak, a2. Correspondingly, Ag (II) and Ag (I) are reduced to Ag (I) and Ag (0) respectively during the subsequent cathodic scan.

Surface oxidation of the Ag from Ag (0) to Ag (I) (peak a2) and the reduction of Ag_2O to Ag (0) (c2) coincides with the redox peaks of polycrystalline Au electrode. When polycrystalline Au electrode is cycled in alkaline media, it generates a pair of redox peaks at 0.3 V and 0.08 V (vs. SCE). The former peak is associated with surface oxidation of Au (0) to Au (I) oxides during the anodic scan while the latter peak is associated with the subsequent reduction of Au (I) back to Au (0) during the cathodic scan. It is likely that the redox peaks associated with the oxidation and reduction of Au were shielded by the redox peaks of Ag species as they possessed higher peak currents. Hence, redox peaks typically associated with polycrystalline Au electrodes cannot be clearly distinguished from the Ag redox peaks in the CV.[270] Selective dissolution of Ag resulted in great changes in the CV profile, even though the etching time was only 15 min (Fig. 5.18). Shape of the CV obtained for the 15 min dealloyed sample resembles that of the polycrystalline Au electrode.[270]

5.4.6. Catalytic activity for glycerol electro-oxidation

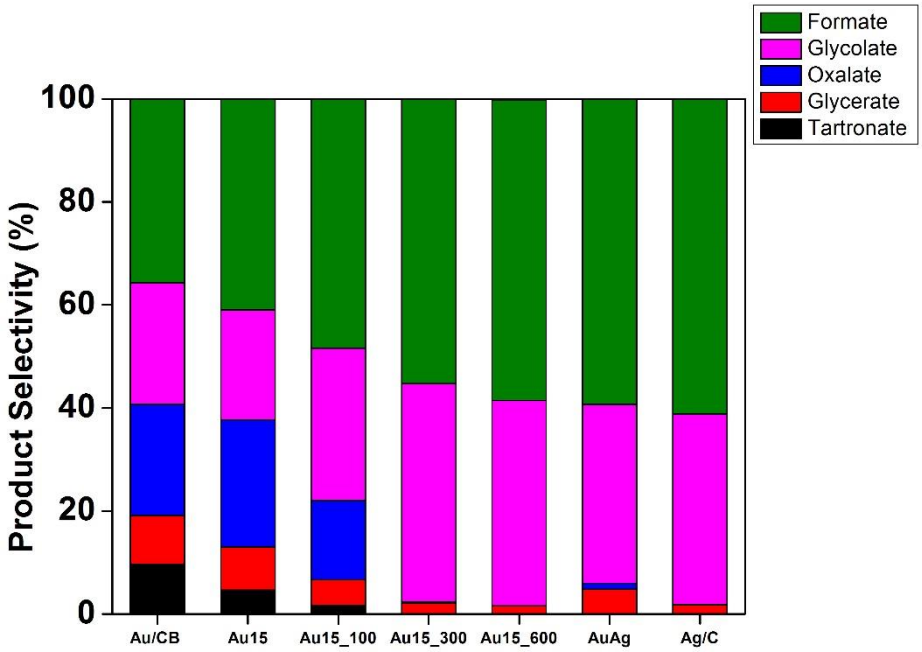

Fig. 5.19. Glycerol electro-oxidation in alkaline medium using catalysts prepared at different conditions.

Table 5.7. Total concentration of oxidation products obtained for the different catalysts.

Sample	Total concentration of products (mM)
AuAg	7.12
Au15	44.53
Au15_100	74.48
Au15_300	25.29
Au15_600	8.59

As-prepared Ag containing porous Au structures were tested for glycerol electro-oxidation. Fig. 5.19 shows the product selectivity obtained by the respective catalysts when glycerol electro-oxidation was carried out in 15 ml of 0.5 M glycerol + 0.5 M NaOH solution at +0.1 V for 2 h. Formate and glycolate were the dominant products generated in all cases despite significant differences in catalysts morphologies. This is indicative that product distribution and selectivity are not controlled by catalyst morphology.

Product distribution and electrochemical activity exhibited by AuAg was similar to that of Ag/C due to its Ag rich nature. Although AuAg was highly selective to formate (59.31%) and glycolate (34.72%) its electrochemical activity was extremely poor and current attained at the end of the 2 h run was only 1.35 mA (Table 5.8, Fig. 5.23f).

Dealloying AuAg for 15 min resulted in a significant enhancement in electrochemical activity. Au15 recorded a current that was roughly 30 times higher than that of AuAg (Table 5.8, Fig. 5.23b). Glycerol conversion increased in tandem with the higher electrochemical activity and total product concentration obtained by Au15 was about 6 times higher than that of AuAg (Table 5.7). Additionally, product distribution of Au15 closely mirrored that of Au nanoparticles supported on carbon black (Au/CB). Differences in product distribution between Au15 and AuAg is attributed to the significant increase in surface Au content in the former. Surface Au content of Au15 was 7.5 times higher than that of AuAg and thus Au15 models "Au-like" behaviour (Table 5.6). Having said that, although Au15 observed a 23% increase in oxalate selectivity relative to AuAg, formate (40.96%) and glycolate (21.33%) are the 2 most dominant products and their high selectivity is attributed to the presence of residual Ag confined within the nanoporous structure.

Au15 was subsequently annealed at increasing temperatures from 100 ^{o}C to 600 ^{o}C. Notably, annealing Au15 at 100 ^{o}C gave rise to even further improvements in electrochemical activity and current exhibited by Au15_100 was about 11 mA higher than that of Au15 (Table 5.8, Fig. 5.23a). Correspondingly, concentration of products attained by Au15_100 was about 1.7 times higher than that of Au15 (Table 5.7). However, annealing Au15 at increasingly higher temperatures, resulted in a gradual shift towards "Ag-like behaviour" as the catalyst surface became increasingly Ag rich. In terms of product distribution, oxalate selectivity decreased whilst selectivity to formate and glycolate increased significantly. Both Au15_300 and

Au15_600 achieved to roughly 98% selectivity formate and glycolate. On the other hand, electrochemical activity and product conversion decreased (Table 5.8, Fig 5.23d and 8e).

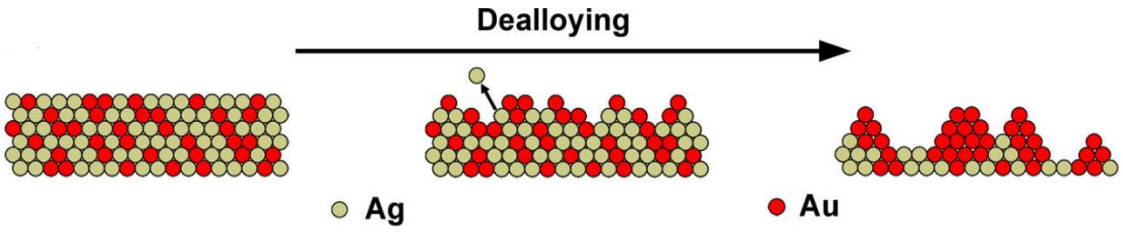

Fig. 5.20. Schematic representation of the mechanism of pattern formation during dealloying. Selective leaching of Ag surface atoms produces Au islands that locally passivate the surface against further corrosion, thus leading to the development of a 3D nanoporous structure. Reprinted with permission from ref 265. Copyright 2015, ACS Publications.[265]

Ag rich AuAg alloyed sheet catalyses glycerol electro-oxidation poorly due to the inherently poor catalytic activity of Ag/C for glycerol electro-oxidation. After AuAg is dealloyed, Au adatoms and vacancies are created in Au15. These adatoms subsequently cluster to form a pit-and-mound surface morphology that further develops into a 3D nanoporous structure as the nucleated Au clusters locally passivate the surface against further corrosion (Fig. 5.20).[265, 271] Most importantly, the two-dimensionally curved surfaces which are characteristic of the ligaments of nanoporous Au structures contain a high concentration of step edge and kink site surface atoms which are more active for catalysis compared to the more highly co-ordinated terrace atoms.[272] As such, Au15 gave rise to considerably higher product conversion compared to Au/C (Table 5.7).

Residual Ag present within the nanoporous structure may not actively take part in the reaction. However, it does play a crucial role when nanoporous Au was applied to CO-oxidation,[258, 271, 273] ester synthesis,[274, 275] and oxidative coupling of alcohols[276-278]. Furthermore, DFT studies show that atomic oxygen and surface intermediates prefer to bind on threefold hollow Au sites (Fig. 5.21).[279] Given that glycerol electro-oxidation is a structure-sensitive reaction,[280, 281]

composition of these threefold sites could influence possibly influence the electro-oxidation process.

Our Ag containing nanoporous Au catalysts also contained 3 types of surface sites, namely, Au-like, mixed and Ag-like sites which are defined as having 3, 1 or 2, and 0 neighbouring Au atoms, respectively.[276] Ag/Au atomic ratio of Au15 and Au15_100 is 0.26 and 0.51 respectively. This means that for Au15, there is 1 Ag atom for every 4 Au atoms while for Au15_100, there is 1 Ag atom for every 2 Au atoms (Fig. 5.22). Au15 thus possessed a higher proportion of Au like sites whilst Au15_100 possessed a higher proportion of mixed sites. Additionally, given that the atomic radius of Au and Ag are 1.79 $\dot{A}$ and 1.75 $\dot{A}$ respectively while the C-C bond length is 1.53 $\dot{A}$, each glycerol molecule thus adsorbs onto a set of Au-like sites and mixed sites in Au15 and Au15_100 respectively. Higher concentration of products attained over Au15_100 is indicative that mixed sites are catalytically more active for glycerol electro-oxidation compared to Au only sites. This may be due to the enhanced stability afforded to the glycerolate intermediate upon binding thereon.[276] Enhanced stability upon binding in turn facilitates the second metal surface catalysed step of the glycerol oxidation reaction.[281]

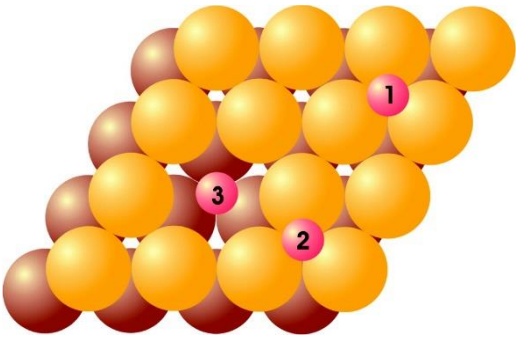

Fig. 5.21. Adsorption sites for atomic oxygen on an Au (111) surface containing one vacancy. The orange spheres represent the top layer of gold, while dark spheres represent the second layer of gold atoms. Calculations revealed that adsorption of oxygen in 3-fold sites near the vacancy is more favourable compared to the (1×1) surface. Reprinted with permission from ref 278. Copyright 2009 American Chemical Society.

On the other hand, further increasing annealing temperature to 600 ^{o}C resulted in a drastic drop in glycerol conversion (Table 5.7). Ag/Au atomic ratio increased from 0.26 in Au15 to 1.68 in

Au15_600 (Table 5.6). This means that for Au15_600, there are nearly 2 Ag atoms for every Au atom. The inherently poor activity of Ag/C for glycerol electro-oxidation thus lead to the drop in product conversion and electro-chemical activity observed. In comparison, glycolate and formate selectivity increases with increasing Ag surface content. As mentioned above, glycerolate likely binds with enhanced stability over mixed sites. Further increasing the ratio of Ag: Au within the mixed site possibly resulted in even greater binding stability compared to that in Au15_100. Greater stability thus gave rise to stronger binding and/or longer binding times and thus elevated C-C bond cleavage was observed. As a result, surface Ag rich catalysts favour formation of C-C and C-C-C bond breaking products during glycerol (electro)-oxidation. Interestingly, oxalate selectivity increased measurably after dealloying. Oxalate selectivity obtained by AuAg and Au15 was 1.17% and 24.71% respectively. However, selectivity decreased by 8% when the sample was annealed at 100 ^{o}C while little to no oxalate was observed with Au15_300 and Au15_600. Collectively, these results indicate that Au rich sites favour further oxidation of glycerate to tartronate as well as the subsequent oxidation of glycolate to oxalate while Ag rich sites favour C-C bond breaking of glycerate to glycolate and formate.

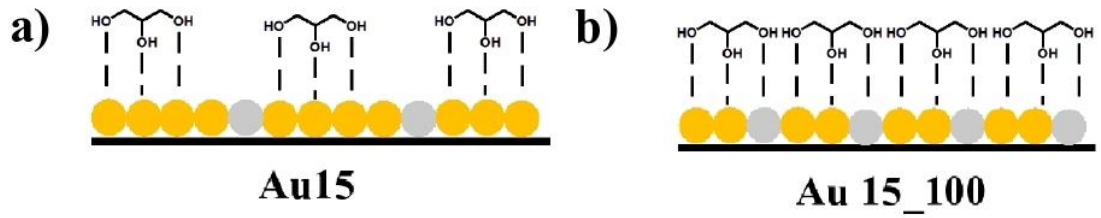

Fig. 5.22. Schematic drawing of Au and Ag atomic arrangement on the surface of a) Au15 and b) Au15_100.

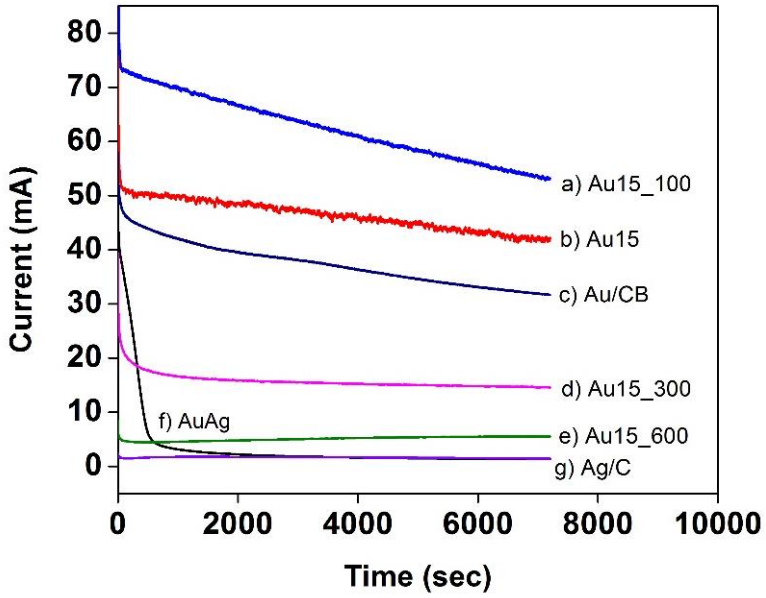

Fig. 5.23. Chronoamperograms of a) Au15_100 b) Au15 c) Au/CB d) Au15_300 e) Au15_600 f) AuAg g) Ag/C

Table. 5.8. Final current attained by each catalyst after glycerol electro-oxidation has taken place for 2 h, at +0.1V.

Sample	Final current (mA)
Au/CB	31.67
Au15	41.77
Au15_100	53.1
Au15_300	14.57
Au15_600	5.53
AuAg	1.35
Ag/C	1.43

5.5. Conclusions

Herein we present porous Au catalysts that demonstrates highly selectivity towards glycolate and formate due to the presence of residual Ag embedded within its porous network. Unlike AuAg alloys, our optimized catalyst also exhibited extremely high electrochemical activity due to its Au rich surface. As such, we have successfully circumvented the problem of low electro-catalytic activity that usually plagues Ag containing catalysts, owing to the inherently poor electrochemical activity of Ag for glycerol electro-oxidation. Low temperature annealing at 100 ^{o}C improved selectivity and electrochemical activity relative to the dealloyed sample.

However, annealing at higher temperatures of 300 ^{o}C and 600 ^{o}C caused electrochemical activity to decrease sharply due to the enhancement of Ag content on the catalyst surface. Formate and glycolate selectivity improved marginally with increased surface Ag content. The dealloyed sample that was annealed at 100 ^{o}C gave rise to the best overall catalytic performance as it managed to achieve high electrochemical activity coupled with high selectivity to both formate and glycolate.

5.6 Summary: Comparison between different catalytic systems

	Cu modified carbon supported Au nanoparticles
Selectivity	- Cu modified carbon supported Au nanoparticles show improved C3 selectivity compared to pure Au/CB - Improvements to selectivity can be further optimized by tuning electro-deposition potential and time
Electrochemical activity	- No significant improvements to electrochemical activity is observed post Cu electro-deposition - Current obtained by Cu modified carbon supported Au nanoparticles are relatively similar to that of Au/CB
Comparison with literature	To the best of our knowledge, supported Au-Cu catalysts have yet to be investigated for glycerol electro-oxidation. Our report is the first to examine the promotional effect of Cu oxides on Au/CB for glycerol electro-oxidation. Having said that, it is interesting to note that alloying Au with Cu (as in $AuCu/Nb_2O_5$) resulted in increased C-C bond cleavage and higher selectivity to glycolic acid and formic acid was observed. Similarly, Cu/CoO also exhibited high selectivity to C-C bond breaking products when tested for glycerol oxidation. On the other hand, with our preparation method and in our experimental set-up, irreversibly adsorbed Cu gave rise to improved C3 selectivity instead. Electron transfer occurred between Cu and Au such that an active Au^+ species was generated in the resultant catalyst. Au^+ was identified as the dominant catalytic species as catalysts containing higher amounts of Au^+ exhibited higher activity. Similarly, Au^+ is posited to be the main driving force for increased selectivity to glycerate and tartronate.

	Ni modified carbon supported Au nanoparticles
Selectivity	- Ni electro-deposition over Au/CB improved its C3 selectivity. However, extent of improvement is significantly lower than that resulting from Cu modification.
Electrochemical activity	- No significant improvements to electrochemical activity is observed post Cu electro-deposition. - Current obtained by Ni modified carbon supported Au nanoparticles are relatively similar to that of Au/CB
Comparison with literature	To the best of our knowledge, there is only one report on bimetallic Au-Ni catalysts for glycerol electro-oxidation. Xu and co-workers previously synthesized Au/Ni Core/shell three dimensional catalysts for glycerol oxidation.[282] However, their report mainly focused on the effect of Ni on the electro-chemical activity of Au for glycerol electro-oxidation but did not discuss its effect on Au selectivity. Furthermore,

	their chronoamperometric studies were only conducted over a very short time length of 8 min. Thus it is very difficult to compare results of their chronoamperometric studies with ours which takes place over 2 h.

	Ag containing porous Au structures
Selectivity	- Presence of Ag steers the catalytic pathway towards C-C bond breaking. High selectivity towards formate and glycolate is observed with Ag containing catalysts in general - In comparison, both Cu and Ni favour C-OH oxidation
Electrochemical activity	- Residual Ag containing porous Au structures are highly active for glycerol electro-oxidation as observed from the large currents obtained during chronoamperometry
Comparison with literature	Residual Ag containing porous Au catalysts show similarly high selectivity to glycolate and formate compared to state of the art AuAg bimetallic catalysts Additionally, porous Au catalysts demonstrate significantly higher electrochemical activity during glycerol electro-oxidation Ag tends to segregate on the surface of the AuAg alloys. However, Ag/C promotes glycerol electro-oxidation poorly.[252] Thus the resulting catalysts suffer from poor electrochemical activity. Segregation of Ag on the alloy surface also reduces the amount of Au available for catalysis. In comparison, our optimized porous Au catalyst only contain small amounts of residual Ag which is embedded within the porous structure. Large surface areas of Au remain exposed to the reaction solution and porous Au structures are thus able to exhibit high electrochemical activity whilst maintaining high selectivity towards glycolate and formate.
How Ag containing Au catalysts work differently from Cu and Ni containing Au catalyst	Residual Ag containing porous Au catalysts exhibit vastly different selectivities compared to Cu and Ni modified carbon supported Au nanoparticles. The former favours C-C bond breaking whilst the latter two favour C-OH oxidation. Porous Au catalysts also demonstrate higher electrochemical activity for glycerol oxidation compared to Au/CB. However, electro-deposition of Cu and Ni onto Au/CB does not result in any improvements in electrochemical activity. **Why does porous Au exhibit higher electrochemical activity compared to Cu and Ni modified carbon supported Au nanoparticles?** Dealloying AuAg generated Au adatoms and vacancies in the dealloyed catalyst. These adatoms subsequently cluster to form a pit-and-mound surface morphology that further develops into a 3D nanoporous structure as the nucleated Au clusters locally passivate the surface against further corrosion. Most importantly, the two-

	dimensionally curved surfaces which are characteristic of the ligaments of nanoporous Au structures contain a high concentration of step edge and kink site surface atoms which are more active for catalysis compared to the more highly co-ordinated terrace atoms. In comparison, Cu and Ni modified carbon supported Au nanoparticles are synthesized by electro-deposition of Cu or Ni over Au/CB. This process does not generate a higher proportion of step edge or kink site surface atoms in the resulting catalysts. As such, Cu and Ni modified Au/CB likely contain a higher concentration of terrace atoms compared to porous Au. Thus, their electrochemical activity during glycerol electro-oxidation is lower than that of porous Au. **Why does porous Au exhibit different selectivities compared to Cu and Ni modified Au nanoparticles?** Differences in selectivities exhibited by porous Au and Cu and Ni modified Au nanoparticles can be attributed to differences in catalyst surface morphology. DFT studies have shown that atomic oxygen and surface intermediates prefer to bind on threefold hollow Au sites. Given the structure sensitive nature of glycerol electro-oxidation[280, 281], the composition of these threefold sites might influence catalytic performance. Porous Au contains 3 types of surface sites, namely, Au-like, mixed and Ag-like sites which are defined as having 3, 1 or 2, and 0 neighbouring Au atoms, respectively. Catalysts possessing a higher proportion of Au like sites exhibit selectivities similar to that of Au nanoparticles. On the other hand, a higher number of mixed and Ag like sites resulted in significantly greater selectivity to C-C bond breaking products, glycolate and formate. Ag is likely not an active participant in the electro-oxidation process. However, its presence in the threefold site affords enhanced stability to the glycerolate intermediate upon binding thereon. Enhanced stability upon binding in turn facilitates the second metal surface catalysed step of the glycerol oxidation reaction. Furthermore, increasing the ratio of Ag : Au within the mixed site possibly resulted in even greater binding stability. This in turn gave rise to stronger binding and/or longer binding times. Thus elevated C-C bond cleavage was observed in porous Au catalysts which were annealed at temperatures above 100 ^{o}C. Atomic oxygen adsorption on Cu-Au is also strongly site specific, with the 4-fold hollow being the most favourable. Most importantly, extensive DFT calculations carried out for CO oxidation over Cu modified Au surfaces indicate that Cu layer on Au slab significantly affects O_2 and CO binding. Adsorption energy and bond activation increases when O_2 binds onto Cu-Au (100). CO adsorption energy on Cu-Au (100) is also more than two times that on Au (100). Presence of Cu on Au thus offers less activation barrier and higher thermodynamic

	favourability, which serves as a driving force for the reaction on the catalytic surface. Unlike mixed or Ag like sites in porous Au, Cu mainly affects ease of reactant binding and does not affect its subsequent stability. As such, glycerate and tartronate remain the dominant products when glycerol oxidation is carried out over Cu modified Au nanoparticles. However, selectivity to these products increases due to the reduced activation barrier and increased thermodynamic favourability of the oxidation reaction. Amongst the three catalysts synthesized, Ni modified Au nanoparticles performed the worst in terms of improving catalytic performance vis-à-vis Au/CB. Since both Cu and Ni modified Au nanoparticles were prepared in a similar manner, it maybe that Ni is less effective than Cu in reducing activation energy barrier of the reaction and improving thermodynamic favourability. Hence the resulting catalyst post Ni modification does not show significantly improved selectivity for glycerate and tartronate.

1. J.-H. Song, J.-Y. Yu, M.-Z. Zhang, Y.-J. Liang and C.-W. Xu, Int. J. Electrochem. Sci., 2012, 7, 4362-4368.
2. A. G. Garcia, P. P. Lopes, J. F. Gomes, C. Pires, E. B. Ferreira, R. G. M. Lucena, L. H. S. Gasparotto and G. Tremiliosi-Filho, New Journal of Chemistry, 2014, 38, 2865-2873.
3. A. C. Garcia, M. J. Kolb, C. van Nierop y Sanchez, J. Vos, Y. Y. Birdja, Y. Kwon, G. Tremiliosi-Filho and M. T. M. Koper, ACS Catalysis, 2016, 6, 4491-4500.
4. B. N. Zope, D. D. Hibbitts, M. Neurock and R. J. Davis, Science, 2010, 330, 74-78.

Chapter 6

Conclusions and recommendations for future work

6.1. Conclusions

Au based catalysts are one of the most extensively investigated catalytic systems for glycerol electro-oxidation. A variety of products including, glycerate, tartronate, glycolate, oxalate and formate were generated when glycerol electro-oxidation was carried out over Au based catalysts under our experimental conditions. A diverse range of catalytic systems have been developed to improve the selectivity of Au toward specific products during catalysis. Alternatively, reaction conditions such as applied potential and catalyst loading can be optimized to improve selectivity. However, hitherto, there has been no unified system which enables one to easily steer selectivity of Au towards different products in the oxidation pathway.

In this thesis, we investigated whether the simple electro-deposition of transition metal species onto Au/C could alter the selectivity of Au towards different products in the glycerol oxidation pathway. We determined that electro-deposition of Cu and Ni onto Au/C effectively tuned selectivity towards glycerate and tartronate. Moreover, we synthesized residual Ag containing porous Au structures which exhibited both high catalytic activity and selectivity to formate. More specifically, our major findings are:

1) Cu electro-deposition onto Au/C led to significant improvements in C3 selectivity. Greatest enhancement in C3 selectivity was observed when Cu electro-deposition occurred at -0.1 V and +0.015 V. High selectivity is attributed to the presence of an Au^{+} species which was generated when Au interacted with electrodeposited Cu_2O. Furthermore, when electro-deposition occurred at +0.015 V for 90 min, Au^{+} content increased by three times. This in turn enabled $Cu_{+0.015V,\ 90min}$-Au/C to double C3 selectivity relative to Au/C when glycerol electro-oxidation occurred at 0.1 V.

2) Ni electro-deposition onto Au/C also led to improvements in C3 selectivity. Similarly, high selectivity is attributed to the presence of an Au^{+} species that was identified in the most selective catalysts. In this case, Au^{+} was generated when Au interacted with NiOOH, which was generated when the electro-deposited Ni species was cycled in NaOH post electro-deposition.
3) Ni electro-deposition onto Au/C is optimized at -0.3 V. When electro-deposition occurs at applied potentials more negative than -0.3 V, a significantly thicker Ni layer is deposited onto Au/C. The thicker Ni surface partially shielded the Au nanoparticles from the glycerol solution and thus severely limited their activity. C3 selectivity of the Ni-Au/CB catalysts prepared under these conditions are relatively similar to that of pure Au/CB. Any possible synergistic effect between Au and Ni was thus nullified by the thick Ni surface coverage.
4) Ag is known to favour C-C bond breaking of glycerol. However, Ag-Au based catalysts such as AuAg alloys also typically exhibit low electro-chemical activity due to the poor conductivity of Ag. It is thus necessary to develop Ag containing catalysts that possessed an Au rich surface in order to achieve high electrochemical activity whilst maintaining high selectivity.
5) Residual Ag containing porous Au structures are highly active and selective catalysts for glycerol electro-oxidation. Porous Au structures possessed an Au rich surface which enabled high electro-catalytic activity. Furthermore, presence of residual amounts of Ag embedded deep within the porous structure lead to high selectivity towards glycolate and formate.
6) Low temperature annealing of the porous Au structure led to further improvements in formate selectivity and conversion. Formate selectivity improved due to the higher surface Ag content. On the other hand, annealing also resulted in atomic rearrangement

on the catalyst surface, which subsequently improved conversion. The dealloyed only sample was Au rich and this lead to the isolation of Ag sites on the catalyst surface. However, after annealing, Au and Ag atoms were rearranged such that all atoms present on the catalyst surface necessarily participated during the reaction. In this way, glycerol molecules were more likely evenly adsorbed onto the metal surface and this gave rise to the higher product conversion.

6.2. Recommendations for future work

To further tune selectivity towards glycerate and tartronate, it is important to understand how specific interactions between transitional metal species and Au/C affect glycerol binding and surface reaction. Electro-deposition can only be used as means to provide surface coverage onto Au/C. It cannot be used to deposit transition metals selectively onto specific facets of the Au particle. As such, it is necessary to design and synthesize Au nanoparticle catalysts which have specific facets covered or replaced with transition metal species. Through this, the catalytic performance of Au/C can be further tuned and the specific interaction between transition metal species and Au/C be understood in greater depth.

In addition, electro-deposition also covers the Au/C surface with a mixture of metals and their corresponding oxides. However, as evaluated, different metals and/or oxides give rise to different catalytic performances. To further tune selectivity, Au/C catalysts should be deposited or alloyed with specific metallic species in order to optimize activity and/or further elucidate differences in catalytic performance.

References

1. B. Katryniok, H. Kimura, E. Skrzynska, J.-S. Girardon, P. Fongarland, M. Capron, R. Ducoulombier, N. Mimura, S. Paul and F. Dumeignil, Green Chemistry, 2011, 13, 1960-1979.
2. R. Ciriminna, C. D. Pina, M. Rossi and M. Pagliaro, European Journal of Lipid Science and Technology, 2014, 116, 1432-1439.
3. A. Ilie, M. Simoes, S. Baranton, C. Coutanceau and S. Martemianov, Journal of Power Sources, 2011, 196, 4965-4971.
4. G. Caselli, M. Mantovanini, C. A. Gandolfi, M. Allegretti, S. Fiorentino, L. Pellegrini, G. Melillo, R. Bertini, W. Sabbatini, R. Anacardio, G. Clavenna, G. Sciortino and A. Teti, Journal of Bone and Mineral Research, 1997, 12, 972-981.
5. P. M. Bizot, B. R. Bailey and P. D. Hicks, Journal, 1998.
6. R. Ciriminna and M. Pagliaro, Advanced Synthesis & Catalysis, 2003, 345, 383-388.
7. H. Kimura, Journal of Polymer Science Part A: Polymer Chemistry, 1998, 36, 195-205.
8. P. S. Fernández, M. E. Martins and G. A. Camara, Electrochimica Acta, 2012, 66, 180-187.
9. J. Gao, D. Liang, P. Chen, Z. Hou and X. Zheng, Catal Lett, 2009, 130, 185-191.
10. R. Garcia, M. Besson and P. Gallezot, Applied Catalysis A: General, 1995, 127, 165-176.
11. E. G. Rodrigues, M. F. R. Pereira, X. Chen, J. J. Delgado and J. J. M. Órfão, Industrial & Engineering Chemistry Research, 2013, 52, 17390-17398.
12. S. Carrettin, P. McMorn, P. Johnston, K. Griffin, C. J. Kiely and G. J. Hutchings, Physical Chemistry Chemical Physics, 2003, 5, 1329-1336.
13. C. Bianchini and P. K. Shen, Chemical Reviews, 2009, 109, 4183-4206.
14. N. Dimitratos, C. Messi, F. Porta, L. Prati and A. Villa, Journal of Molecular Catalysis A: Chemical, 2006, 256, 21-28.
15. M. Zhang, J. Shi, Y. Sun, W. Ning and Z. Hou, Catalysis Communications, 2015, 70, 72-76.
16. D. Liang, J. Gao, J. Wang, P. Chen, Z. Hou and X. Zheng, Catalysis Communications, 2009, 10, 1586-1590.
17. D. Liang, J. Gao, H. Sun, P. Chen, Z. Hou and X. Zheng, Applied Catalysis B: Environmental, 2011, 106, 423-432.
18. D. Liang, J. Gao, J. Wang, P. Chen, Y. Wei and Z. Hou, Catalysis Communications, 2011, 12, 1059-1062.
19. Z. Lin, H. Chu, Y. Shen, L. Wei, H. Liu and Y. Li, Chemical Communications, 2009, DOI: 10.1039/B917235A, 7167-7169.
20. W. Hong, C. Shang, J. Wang and E. Wang, Energy & Environmental Science, 2015, DOI: 10.1039/C5EE01988E.
21. Y. Li and F. Zaera, Journal of Catalysis, 2015, 326, 116-126.
22. A. C. Garcia, M. J. Kolb, C. van Nieropy y. Sanchez, J. Vos, Y. Y. Birdja, Y. Kwon, G. Tremiliosi-Filho and M. T. M. Koper, ACS Catal., 2016, DOI: 10.1021/acscatal.6b00709, Ahead of Print.
23. M. Besson and P. Gallezot, Catalysis Today, 2000, 57, 127-141.
24. T. Mallat and A. Baiker, Catalysis Today, 1994, 19, 247-283.
25. T. Mallat and A. Baiker, Chemical Reviews, 2004, 104, 3037-3058.
26. in The Future of Glycerol (2), The Royal Society of Chemistry, 2010, DOI: 10.1039/9781849731089-00115, pp. 115-134.
27. S. Biella, G. L. Castiglioni, C. Fumagalli, L. Prati and M. Rossi, Catalysis Today, 2002, 72, 43-49.
28. M. Haruta, T. Kobayashi, H. Sano and N. Yamada, Chemistry Letters, 1987, 16, 405-408.
29. M. Haruta and H. Sano, in Studies in Surface Science and Catalysis, eds. P. G. G. Poncelet and P. A. Jacobs, Elsevier, 1983, vol. Volume 16, pp. 225-236.

30. M. Haruta, N. Yamada, T. Kobayashi and S. Iijima, Journal of Catalysis, 1989, 115, 301-309.
31. M. Haruta, S. Tsubota, T. Kobayashi, H. Kageyama, M. J. Genet and B. Delmon, Journal of Catalysis, 1993, 144, 175-192.
32. L. Prati and M. Rossi, Journal of Catalysis, 1998, 176, 552-560.
33. S. Biella and M. Rossi, Chemical Communications, 2003, DOI: 10.1039/B210506C, 378-379.
34. A. Gaiassi and L. Prati, Catalysis Today, 2009, 141, 378-384.
35. A. Villa, S. Campisi, M. Schiavoni and L. Prati, Materials, 2013, 6, 2777-2788.
36. S. Yongprapat, A. Therdthianwong and S. Therdthianwong, J. Appl. Electrochem., 2015, 45, 487-494.
37. W. C. Ketchie, Y.-L. Fang, M. S. Wong, M. Murayama and R. J. Davis, Journal of Catalysis, 2007, 250, 94-101.
38. S. Carrettin, P. McMorn, P. Johnston, K. Griffin and G. J. Hutchings, Chemical Communications, 2002, DOI: 10.1039/B201112N, 696-697.
39. L. Prati and G. Martra, Gold Bull, 1999, 32, 96-101.
40. F. Porta, L. Prati, M. Rossi, S. Coluccia and G. Martra, Catalysis Today, 2000, 61, 165-172.
41. F. Porta and L. Prati, Journal of Catalysis, 2004, 224, 397-403.
42. E. G. Rodrigues, S. A. C. Carabineiro, X. Chen, J. J. Delgado, J. L. Figueiredo, M. F. R. Pereira and J. J. M. Órfão, Catal Lett, 2010, 141, 420-431.
43. N. Dimitratos, A. Villa, C. L. Bianchi, L. Prati and M. Makkee, Applied Catalysis A: General, 2006, 311, 185-192.
44. T. Ntho, J. Aluha, P. Gqogqa, M. Raphulu and G. Pattrick, Reac Kinet Mech Cat, 2013, 109, 133-148.
45. S. M. Rogers, C. R. A. Catlow, C. E. Chan-Thaw, D. Gianolio, E. K. Gibson, A. L. Gould, N. Jian, A. J. Logsdail, R. E. Palmer, L. Prati, N. Dimitratos, A. Villa and P. P. Wells, ACS Catalysis, 2015, 5, 4377-4384.
46. A. Villa, D. Wang, D. S. Su and L. Prati, ChemCatChem, 2009, 1, 510-514.
47. A. Villa, D. Wang, D. Su, G. M. Veith and L. Prati, Physical Chemistry Chemical Physics, 2010, 12, 2183-2189.
48. S. Biella, L. Prati and M. Rossi, Journal of Catalysis, 2002, 206, 242-247.
49. C. D. Evans, S. A. Kondrat, P. J. Smith, T. D. Manning, P. J. Miedziak, G. L. Brett, R. D. Armstrong, J. K. Bartley, S. H. Taylor, M. J. Rosseinsky and G. J. Hutchings, Faraday Discussions, 2016, 188, 427-450.
50. A. Villa, D. Wang, G. M. Veith, F. Vindigni and L. Prati, Catalysis Science &Technology, 2013, 3, 3036-3041.
51. S. Campisi, C. E. Chan-Thaw, D. Wang, A. Villa and L. Prati, Catalysis Today, 2016, 278, Part 1, 91-96.
52. M. Sankar, N. Dimitratos, P. J. Miedziak, P. P. Wells, C. J. Kiely and G. J. Hutchings, Chemical Society Reviews, 2012, 41, 8099-8139.
53. D. M. Alonso, S. G. Wettstein and J. A. Dumesic, Chemical Society Reviews, 2012, 41, 8075-8098.
54. L. Prati, A. Villa, C. Campione and P. Spontoni, Top Catal, 44, 319-324.
55. N. Dimitratos, A. Villa, D. Wang, F. Porta, D. Su and L. Prati, Journal of Catalysis, 2006, 244, 113-121.
56. C. L. Bianchi, P. Canton, N. Dimitratos, F. Porta and L. Prati, Catalysis Today, 2005, 102–103, 203-212.
57. H. Zhang, T. Watanabe, M. Okumura, M. Haruta and N. Toshima, Nat Mater, 2012, 11, 49-52.
58. S. Xie, H. Tsunoyama, W. Kurashige, Y. Negishi and T. Tsukuda, ACS Catalysis, 2012, 2, 1519-1523.
59. D. I. Enache, J. K. Edwards, P. Landon, B. Solsona-Espriu, A. F. Carley, A. A. Herzing, M. Watanabe, C. J. Kiely, D. W. Knight and G. J. Hutchings, Science, 2006, 311, 362-365.

60. A. Villa, C. Campione and L. Prati, Catal Lett, 2007, 115, 133-136.
61. N. Dimitratos, J. A. Lopez-Sanchez, D. Lennon, F. Porta, L. Prati and A. Villa, Catal Lett, 2006, 108, 147-153.
62. N. Dimitratos, J. A. Lopez-Sanchez and G. J. Hutchings, Top Catal, 2009, 52, 258-268.
63. J. A. Lopez-Sanchez, N. Dimitratos, N. Glanville, L. Kesavan, C. Hammond, J. K. Edwards, A. F. Carley, C. J. Kiely and G. J. Hutchings, Applied Catalysis A: General, 2011, 391, 400-406.
64. D. Wang, A. Villa, F. Porta, D. Su and L. Prati, Chemical Communications, 2006, DOI: 10.1039/B518069D, 1956-1958.
65. W. C. Ketchie, M. Murayama and R. J. Davis, Journal of Catalysis, 2007, 250, 264-273.
66. N. Dimitratos, J. A. Lopez-Sanchez, J. M. Anthonykutty, G. Brett, A. F. Carley, R. C. Tiruvalam, A. A. Herzing, C. J. Kiely, D. W. Knight and G. J. Hutchings, Physical Chemistry Chemical Physics, 2009, 11, 4952-4961.
67. A. Villa, C. Campione and L. Prati, Catal Lett, 2007, 115, 133-136.
68. D. Wang, A. Villa, F. Porta, L. Prati and D. Su, The Journal of Physical Chemistry C, 2008, 112, 8617-8622.
69. A. Villa, N. Janjic, P. Spontoni, D. Wang, D. S. Su and L. Prati, Applied Catalysis A: General, 2009, 364, 221-228.
70. S. F. J. Hackett, R. M. Brydson, M. H. Gass, I. Harvey, A. D. Newman, K. Wilson and A. F. Lee, Angewandte Chemie International Edition, 2007, 46, 8593-8596.
71. K. Mori, T. Hara, T. Mizugaki, K. Ebitani and K. Kaneda, Journal of the American Chemical Society, 2004, 126, 10657-10666.
72. P. Han, S. Axnanda, I. Lyubinetsky and D. W. Goodman, Journal of the American Chemical Society, 2007, 129, 14355-14361.
73. Z. Zhao, J. Arentz, L. A. Pretzer, P. Limpornpipat, J. M. Clomburg, R. Gonzalez, N. M. Schweitzer, T. Wu, J. T. Miller and M. S. Wong, Chemical Science, 2014, 5, 3715-3728.
74. Z. Zhao, J. Miller, T. Wu, N. Schweitzer and M. Wong, Top Catal, 2015, 58, 302-313.
75. D. Tongsakul, S. Nishimura and K. Ebitani, ACS Catalysis, 2013, 3, 2199-2207.
76. A. Villa, G. M. Veith and L. Prati, Angewandte Chemie International Edition, 2010, 49, 4499-4502.
77. G. L. Brett, Q. He, C. Hammond, P. J. Miedziak, N. Dimitratos, M. Sankar, A. A. Herzing, M. Conte, J. A. Lopez-Sanchez, C. J. Kiely, D. W. Knight, S. H. Taylor and G. J. Hutchings, Angewandte Chemie International Edition, 2011, 50, 10136-10139.
78. S. Hirasawa, Y. Nakagawa and K. Tomishige, Catalysis Science &Technology, 2012, 2, 1150-1152.
79. S. A. Kondrat, P. J. Miedziak, M. Douthwaite, G. L. Brett, T. E. Davies, D. J. Morgan, J. K. Edwards, D. W. Knight, C. J. Kiely, S. H. Taylor and G. J. Hutchings, ChemSusChem, 2014, 7, 1326-1334.
80. P. Suramanee, S. Poompradub, R. Rojanathanes and P. Thamyongkit, Catal Lett, 2011, 141, 1677-1684.
81. E. Skrzyńska, J. Ftouni, J.-S. Girardon, M. Capron, L. Jalowiecki-Duhamel, J.-F. Paul and F. Dumeignil, ChemSusChem, 2012, 5, 2065-2078.
82. D. W. Goodman, Catal Lett, 99, 1-4.
83. R. W. Joyner, J. B. Pendry, D. K. Saldin and S. R. Tennison, Surface Science, 1984, 138, 84-94.
84. S. J. Tauster, Accounts of Chemical Research, 1987, 20, 389-394.
85. G. C. Bond, C. D. Louis and D. T. D. Thompson, Catalysis by gold. [electronic resource], London : Imperial College Press ; Singapore : Distributed by World Scientific Pub., 2006., 2006.
86. F. Rodríguez-reinoso, Carbon, 1998, 36, 159-175.
87. S. Demirel, P. Kern, M. Lucas and P. Claus, Catalysis Today, 2007, 122, 292-300.
88. S. Demirel, K. Lehnert, M. Lucas and P. Claus, Applied Catalysis B: Environmental, 2007, 70, 637-643.

89. S. Demirel-Gülen, M. Lucas and P. Claus, Catalysis Today, 2005, 102–103, 166-172.
90. A. Fási, K. Hernádi, I. Pálinkó and G. Galbács, Reaction Kinetics and Catalysis Letters, 87, 343-348.
91. S. Gil, M. Marchena, C. M. Fernández, L. Sánchez-Silva, A. Romero and J. L. Valverde, Applied Catalysis A: General, 2013, 450, 189-203.
92. S. Gil, L. Muñoz, L. Sánchez-Silva, A. Romero and J. L. Valverde, Chemical Engineering Journal, 2011, 172, 418-429.
93. Z. C. Kang and Z. L. Wang, Journal of Molecular Catalysis A: Chemical, 1997, 118, 215-222.
94. D. Wang, A. Villa, D. Su, L. Prati and R. Schlögl, ChemCatChem, 2013, 5, 2717-2723.
95. J. R. Copeland, I. A. Santillan, S. M. Schimming, J. L. Ewbank and C. Sievers, The Journal of Physical Chemistry C, 2013, 117, 21413-21425.
96. A. Villa, N. Dimitratos, C. E. Chan-Thaw, C. Hammond, L. Prati and G. J. Hutchings, Accounts of Chemical Research, 2015, 48, 1403-1412.
97. S. E. Davis, M. S. Ide and R. J. Davis, Green Chemistry, 2013, 15, 17-45.
98. C. Xu, Y. Du, C. Li, J. Yang and G. Yang, Applied Catalysis B: Environmental, 2015, 164, 334-343.
99. A. Villa, S. Campisi, K. M. H. Mohammed, N. Dimitratos, F. Vindigni, M. Manzoli, W. Jones, M. Bowker, G. J. Hutchings and L. Prati, Catalysis Science &Technology, 2015, 5, 1126-1132.
100. A. Tsuji, K. T. V. Rao, S. Nishimura, A. Takagaki and K. Ebitani, ChemSusChem, 2011, 4, 542-548.
101. D. P. Debecker, E. M. Gaigneaux and G. Busca, Chemistry – A European Journal, 2009, 15, 3920-3935.
102. F. Figueras, M. Lakshmi Kantam and B. Manoranjan Choudary, Current Organic Chemistry, 2006, 10, 1627-1637.
103. K. Yamaguchi, K. Mori, T. Mizugaki, K. Ebitani and K. Kaneda, The Journal of Organic Chemistry, 2000, 65, 6897-6903.
104. F. Zhang, J. Chen, X. Zhang, W. Gao, R. Jin, N. Guan and Y. Li, Langmuir, 2004, 20, 9329-9334.
105. B. F. Sels, D. E. De Vos and P. A. Jacobs, Catalysis Reviews, 2001, 43, 443-488.
106. A. Villa, A. Gaiassi, I. Rossetti, C. L. Bianchi, K. van Benthem, G. M. Veith and L. Prati, Journal of Catalysis, 2010, 275, 108-116.
107. L. P. R. Profeti, E. A. Ticianelli and E. M. Assaf, International Journal of Hydrogen Energy, 2009, 34, 5049-5060.
108. M. Xiao, Y. Miao, W. Li, Y. Yang and X. Liang, Electrochimica Acta, 2015, 178, 209-216.
109. S. Adhikari, S. D. Fernando and A. Haryanto, Energy Conversion and Management, 2009, 50, 2600-2604.
110. A. Iriondo, V. L. Barrio, J. F. Cambra, P. L. Arias, M. B. Güemez, R. M. Navarro, M. C. Sánchez-Sánchez and J. L. G. Fierro, Top Catal, 2008, 49, 46-58.
111. V. Nichele, M. Signoretto, F. Menegazzo, A. Gallo, V. Dal Santo, G. Cruciani and G. Cerrato, Applied Catalysis B: Environmental, 2012, 111–112, 225-232.
112. V. L. Oliveira, C. Morais, K. Servat, T. W. Napporn, G. Tremiliosi-Filho and K. B. Kokoh, Journal of Electroanalytical Chemistry, 2013, 703, 56-62.
113. A. Villa, C. E. Chan-Thaw, G. M. Veith, K. L. More, D. Ferri and L. Prati, ChemCatChem, 2011, 3, 1612-1618.
114. A. Villa, G. M. Veith, D. Ferri, A. Weidenkaff, K. A. Perry, S. Campisi and L. Prati, Catalysis Science & Technology, 2013, 3, 394-399.
115. S.-S. Liu, K.-Q. Sun and B.-Q. Xu, ACS Catalysis, 2014, 4, 2226-2230.
116. S. Gil, M. Marchena, L. Sánchez-Silva, A. Romero, P. Sánchez and J. L. Valverde, Chemical Engineering Journal, 2011, 178, 423-435.
117. N. Dimitratos, A. Villa and L. Prati, Catal Lett, 2009, 133, 334-340.
118. B. Zope, S. Davis and R. Davis, Top Catal, 2012, 55, 24-32.

119. V. Bambagioni, C. Bianchini, A. Marchionni, J. Filippi, F. Vizza, J. Teddy, P. Serp and M. Zhiani, Journal of Power Sources, 2009, 190, 241-251.
120. H. Kimura, Applied Catalysis A: General, 1993, 105, 147-158.
121. W. Hu, D. Knight, B. Lowry and A. Varma, Industrial & Engineering Chemistry Research, 2010, 49, 10876-10882.
122. H. J. Kim, J. Lee, S. K. Green, G. W. Huber and W. B. Kim, ChemSusChem, 2014, 7, 1051-1056.
123. B. Zope and R. Davis, Top Catal, 2009, 52, 269-277.
124. N. Worz, A. Brandner and P. Claus, The Journal of Physical Chemistry C, 2010, 114, 1164-1172.
125. S. D. Pollington, D. I. Enache, P. Landon, S. Meenakshisundaram, N. Dimitratos, A. Wagland, G. J. Hutchings and E. H. Stitt, Catalysis Today, 2009, 145, 169-175.
126. X. Deng, G. Dodekatos, K. Pupovac, C. Weidenthaler, W. N. Schmidt, F. Schüth and H. Tüysüz, ChemCatChem, 2015, 7, 3832-3837.
127. C.-H. Zhou, J. N. Beltramini, C.-X. Lin, Z.-P. Xu, G. Q. Lu and A. Tanksale, Catalysis Science & Technology, 2011, 1, 111-122.
128. G. Wu, X. Wang, Y. a. Huang, X. Liu, F. Zhang, K. Ding and X. Yang, Journal of Molecular Catalysis A: Chemical, 2013, 379, 185-191.
129. I. Sobczak and Ł. Wolski, Catalysis Today, 2015, 254, 72-82.
130. Y. Kwon, K. J. P. Schouten and M. T. M. Koper, ChemCatChem, 2011, 3, 1176-1185.
131. Y. Kwon and M. T. M. Koper, Analytical Chemistry, 2010, 82, 5420-5424.
132. C. A. Martins, M. J. Giz and G. A. Camara, Electrochimica Acta, 2011, 56, 4549-4553.
133. W. Ketchie, M. Murayama and R. Davis, Top Catal, 2007, 44, 307-317.
134. Y. Kwon, S. C. S. Lai, P. Rodriguez and M. T. M. Koper, Journal of the American Chemical Society, 2011, 133, 6914-6917.
135. G. Tremiliosi-Filho, E. R. Gonzalez, A. J. Motheo, E. M. Belgsir, J. M. Léger and C. Lamy, Journal of Electroanalytical Chemistry, 1998, 444, 31-39.
136. H. Wang, L. Thia, N. Li, X. Ge, Z. Liu and X. Wang, Applied Catalysis B: Environmental, 2015, 166–167, 25-31.
137. H. Wang, L. Thia§, N. Li, X. Ge, Z. Liu and X. Wang, ACS Catalysis, 2015, 5, 3174-3180.
138. J. A. van Bokhoven and J. T. Miller, The Journal of Physical Chemistry C, 2007, 111, 9245-9249.
139. T. Holme, Y. Zhou, R. Pasquarelli and R. O'Hayre, Physical Chemistry Chemical Physics, 2010, 12, 9461-9468.
140. M. J. Allen, V. C. Tung and R. B. Kaner, Chemical Reviews, 2010, 110, 132-145.
141. J. Long, X. Xie, J. Xu, Q. Gu, L. Chen and X. Wang, ACS Catalysis, 2012, 2, 622-631.
142. A. K. Geim, Science, 2009, 324, 1530-1534.
143. D. Chen, H. Feng and J. Li, Chemical Reviews, 2012, 112, 6027-6053.
144. Y. Shao, J. Wang, M. Engelhard, C. Wang and Y. Lin, Journal of Materials Chemistry, 2010, 20, 743-748.
145. D. A. C. Brownson and C. E. Banks, Analyst, 2010, 135, 2768-2778.
146. G. G. Wildgoose, C. E. Banks and R. G. Compton, Small, 2006, 2, 182-193.
147. R. H. Baughman, A. A. Zakhidov and W. A. de Heer, Science, 2002, 297, 787-792.
148. A. Villa, D. Wang, N. Dimitratos, D. Su, V. Trevisan and L. Prati, Catalysis Today, 2010, 150, 8-15.
149. C. Wang, M. Waje, X. Wang, J. M. Tang, R. C. Haddon and Yan, Nano Letters, 2004, 4, 345-348.
150. V. Selvaraj, M. Vinoba and M. Alagar, J. Colloid Interface Sci., 2008, 322, 537-544.
151. R. Nie, D. Liang, L. Shen, J. Gao, P. Chen and Z. Hou, Applied Catalysis B: Environmental, 2012, 127, 212-220.
152. J. Qi, L. Xin, Z. Zhang, K. Sun, H. He, F. Wang, D. Chadderdon, Y. Qiu, C. Liang and W. Li, Green Chem., 2013, 15, 1133-1137.
153. H. J. Kim, S. M. Choi, M. H. Seo, S. Green, G. W. Huber and W. B. Kim, Electrochemistry Communications, 2011, 13, 890-893.

154. L. Gao, W. Yue, S. Tao and L. Fan, Langmuir, 2013, 29, 957-964.
155. S. Bong, Y.-R. Kim, I. Kim, S. Woo, S. Uhm, J. Lee and H. Kim, Electrochemistry Communications, 2010, 12, 129-131.
156. J. Gao, D. Liang, P. Chen, Z. Hou and X. Zheng, Catal. Lett., 2009, 130, 185-191.
157. S.-S. Li, Y.-Y. Hu, J.-J. Feng, Z.-Y. Lv, J.-R. Chen and A.-J. Wang, International Journal of Hydrogen Energy, 2014, 39, 3730-3738.
158. Y. Shen, Z. Zhang, K. Xiao and J. Xi, Physical Chemistry Chemical Physics, 2014, 16, 21609-21614.
159. Z. Zhang, L. Xin, J. Qi, Z. Wang and W. Li, Green Chemistry, 2012, 14, 2150-2152.
160. L. Xin, Z. Zhang, Z. Wang and W. Li, ChemCatChem, 2012, 4, 1105-1114.
161. O. O. Fashedemi, H. A. Miller, A. Marchionni, F. Vizza and K. I. Ozoemena, Journal of Materials Chemistry A, 2015, 3, 7145-7156.
162. K. Fugane, T. Mori, D. R. Ou, P. Yan, F. Ye, H. Yoshikawa and J. Drennan, Langmuir, 2012, 28, 16692-16700.
163. D. R. Ou, T. Mori, K. Fugane, H. Togasaki, F. Ye and J. Drennan, The Journal of Physical Chemistry C, 2011, 115, 19239-19245.
164. W. Yuan, J. Zhang, P. K. Shen, C. M. Li and S. P. Jiang, Electrochimica Acta, 2016, 190, 817-828.
165. L. Zhang and Y. Shen, ChemElectroChem, 2015, 2, 887-895.
166. H. Qian, M. Zhu, Z. Wu and R. Jin, Accounts of Chemical Research, 2012, 45, 1470-1479.
167. L. Artiglia, S. Agnoli, A. Vittadini, A. Verdini, A. Cossaro, L. Floreano and G. Granozzi, Journal of the American Chemical Society, 2013, 135, 17331-17338.
168. B. H. Kim, M. J. Hackett, J. Park and T. Hyeon, Chemistry of Materials, 2014, 26, 59-71.
169. F. Jiao and H. Frei, Energy & Environmental Science, 2010, 3, 1018-1027.
170. X. Ning, H. Yu, F. Peng and H. Wang, Journal of Catalysis, 2015, 325, 136-144.
171. J. Wu, X. Z. Yuan, J. J. Martin, H. Wang, J. Zhang, J. Shen, S. Wu and W. Merida, Journal of Power Sources, 2008, 184, 104-119.
172. L. S. R. Silva, F. E. Lopez-Suarez, M. Perez-Cadenas, S. F. Santos, L. P. da Costa, K. I. B. Eguiluz and G. R. Salazar-Banda, Appl. Catal., B, 2016, 198, 38-48.
173. A. Zalineeva, A. Serov, M. Padilla, U. Martinez, K. Artyushkova, S. Baranton, C. Coutanceau and P. B. Atanassov, Appl. Catal., B, 2015, 176-177, 429-435.
174. Y. Holade, C. Morais, K. Servat, T. W. Napporn and K. B. Kokoh, ACS Catal., 2013, 3, 2403-2411.
175. Y. Holade, C. Morais, S. Arrii-Clacens, K. Servat, T. W. Napporn and K. B. Kokoh, Electrocatalysis, 2013, 4, 167-178.
176. S. Lee, H. J. Kim, S. M. Choi, M. H. Seo and W. B. Kim, Appl. Catal., A, 2012, 429-430, 39-47.
177. S. Lee, H. J. Kim, E. J. Lim, Y. Kim, Y. Noh, G. W. Huber and W. B. Kim, Green Chem., 2016, 18, 2877-2887.
178. H. J. Kim, S. M. Choi, S. Green, G. A. Tompsett, S. H. Lee, G. W. Huber and W. B. Kim, Applied Catalysis B: Environmental, 2011, 101, 366-375.
179. H. Kimura, K. Tsuto, T. Wakisaka, Y. Kazumi and Y. Inaya, Applied Catalysis A: General, 1993, 96, 217-228.
180. Y. Kwon, Y. Birdja, I. Spanos, P. Rodriguez and M. T. M. Koper, ACS Catalysis, 2012, 2, 759-764.
181. Y. Kwon, T. P. Hersbach and M. M. Koper, Top Catal, 2014, 57, 1272-1276.
182. S. Yongprapat, S. Therdthianwong and A. Therdthianwong, Electrochim. Acta, 2012, 83, 87-93.
183. J. F. Gomes, A. C. Garcia, L. H. S. Gasparotto, N. E. de Souza, E. B. Ferreira, C. Pires and G. Tremiliosi-Filho, Electrochimica Acta, 2014, 144, 361-368.
184. A. C. Garcia, J. Caliman, E. B. Ferreira, G. Tremiliosi-Filho and J. J. Linares, ChemElectroChem, 2015, 2, 1036-1041.

185. J. Qi, L. Xin, D. J. Chadderdon, Y. Qiu, Y. Jiang, N. Benipal, C. Liang and W. Li, Applied Catalysis B: Environmental, 2014, 154–155, 360-368.
186. Z. Zhang, L. Xin and W. Li, International Journal of Hydrogen Energy, 2012, 37, 9393-9401.
187. Z. Zhang, L. Xin, J. Qi, D. J. Chadderdon, K. Sun, K. M. Warsko and W. Li, Applied Catalysis B: Environmental, 2014, 147, 871-878.
188. M. Simões, S. Baranton and C. Coutanceau, Applied Catalysis B: Environmental, 2010, 93, 354-362.
189. R. Ciriminna and M. Pagliaro, Tetrahedron Letters, 2004, 45, 6381-6383.
190. P. Fordham, M. Besson and P. Gallezot, Catal Lett, 1997, 46, 195-199.
191. P. Fordham, M. Besson and P. Gallezot, in Studies in Surface Science and Catalysis, eds. A. B. H.U. Blaser and R. Prins, Elsevier, 1997, vol. Volume 108, pp. 429-436.
192. I. Sobczak, K. Jagodzinska and M. Ziolek, Catalysis Today, 2010, 158, 121-129.
193. R. Ciriminna, G. Palmisano, C. D. Pina, M. Rossi and M. Pagliaro, Tetrahedron Letters, 2006, 47, 6993-6995.
194. H. D. Speckmann, S. Haupt and H. H. Strehblow, Surface and Interface Analysis, 1988, 11, 148-155.
195. H. H. Strehblow and B. Titze, Electrochimica Acta, 1980, 25, 839-850.
196. P. Keil, D. Lützenkirchen‐Hecht and R. Frahm, AIP Conference Proceedings, 2007, 882, 490-492.
197. A. M. Visco, F. Neri, G. Neri, A. Donato, C. Milone and S. Galvagno, Physical Chemistry Chemical Physics, 1999, 1, 2869-2873.
198. Y. Joseph, I. Besnard, M. Rosenberger, B. Guse, H.-G. Nothofer, J. M. Wessels, U. Wild, A. Knop-Gericke, D. Su, R. Schlögl, A. Yasuda and T. Vossmeyer, The Journal of Physical Chemistry B, 2003, 107, 7406-7413.
199. T. F. Jaramillo, S.-H. Baeck, B. R. Cuenya and E. W. McFarland, Journal of the American Chemical Society, 2003, 125, 7148-7149.
200. M.-J. Kim, H.-J. Na, K. C. Lee, E. A. Yoo and M. Lee, Journal of Materials Chemistry, 2003, 13, 1789-1792.
201. M. P. Casaletto, A. Longo, A. Martorana, A. Prestianni and A. M. Venezia, Surface and Interface Analysis, 2006, 38, 215-218.
202. J. Pal, M. Ganguly, S. Dutta, C. Mondal, Y. Negishi and T. Pal, CrystEngComm, 2014, 16, 883-893.
203. M. Pang, Q. Wang and H. C. Zeng, Chemistry – A European Journal, 2012, 18, 14605-14609.
204. J. A. Hernández, S. A. Gómez, T. A. Zepeda, J. C. Fierro-González and G. A. Fuentes, ACS Catalysis, 2015, 5, 4003-4012.
205. Z. Wang, H. Fu, Z. Tian, D. Han and F. Gu, Nanoscale, 2016, 8, 5865-5872.
206. V. Matolín, M. Cabala, I. Matolínová, M. Škoda, J. Libra, M. Václavů, K. C. Prince, T. Skála, H. Yoshikawa, Y. Yamashita, S. Ueda and K. Kobayashi, Journal of Physics D: Applied Physics, 2009, 42, 115301.
207. G. Zhao, H. Hu, W. Chen, Z. Jiang, S. Zhang, J. Huang and Y. Lu, Catalysis Science & Technology, 2013, 3, 404-408.
208. K. Dhara, T. Ramachandran, B. G. Nair and T. G. Satheesh Babu, Journal of Electroanalytical Chemistry, 2015, 743, 1-9.
209. D. R. Kumar, D. Manoj, J. Santhanalakshmi and J.-J. Shim, Electrochimica Acta, 2015, 176, 514-522.
210. J.-S. Lee, A. Katoch, J.-H. Kim and S. S. Kim, Sensors and Actuators B: Chemical, 2016, 222, 307-314.
211. M. S. P. Francisco, V. R. Mastelaro, P. A. P. Nascente and A. O. Florentino, The Journal of Physical Chemistry B, 2001, 105, 10515-10522.
212. J. J. Teo, Y. Chang and H. C. Zeng, Langmuir, 2006, 22, 7369-7377.
213. T. Ghodselahi, M. A. Vesaghi, A. Shafiekhani, A. Baghizadeh and M. Lameii, Applied Surface Science, 2008, 255, 2730-2734.

214. W.-T. Yao, S.-H. Yu, Y. Zhou, J. Jiang, Q.-S. Wu, L. Zhang and J. Jiang, The Journal of Physical Chemistry B, 2005, 109, 14011-14016.
215. A. Primo, I. Esteve-Adell, J. F. Blandez, A. Dhakshinamoorthy, M. Alvaro, N. Candu, S. M. Coman, V. I. Parvulescu and H. Garcia, Nat Commun, 2015, 6.
216. A. Hussain, The Journal of Physical Chemistry C, 2013, 117, 5084-5094.
217. A. M. Venezia, G. Pantaleo, A. Longo, G. Di Carlo, M. P. Casaletto, F. L. Liotta and G. Deganello, The Journal of Physical Chemistry B, 2005, 109, 2821-2827.
218. R. Si and M. Flytzani-Stephanopoulos, Angewandte Chemie, 2008, 120, 2926-2929.
219. Q. Fu, H. Saltsburg and M. Flytzani-Stephanopoulos, Science, 2003, 301, 935-938.
220. M. Jia, H. Bai, Zhaorigetu, Y. Shen and Y. Li, Journal of Rare Earths, 2008, 26, 528-531.
221. Y. Shen, X. Yang, Y. Wang, Y. Zhang, H. Zhu, L. Gao and M. Jia, Applied Catalysis B: Environmental, 2008, 79, 142-148.
222. B. Habibi and N. Delnavaz, RSC Adv., 2016, 6, 31797-31806.
223. V. L. Oliveira, C. Morais, K. Servat, T. W. Napporn, P. Olivi, K. B. Kokoh and G. Tremiliosi-Filho, Electrocatalysis, 2015, DOI: 10.1007/s12678-015-0261-2, 1-8.
224. V. L. Oliveira, C. Morais, K. Servat, T. W. Napporn, G. Tremiliosi-Filho and K. B. Kokoh, Electrochimica Acta, 2014, 117, 255-262.
225. R. M.A. Tehrani and S. Ab Ghani, Electrochimica Acta, 2012, 70, 153-157.
226. X. Liang, M. Xiao, M. Xu, D. Yang, Y. Yan, Y. Tian and Y. Miao, J Appl Electrochem, 2016, 46, 1-8.
227. G. H. Yu, L. R. Zeng, F. W. Zhu, C. L. Chai and W. Y. Lai, Journal of Applied Physics, 2001, 90, 4039-4043.
228. M. A. Peck and M. A. Langell, Chemistry of Materials, 2012, 24, 4483-4490.
229. N. Han, S. Cao, J. Han, Y. Hu, X. Zhang and R. Guo, Journal of Materials Chemistry A, 2016, 4, 2590-2596.
230. J. W. Lee, T. Ahn, D. Soundararajan, J. M. Ko and J.-D. Kim, Chemical Communications, 2011, 47, 6305-6307.
231. J. Yan, W. Sun, T. Wei, Q. Zhang, Z. Fan and F. Wei, Journal of Materials Chemistry, 2012, 22, 11494-11502.
232. H.-Y. Wang, Y.-Y. Hsu, R. Chen, T.-S. Chan, H. M. Chen and B. Liu, Advanced Energy Materials, 2015, 5, n/a-n/a.
233. M. C. Biesinger, B. P. Payne, L. W. M. Lau, A. Gerson and R. S. C. Smart, Surface and Interface Analysis, 2009, 41, 324-332.
234. P. Selvam, B. Viswanathan and V. Srinivasan, Journal of Electron Spectroscopy and Related Phenomena, 1989, 49, 203-211.
235. A. N. Mansour and C. A. Melendres, Surface Science Spectra, 1994, 3, 263-270.
236. N. R. Stradiotto, K. E. Toghill, L. Xiao, A. Moshar and R. G. Compton, Electroanalysis, 2009, 21, 2627-2633.
237. M. A. Abdel Rahim, R. M. Abdel Hameed and M. W. Khalil, Journal of Power Sources, 2004, 134, 160-169.
238. A. Seghiouer, J. Chevalet, A. Barhoun and F. Lantelme, Journal of Electroanalytical Chemistry, 1998, 442, 113-123.
239. Y. Y. Du, Q. Jin, J. T. Feng, N. Zhang, Y. F. He and D. Q. Li, Catalysis Science & Technology, 2015, 5, 3216-3225.
240. G. Zhao, J. Huang, Z. Jiang, S. Zhang, L. Chen and Y. Lu, Applied Catalysis B: Environmental, 2013, 140–141, 249-257.
241. G. Zhao, H. Hu, M. Deng and Y. Lu, Chemical Communications, 2011, 47, 9642-9644.
242. Y. Mao, H. Yang, J. Chen, J. Chen, Y. Tong and X. Wang, Nano Energy, 2014, 6, 10-18.
243. Y. Mao, Y. Cheng, J. Wang, H. Yang, M. Li, J. Chen, M. Chao, Y. Tong and E. Liang, New Journal of Chemistry, 2016, 40, 107-112.
244. S. Berchmans, H. Gomathi and G. P. Rao, Journal of Electroanalytical Chemistry, 1995, 394, 267-270.

245. M. Shamsipur, M. Najafi and M.-R. M. Hosseini, Bioelectrochemistry, 2010, 77, 120-124.
246. N. Spinner and W. E. Mustain, Electrochimica Acta, 2011, 56, 5656-5666.
247. C. Xu, Y. Hu, J. Rong, S. P. Jiang and Y. Liu, Electrochemistry Communications, 2007, 9, 2009-2012.
248. Y.-l. Zhang, M. Zhang, Z. Shen, J.-f. Zhou and X.-f. Zhou, Journal of Chemical Technology & Biotechnology, 2013, 88, 829-833.
249. C. Rice, S. Ha, R. I. Masel, P. Waszczuk, A. Wieckowski and T. Barnard, Journal of Power Sources, 2002, 111, 83-89.
250. S. Uhm, S. T. Chung and J. Lee, Journal of Power Sources, 2008, 178, 34-43.
251. N. Y. Suzuki, P. V. B. Santiago, T. S. Galhardo, W. A. Carvalho, J. Souza-Garcia and C. A. Angelucci, Journal of Electroanalytical Chemistry, DOI: http://dx.doi.org/10.1016/j.jelechem.2016.02.020.
252. A. G. Garcia, P. P. Lopes, J. F. Gomes, C. Pires, E. B. Ferreira, R. G. M. Lucena, L. H. S. Gasparotto and G. Tremiliosi-Filho, New Journal of Chemistry, 2014, 38, 2865-2873.
253. T. M.-H. Lee, H. Cai and I. M. Hsing, Electroanalysis, 2004, 16, 1628-1631.
254. A. de la Escosura-Muñiz, M. Begoña González-García and A. Costa-García, Electroanalysis, 2004, 16, 1561-1568.
255. Y. Ding, Y. J. Kim and J. Erlebacher, Advanced Materials, 2004, 16, 1897-1900.
256. H. Qiu, C. Xu, X. Huang, Y. Ding, Y. Qu and P. Gao, The Journal of Physical Chemistry C, 2008, 112, 14781-14785.
257. J. Zhang, P. Liu, H. Ma and Y. Ding, The Journal of Physical Chemistry C, 2007, 111, 10382-10388.
258. C. Xu, J. Su, X. Xu, P. Liu, H. Zhao, F. Tian and Y. Ding, Journal of the American Chemical Society, 2007, 129, 42-43.
259. R. Li and K. Sieradzki, Physical Review Letters, 1992, 68, 1168-1171.
260. J. Wang, R. Xia, J. Zhu, Y. Ding, X. Zhang and Y. Chen, J Mater Sci, 2012, 47, 5013-5018.
261. L. H. Qian, X. Q. Yan, T. Fujita, A. Inoue and M. W. Chen, Applied Physics Letters, 2007, 90, 153120.
262. M. Hakamada and M. Mabuchi, Scripta Materialia, 2007, 56, 1003-1006.
263. A. Wittstock, B. Neumann, A. Schaefer, K. Dumbuya, C. Kübel, M. M. Biener, V. Zielasek, H.-P. Steinrück, J. M. Gottfried, J. Biener, A. Hamza and M. Bäumer, The Journal of Physical Chemistry C, 2009, 113, 5593-5600.
264. J. Erlebacher, M. J. Aziz, A. Karma, N. Dimitrov and K. Sieradzki, Nature, 2001, 410, 450-453.
265. J. Biener, M. M. Biener, R. J. Madix and C. M. Friend, ACS Catalysis, 2015, 5, 6263-6270.
266. W.-X. Li, C. Stampfl and M. Scheffler, Physical Review Letters, 2003, 90, 256102.
267. H. Zhang, G. Wang, D. Chen, X. Lv and J. Li, Chemistry of Materials, 2008, 20, 6543-6549.
268. M. Hepel and M. Tomkiewicz, Journal of The Electrochemical Society, 1984, 131, 1288-1294.
269. J. Guo, A. Hsu, D. Chu and R. Chen, The Journal of Physical Chemistry C, 2010, 114, 4324-4330.
270. Z. Liu, L. Huang, L. Zhang, H. Ma and Y. Ding, Electrochimica Acta, 2009, 54, 7286-7293.
271. T. Fujita, P. Guan, K. McKenna, X. Lang, A. Hirata, L. Zhang, T. Tokunaga, S. Arai, Y. Yamamoto, N. Tanaka, Y. Ishikawa, N. Asao, Y. Yamamoto, J. Erlebacher and M. Chen, Nat Mater, 2012, 11, 775-780.
272. W.-L. Yim, T. Nowitzki, M. Necke, H. Schnars, P. Nickut, J. Biener, M. M. Biener, V. Zielasek, K. Al-Shamery, T. Klüner and M. Bäumer, The Journal of Physical Chemistry C, 2007, 111, 445-451.
273. C. Xu, X. Xu, J. Su and Y. Ding, Journal of Catalysis, 2007, 252, 243-248.

274. K. J. Stowers, R. J. Madix, M. M. Biener, J. Biener and C. M. Friend, Catal Lett, 2015, 145, 1217-1223.
275. L.-C. Wang, K. J. Stowers, B. Zugic, M. M. Biener, J. Biener, C. M. Friend and R. J. Madix, Catalysis Science & Technology, 2015, 5, 1299-1306.
276. B. Xu, C. G. F. Siler, R. J. Madix and C. M. Friend, Chemistry – A European Journal, 2014, 20, 4646-4652.
277. K. M. Kosuda, A. Wittstock, C. M. Friend and M. Bäumer, Angewandte Chemie International Edition, 2012, 51, 1698-1701.
278. B. Xu and C. M. Friend, Faraday Discussions, 2011, 152, 307-320.
279. T. A. Baker, C. M. Friend and E. Kaxiras, The Journal of Physical Chemistry C, 2009, 113, 3232-3238.
280. A. C. Garcia, M. J. Kolb, C. van Nierop y Sanchez, J. Vos, Y. Y. Birdja, Y. Kwon, G. Tremiliosi-Filho and M. T. M. Koper, ACS Catalysis, 2016, 6, 4491-4500.
281. B. N. Zope, D. D. Hibbitts, M. Neurock and R. J. Davis, Science, 2010, 330, 74-78.
282. J.-H. Song, J.-Y. Yu, M.-Z. Zhang, Y.-J. Liang and C.-W. Xu, Int. J. Electrochem. Sci., 2012, 7, 4362-4368.